

UCSF

UC San Francisco Electronic Theses and Dissertations

Title

Transient and chronic tolerance kinetics of nitoglycerin-induced cyclic GMP accumulation in LLC-PK1 epithelial cells

Permalink

<https://escholarship.org/uc/item/9k41p9bh>

Author

Uchizono, James Alan

Publication Date

2001

Peer reviewed|Thesis/dissertation

Transient and Chronic Tolerance Kinetics of Nitroglycerin-induced
cyclic GMP Accumulation in LLC-PK1 Epithelial Cells

by

James Alan Uchizono
B.S. Chemistry, University of California, Irvine
B.S. Biology, University of California, Irvine
Pharm.D., University of California, San Francisco

DISSERTATION

Submitted in partial satisfaction of the requirements for the degree of

DOCTOR OF PHILOSOPHY

in

Pharmaceutical Chemistry

in the

GRADUATE DIVISION

of the

UNIVERSITY OF CALIFORNIA SAN FRANCISCO

Date

University Librarian

Degree Conferred:

Copyright 2001

by

James Alan Uchizono

**I dedicate this work to:
Mom and Dad**

**And a special dedication to my wife and best friend,
Suzie**

Acknowledgments

First and foremost, I thank God for creating us with minds beyond the mere chemical reactions of the brain and with senses that give us reliable information. This work is for His glory, not mine.

Although many deserve acknowledgement, no one deserves it more than Suzie, my wife. “My greatest achievement was convincing her to marry me.” She has been and is the most tangible expression of God’s care and love for me. She knew when to push me and when to let me be. Thank you for walking with me; you own this work as much as I.

To my parents, who have so generously invested in their children’s education, I love you and thank you with all my heart. I am also greatly indebted to Mom and Dad Tanioka, who “came to the rescue” in the closing days of completing this work. Throughout this journey, my sister and brother have remained steadfast supporters and prayer intercessors – thank you for sharing in the emotional and spiritual battle. I am also grateful to my grandparents for their faithful support. I also would like to extend my appreciation to my surrogate mother, Mrs. Paddy Kakihara, for all the \$10 bills for “da kine haircuts.”

I am thankful for the faculty at the University of California for giving me the opportunity to interact with and learn from international experts. I would like to specifically acknowledge several faculty members. I would like to thank the brilliant Professor Ronald A. Siegel for his guidance and vision for this project. His intellectual honesty and scientific integrity, as well as his “open-door” office hours,

have left a significant impression on me. I endeavor to carry these attributes throughout my career. I am grateful for Professor Lewis Sheiner, who added the needed driving force and expertise to complete this work. Dr. Sheiner showed me tremendous kindness, something I will never forget. I would also like to thank Professor Neal Benowitz for serving on my thesis and oral examination committees. Dr. Benowitz's grasp of pharmacology coupled with his humility inspires and challenges me. I am also indebted to Professor Frank Szoka, who has always provided sound guidance and wisdom. Dr. Szoka master-minded the recovery of my thesis from being an item in the trash bin to a doctoral thesis. Professor Richard H. Guy helped me grow as a researcher and manager of resources; he also provided invaluable guidance for traversing various political minefields. His immediate presence and humor are sorely missed on this side of the Atlantic. I also owe a great deal to Professor Leslie Z. Benet. Professor Benet pulled me out of multiple, proverbial fires. He also taught me how to identify the important issues of my research. Professor Christopher Cullander provided timely research critique and advice. Dr. Cullander was never stingy with encouragement, time, or friendship. I would also like to thank Professor Henning Schröder (Martin Luther University, Halle, Germany) for his generous advice, gifts of nitroglycerin, and time. His excitement and encouragement for nitroglycerin research is contagious. I am also thankful for Professors Davide Verotta, Anthony Hunt, and Palo Vicini (University of Washington) for their help with different mathematical aspects of this work.

Other faculty who have contributed to this work: Professor Kathy Giacomini (cell culture resources), Professor Thomas Scanlan (cell culture resources), and Professor Andy Packard (UC Berkeley, oral examination committee member).

There are many others from the lab I would like to thank. Dr. Vikram Ramanathan taught me all I know about cell culture (I still smile when I think about our years as TA's). Dr. Robert "Bob" Hinz could answer any lab/science (actually anything) question imagined – thanks Dr. Bob! Dr. Garrett Stanley helped stretch my mind and worldview and always provided interesting conversation. Dr. Rae Yuan was always encouraging and provided solid research critique. In addition, I would like to thank: Drs. Yogeshvar Kalia and Aarti Naik for their continued friendship and wit; Drs. Carol Lim and Thomas Cheatham, III for being great flat-mates and for all the great leftovers; Dr. Norris Turner for being such a truly, positive influence on the 11th-floor gang; Dr. Pamela DeMoor for all the encouragement and help with math; Dr. Girish "Rat" Rao for showing me how to electrocute the boss; Dr. John Baker for making the midnight fish-n-chips runs with me; Dr. Murali Ramanathan for all the funny stories, company at AAPS, and math helps; and Drs. Lourdes Nonato, Seung Oh, Delphine Imbert, Lisa Uyechi, and Marci Schaner for all their help and support. I would also like to thank Jim Frazine for his computer help and friendship.

I am also grateful for friends outside of UCSF that helped make this journey liveable. I would like to thank Bing Yeh, Ron Park, and Rob Honma for their continued support, prayers, and friendship – as well as computer help. I thank Richard Ma lending me a laptop. I would also like to thank the "bros," who have always been

a source of strength, encouragement, and great laughter: Brian “RT” Takushi, Curt “Oly” Ogawa, Rich “Speedo” Wada, Kevin “Hebe” Hayashida, Eric “Yaki” Yakura, and Rob “Corn” Honma. I also thank Felix Yu and Dr. Yan Chin for their hospitality and support, especially in the final days. Finally, I would like to thank my new colleagues at the University of the Pacific for their support and patience, especially Professors Xiaoling Li, William Chan, and Samir Kouzi.

Abstract

Transient and Chronic Tolerance Kinetics of Nitroglycerin-induced Cyclic GMP Accumulation in LLC-PK₁ Epithelial Cells

by

James Alan Uchizono

Doctor of Philosophy in Pharmaceutical Chemistry

University of California at San Francisco

Professor Lewis B. Sheiner, M.D., Chair

Professor Ronald A. Siegel, Sc.D.

Professor Neal Benowitz, M.D.

In this work, we present experiments and mathematical models characterizing the transient and chronic tolerance kinetics of nitroglycerin-induced cGMP accumulation in LLC-PK₁ (PK1) cells. PK1 cells were exposed to various concentrations of nitroglycerin (GTN) and were sampled for their cGMP content. Three major aspects were studied and are presented in this thesis: 1) characterization of transient cGMP responses (0 to 600 seconds) to multiple GTN concentrations;

2) characterization of chronic, tolerance kinetics – development and recovery, to multiple GTN concentrations; and 3) mathematical modeling of the transient and chronic kinetics.

In the transient kinetic experiments, cells were pre-incubated (5 minutes) with 3-isobutyl-1-methylxanine (IBMX), a phosphodiesterase inhibitor used to amplify the cGMP signal by preventing its rapid endogenous degradation. Various GTN concentrations (10^{-4} , 10^{-5} , 10^{-6} , 10^{-7} , 10^{-8} M) were used to stimulate cGMP production for prescribed amounts of time (15, 30, 45, 60, 90, 180, 300, 600 sec). Cells were lysed and measured for cGMP using ^3H -cGMP radioimmunoassay (RIA). Initial rates of cGMP production increased with increased GTN concentrations. However, maximal peak height for 10^{-5} M was higher than 10^{-4} M, and therefore, 10^{-5} M for 180 sec was used as the GTN rechallenge probe in the chronic, tolerance experiments. In chapter 3, we compare five and six parameter fits to the above described transient data.

In the chronic experiments, responsiveness to GTN was determined by using the rechallenge probe discussed above. In the tolerance development experiments, five GTN concentrations (10^{-6} , 5×10^{-7} , 2.5×10^{-7} , 10^{-7} , 5×10^{-8} M) were used to induce tolerance. At prescribed times (1, 5, 10, 15, 30, 45, 60, 90, 120, 150, 240 min), cGMP measurements were made. In the recovery experiments, cells were incubated with three different GTN concentrations (5×10^{-7} , 2.5×10^{-7} , 10^{-7} M) for two hours. The cells were allowed to recover in GTN-free media and were sampled at various times after the two GTN incubation (0, 6, 12, 20, 3 hrs). The extent and initial rate of tolerance

development increased with GTN concentration. Tolerance development at our highest concentration, 10^{-6} M, was incomplete. The cells did not fully recover – only returning to approximately 60% of the naïve control. In Chapter 4 we compare two two-parameter fits, as well as, show a phenomenological fit.

We were able to independently fit the transient and chronic data. However, attempts to integrate the two models failed, in that the $F_I(0)$ parameter estimated in the transient fit (0.598) did not match the chronic fit (0.373). In Chapter 4, we also compare the recovery rate constant, r , from the mechanism-based model fit to a phenomenological fit.



Professor Lewis B. Sheiner, M.D.
Dissertation Committee, Chair

Contents

Abstract	viii
List of Tables	xiv
List of Figures	xv
List of Figures	xv
1 Introduction	1
2 Background	4
2.1 Drug Tolerance	5
2.1.1 <i>Models of Drug Tolerance</i>	6
2.1.2 <i>Pharmacokinetic Phenomena Appearing to be Pharmacodynamic Tolerance</i>	12
2.1.3 <i>Ideal Kinetic Characteristics of Drugs used in Tolerance Studies</i>	13
2.2 Nitroglycerin (GTN)	14
2.2.1 <i>History and Background</i>	14
2.2.2 <i>Clinical Use</i>	19
2.2.3 <i>Mechanisms of GTN Action and Tolerance</i>	20
2.3 LLC-PK ₁ Epithelial Cell Culture	24
2.3.1 <i>Cyclic GMP (cGMP) and Phosphodiesterases</i>	25
2.4 References.....	27
3 Kinetics of Nitroglycerin-induced cGMP Accumulation in LLC-PK₁ Epithelial Cells at Multiple Nitroglycerin Concentrations. Part 1: Acute, Transient Kinetics.	44
3.1 Abstract.....	45
3.2 Introduction.....	46
3.3 Materials and Methods.....	48
3.3.1 <i>Materials</i>	48
3.3.2 <i>Cell Culture</i>	49
3.3.3 <i>Solution Preparation</i>	49
3.3.4 <i>Acute GTN/cGMP Kinetics</i>	50
3.3.5 <i>SNAP/cGMP degradation kinetics</i>	50
3.4 Experimental Results	51
3.5 Modeling	52
3.6 Discussion	56
3.7 References.....	60
3.8 Figure and Table Captions	64

4	Kinetics of Nitroglycerin-induced cGMP Accumulation in LLC-PK₁ Epithelial Cells at Multiple Nitroglycerin Concentrations. Part 2: Chronic, Tolerance Kinetics.	71
4.1	Abstract	72
4.2	Introduction	73
4.3	Materials and Methods	74
4.3.1	<i>Materials</i>	74
4.3.2	<i>Cell Culture</i>	75
4.3.3	<i>Solution Preparation</i>	75
4.3.4	<i>Rechallenge Probe</i>	75
4.3.5	<i>Tolerance Development</i>	75
4.3.6	<i>Tolerance Recovery</i>	76
4.4	Experimental Results	76
4.5	Modeling	77
4.6	Discussion	82
4.7	Figure and Table Captions	86
4.8	References	95
5	Conclusions	101
6	Future Work	106
7	Appendix A	107
7.1	Lysis, Extraction, RIA Preparation, and Miscellaneous Procedure	107
7.1.1	<i>Cell Lysis and Intracellular cGMP Extraction</i>	107
7.1.2	<i>RIA Sample Preparation and Dilutions</i>	108
7.2	Cell Culture Procedures	109
7.2.1	<i>Preparation for Media Used in Cell Culture Maintenance</i>	109
7.3	Cell Passaging	110
7.3.1	<i>Maintenance of Cell Pool Reservoir: T-150 or T-75 Flasks</i>	110
7.3.2	<i>Plating for Experiments: Falcon 6-well Plates</i>	112
7.4	Cell Counting	113
7.4.1	<i>Cell Counting for T-150 and T-75 Flasks and 6-well Plate Seeding</i>	113
7.4.2	<i>Cell Counting for 6-well Plates Used in Experiments</i>	115
7.5	Preparation of Commonly Used Solutions	116
7.5.1	<i>Nitroglycerin Solutions</i>	116
7.5.2	<i>IBMX Solutions</i>	117
7.5.3	<i>SNAP Solutions</i>	118
7.5.4	<i>DETA-NONO Solutions</i>	119
7.5.5	<i>Buffer Solutions</i>	119
7.6	Materials and Equipment	120
7.6.1	<i>Cell Culture</i>	120
7.6.2	<i>Chemicals, Solvents, and Miscellaneous</i>	123
7.6.3	<i>Radioimmunoassay</i>	124
7.6.4	<i>Experimental Apparatus and Equipment</i>	125

7.7	References.....	126
8	Appendix B.....	127
8.1	Chi-squared statistic.....	127
8.2	Correlation Matrix	128
8.3	References.....	131

List of Tables

Table 2.1. Key Characteristics of Various NO Donors. Adapted from [5, 24].	19
Table 3.1. Optimal Parameters and 95% Likelihood Profile Confidence Intervals.....	66
Table 4.1. Parameter Estimates for 2-parameter development fit shown	
in Figure 4.2A	93
Table 4.2. Parameter Estimates for 3 parameter recovery fit shown in Figure 4.2.B..	93
Table 4.3. Parameter Estimates for 5 parameter development fit shown in	
Figures 4.3A-B.....	93
Table 4.4. AIC values for Mechanistic Fits	94
Table 4.5 – Optimal parameters for Figure 4.4A-B.....	94
Table 4.6. Optimal parameters for Figure 4.5A-B.....	94

List of Figures

Figure 2.1. Nitroglycerin Chemical Structure.....	15
Figure 2.2. Schematic of Smooth Muscle Relaxation.....	17
Figure 2.3. Schematic diagram showing proposed mechanisms of action for various NO donors.....	22
Figure 3.1 Diagram showing transient model.....	67
Figure 3.2. Transient kinetic behavior at multiple GTN concentrations	68
Figure 3.3. Degrådation of cGMP.....	69
Figure 3.4. Surface plot showing relationship between initial conditions of f_1 and f_2 and cGMP accumulation.....	70
Figure 4.1. Diagram showing tolerance model.....	88
Figures 4.2A-B. Phenomenological Fit – 2 parameter development fit and 3 parameter recovery fit.....	89
Figure 4.3A-B. Phenomenological Fit – 5 parameter development fit and recovery trajectories using development parameters.....	90
Figure 4.4A-B. Mechanistic Fit – 2 parameter chronic fit and 7 parameter transient fit.	91
Figure 4.5A-B. Mechanistic Fit – 2 parameter chronic fit and 6 parameter transient fit.	92

1 Introduction

Despite the many years of clinical and basic research on glyceryl trinitrate (GTN or nitroglycerin) tolerance, clinicians still rely heavily on empirical dosing regimens of GTN in attempts to provide efficacious aid to patients suffering from angina or congestive heart failure. Our work seeks to quantify GTN kinetics of tolerance development and recovery in a model system; and in future studies, our work will provide a simple living system (LLC-PK₁ cell culture) in which more theoretically based dosing regimens can be tested. Since a simple living system provides an environment in which theoretical models and predictions can be easily tested, modified, and retested, an *in vitro* system was chosen over an *in vivo* system. Of course, as the accuracy and robustness of these models improves, *in vivo* and human subjects would be desirable and more realistic, and ultimately rational, quantitative dosing regimens could be determined for a given patient with cardiovascular disease (CVD).

Diseases of the heart are the leading cause of mortality and morbidity in the United States. This morbidity and mortality is associated with staggering losses of productivity in our work force, which results in a negative impact on social, health-care, and economic structures. In a fair portion of these heart disease patients, angina pectoris (AP) is the first clinical sign. For over a century, GTN has been given to abort AP; most physicians still consider GTN to be an effective antianginal and antiischemic agent.

Although nitrates have been the subject of over a century's worth of research, we find that we still do not understand the kinetics of nitrate GTN tolerance well enough to prescribe rational dosing strategies. One simply needs to observe the different delivery forms of nitrates and the prescribing patterns of clinicians to realize that nitrate therapy and the development of nitrate drug delivery systems are still empirically based. We observe delivery systems from the virtually instantaneous (sublingual, translingual sprays, and IV) to virtually zero-order, constant rate delivery systems (patches and ointment) and even dosage forms that are intermediate acting (isosorbide dinitrate). Yet, with this arsenal of dosage forms, we still do not know which form or combination of dosage forms will provide the patient with the greatest amount of prophylactic benefit. Our long-term goal is to develop and verify mathematical tools and models that will ultimately help the clinician prescribe a GTN regimen based on strong theoretical underpinnings that will maximize patient care.

Our short-term goal is to develop and characterize a cell culture system that will allow us to quantitate the kinetics of tolerance development and recovery. The work presented here reflects our efforts towards accomplishing this short-term goal. In this work, we chose to use nitroglycerin (GTN or glycerol trinitrate) as the drug exhibiting tolerance. The cell system was the LLC-PK₁ cell line, and we chose to measure cGMP as the surrogate marker for cell response. Chapter 2 presents relevant background information on GTN, the PK₁ cell line, and mathematical tolerance models. Chapter 3 covers the characterization and mathematical modeling of the cells' transient response to GTN at varying times and concentrations. Chapter 4 deals

with response kinetics, both tolerance development and recovery, when the cells experience prolonged exposure to GTN. Chapter 5 represents our conclusions and comments about future work. Appendices have been added to supplement the chapters; detailed experimental protocols are given as well as detailed derivations and explanations used in determining the optimal parameter sets and statistics.

2 Background

Most consider adaptation to be one of the traits distinguishing between living from nonliving systems. In contrast with non-living material undergoing degradative changes, living systems can detect stimuli and adapt. Technological advances have improved our ability to detect and measure intracellular effectors; these tools have revealed elegant stimulus detection systems coupled to adaptive intracellular remodeling. Koshland [49] cites the example of bacteria responding to a chemical attractant. When the attractant is suddenly increased, the bacteria change their migratory behavior. However, the bacteria soon adapt and return to their naïve migratory behavior despite the continued presence of attractant. Adaptation need not occur solely within intracellular boundaries. In the following example multiple tissue systems are involved; when a person walks out of a movie theater into the bright afternoon sunlight, his perception of light is highly amplified. His eyes rapidly accommodate by decreasing pupil size. However, this aperture adjustment alone is not sufficient; rapid photo bleaching of the protein rhodopsin, found in rods and cones, combines with pupil changes to attenuate the potential over stimulation of visual pathways. These intracellular and multi-system compensatory mechanisms are present throughout many biological systems. Our interests lie within a subset of adaptation known as drug tolerance. In our case, drug is the stimulus and the drug's desired effect is reduced under prolonged stimulation, leading to drug tolerance or adaptation. Specifically, this work addresses tolerance seen in LLC-PK₁ epithelial cells when stimulated with nitroglycerin (GTN).

2.1 Drug Tolerance

Drug tolerance is the source of much discussion in the literature. Although many have qualitatively described this phenomenon, until recently, few investigators have attempted to kinetically model or quantitate it, and even fewer have developed rational dosing schemes to circumvent it. For the purposes of this paper, we define tolerance as “the lessening of drug effect with time, when the drug level is maintained constant.” When tolerance is present, clockwise hysteresis between drug concentration and effect is observed.

For most drugs that do not exhibit tolerance, a “gold-standard” for dosing has been established and is easily understood and obtained. This gold standard consists of maintaining a steady-state concentration of drug between the MEC (minimum effective concentration) and the MTC (minimum toxic concentration). In these systems, as long as the drug is constantly maintained, the drug effect remains constant. In systems exhibiting tolerance, this dosing gold standard fails to provide optimal therapy. Intuitively, one doses drugs that exhibit tolerance as bolus doses at periods that are spaced far enough apart so that the tolerance from the previous dose has worn off. Although this dosing scheme makes intuitive sense, few have made efforts to theoretically or quantitatively justify this scheme. In our early work, which was relatively unsuccessful, we tried to substantiate the “intuitive” dosing scheme for nicotine in humans through brute force and dynamic programming optimizations. Although we did derive theoretically optimal dosing regimens for different sets of assumptions, realization of these complex dosing schemes in human subjects was not

accomplished because of experimental barriers – cost and ethical considerations. This experience led us to the characterized a biological system that demonstrated tolerance to drug stimulus and allowed us to easily test multiple dosing regimens.

2.1.1 Models of Drug Tolerance

The mathematical distinctions between various models provides insight into differentiating between underlying mechanisms of tolerance. For example, some models of tolerance predict an identical onset and recovery rates [76], while other models predict asymmetrical onset and recovery rates [44, 55, 78, 86, 87, 104, 105]. Although models can be powerful tools for prediction and description, they do not, alone, prove the veracity of a mechanism. For a more complete comparison of current models, the reader is directed to [29].

Five major models/mechanisms that can encompass most tolerance mechanisms are explained below. The first model is probably the best-known, receptor down-regulation [45, 55]. Drug action is often initiated by the binding of drug to a cell surface receptor. The drug-receptor complex is internalized or endocytosed, leading to a decrease in the number of available surface receptors. In the presence of constant drug stimulation (assuming that drug effect is proportional to the number or concentration of drug-receptor complexes), the pool of surface receptors is depleted, which leads to an attenuated response/effect. Tolerance in this model is asymmetrical with respect to development and recovery rates. Mathematically, this model can be expressed as

$$\frac{d[R]}{dt} = r_0 - (q + s[drug])[R] \quad (2.1)$$

where R is the receptor, r_0 is a zero-order rate constant for receptor production, q is an apparent first-order rate constant for constitutive receptor removal, and s is an apparent second-order rate constant (if $[drug]$ is constant, then $s[drug]$ and q can be combined to form a single apparent 1st-order rate constant). In this model, the system moves between two steady-state levels, $[R]_{ss(1)} = r_0/q$ and $[R]_{ss(2)} = r_0/(q + s[drug])$, corresponding to the completely naïve and fully tolerant states, respectively. Since moving from state 1 to 2 occurs more rapidly than vice versa, this model predicts an asymmetry between tolerance development and recovery. Since we must have $[drug] \geq 0$, the rate of tolerance development, $(q + s[drug])$, will always be greater than the rate of recovery, q .

The second mechanism is known as receptor desensitization [44, 86, 105]; Katz and Thesleff [44] developed the receptor desensitization model to explain acetylcholine-induced motor-end plate refractoriness. Even eleven years later, their model was still considered too esoteric; Waud [104] states in *Pharmacological Reviews*, “I expect that their [Katz and Thesleff] results will become explicable at one of these later stages, so that the cumbersome receptor model will not be necessary.” Waud believed the desensitization resulted from “changes in events following receptor activation” rather than strictly “a receptor phenomenon.” Rang and Ritter [78] and Weiland et al. [105] presented evidence further supporting the four-state receptor model of Katz and Thesleff. In 1986, Segel et al. added further to the Katz and Thesleff model; they modeled adaptation as a linear combination of the four possible

states. In this mechanism, the total number of receptors available for drug binding remains constant, but the receptors can exist in two forms, sensitized/activated or desensitized/inactivated, each form capable of binding drug. Although only drug bound to sensitized receptors elicits the response, the distribution of drug across all receptors determines the response magnitude. This model is described by

$$\begin{bmatrix} \dot{R} \\ \dot{X} \\ \dot{Y} \\ \dot{D} \end{bmatrix} = \begin{bmatrix} -(k_1 + k_r L) & k_{-r} & 0 & k_{-1} \\ k_r L & -(k_2 + k_{-r}) & k_{-2} & 0 \\ 0 & k_2 & -(k_{-2} + k_{-d}) & k_d L \\ k_1 & 0 & k_{-d} & -(k_{-1} + k_d L) \end{bmatrix} \begin{bmatrix} R \\ X \\ Y \\ D \end{bmatrix} \quad (2.2)$$

where R and X are the unbound and bound activated states, respectively, D and Y are the unbound and bound inactivated states, respectively, k_1 , k_{-1} , k_2 , k_{-2} are first-order rate constants, k_r , k_{-r} , k_d , k_{-d} are second-order rate constants, and L is the drug or ligand. The total receptor pool remains constant, $R_T = R + X + D + Y$. The binding rate constants, r and d subscripts, are rapid compared to the activated/inactivated isomerization rate constants. Inspection of the above matrix reveals an asymmetry in the rates of development and recovery. However, this model lacks the “development rate > recovery rate” constraint seen in the above down-regulation model. Interestingly, this model is mathematically similar to the non-competitive inhibition enzyme kinetics model, where enzyme (E), inhibitor (I), and substrate (S) exist in four combinations: E, ES, EI, and EIS, corresponding to R, X, D, and Y, respectively.

The third mechanism is based upon a kinetic tolerance compartment or state variable [76, 88]. The tolerance compartment, denoted T , attaches is linked to the concentration compartment (usually C or C_e) via a first-order transfer constant. The

first-order, exit rate constant, k_{tol} , for T determines the rate of tolerance development and recovery. If C is the driving compartment, then T becomes a state variable defined as $T = k_{tol}C * e^{-k_{tol}t}$ (where $*$ denotes convolution). At any time, t' , $T(t')$ represents a kind of moving, integrated exposure history of compartment C , which is used to attenuate the system's response to C . In the simplest model, both C and T are directly linked to the effect site. The following equations show two link models, non-competitive (2.3) and competitive antagonistic inhibition (2.4).

$$Effect = \frac{E_{max} \left(\frac{T_{50}}{T_{50} + T} \right) C}{C_{50} + C} \quad (2.3)$$

$$Effect = \frac{E_{max} C}{C_{50} \left(\frac{T_{50} + T}{T_{50}} \right) + C} \quad (2.4)$$

where E_{max} is the maximal effect, C_{50} is the concentration of drug leading to 50% of E_{max} in the absence of tolerance, and T_{50} quantifies the relationship between C_{ss} and T is a parameter relating the growth of T to the attenuation of effect. As T increases, either E_{max} is attenuated (non-competitive) or C_{50} is increased (competitive), both models predict that effect decreases as T increases. When $T=0$, both models reduce to the well-known E_{max} model. Since k_{tol} solely dictates the kinetics of T , this model, irrespective of the link model, predicts that the rate of tolerance development and recovery is symmetrical. Therefore, this model and the first model predict different behaviors with respect to tolerance rate symmetry for receptor down-regulation. In the first model, $(q+s[drug])$ governs the degradation of R and q governs its replenishing – leading to an asymmetrical down-regulation and recovery. On the other hand, the

third mechanism modulates receptor concentration with T , where the kinetics of tolerance development and recovery are symmetrical and governed by k_{tol} alone.

A second interesting difference involves the competitive link model. Unlike simple, classic competitive models, increasing drug concentration C will not overcome the inhibitor's effect T because T will increase proportionately – defeating the gains of increased drug concentration. This model has been used to simulate nicotine tolerance [76], multiple intravenous bolus dose morphine tolerance [69], and tolerance to caffeine's pressor effects [89].

The fourth mechanism involves variations of an adaptive systems approach [59, 73-75, 101]. Despite some major differences, the primary assumption made in all five papers is that the body maintains homeostasis and drugs disturb or trigger counter-regulatory mechanisms. Peper et al. [74] modeled drugs as disturbances in the feedback loop causing alterations to homeostatic balance. The body responds by activating an adaptive regulator that adjusts input, and this regulator “learns” how to better adapt with repeated drug exposures. It is not clear how this model “learns” which drugs exhibit tolerance and which do not. Veng-Pedersen and Modi [101] modeled tolerance as alterations to the input gain block, which controls the body's sensitivity to the drug. The output effect is the product of two terms (endogenous output and drug-induced output). As drug exposure increases, the effect increases – causing a feedback loop to modify the endogenous output. This modification lowers the resulting product of the two above terms. Mandema and Wada [59] based tolerance upon physiological changes, both molecular and cellular. Drug-induced

effect is added to endogenously induced effect to produce the output effect. As the output effect increases, it triggers molecular and cellular processes to produce negative feedback (negative effect) via changes to E_{\max} , EC_{50} , or the Hill coefficient. This model is by far one of the most sophisticated tolerance models in the literature, accounting for both within-systems and between-systems adaptation [48] while simultaneously maintaining mechanistic integrity. These adaptive models have been successfully used to model alfentanil tolerance [59, 101].

A fifth model is embodied in the indirect pharmacodynamics response models (specifically Models I and IV), which have utility well beyond tolerance modeling [19, 42, 50, 87]. The four models are based upon the premise that “a measured response (R) to a drug may be produced by indirect mechanisms” [19]. The following two modified equations show the four possible models:

$$\frac{dR}{dt} = k_{in} \cdot V(S_{1\dots n}, t) - k_{out} \cdot R \quad (2.5)$$

$$\frac{dR}{dt} = k_{in} - k_{out} W(S_{1\dots n}, t) \cdot R \quad (2.6)$$

where k_{in} and k_{out} are zero and first-order rate constants, respectively. The functions $V(S_{1\dots n}, t)$ and $W(S_{1\dots n}, t)$ can be stimulatory or inhibitory, depending on the specific drug-response system. For drug tolerance, we consider the models where V is inhibitory (Model I) or W is stimulatory (Model IV). V and W are explicit functions of other state variables ($S_{1\dots n}$) and can be explicit or implicit functions of time. The flexibility of this model allows for symmetrical and asymmetrical tolerance rates. This basic model has been successfully used to model prolactin release after

remoxipride [64], corticosteroid receptor down-regulation [91], and furosemide tolerance [102].

2.1.2 Pharmacokinetic Phenomena Appearing to be Pharmacodynamic Tolerance

Two distinct pharmacokinetic (PK) phenomena that can masquerade as pharmacodynamic tolerance are rapid drug distribution to the site of drug action, and enzymatic autoinduction. Porchet et al. [77] reported the confounding interaction between distribution kinetics and tolerance to nicotine's acute effects on heart rate. This artifactual "tolerance" occurs when the drug equilibrates more rapidly with the site of action than with the site of sampling (sampling site lags behind the site of action). A multiple dose regimen would be helpful in distinguishing distribution effects from tolerance. Once equilibration has occurred, a multiple-dose regimen will show a one-to-one correspondence between drug concentration and effect. If true tolerance is present, the concentration versus effect curve will continue to show clockwise hysteresis.

The second PK phenomenon appears when enzymatic autoinduction is present. In these systems, drug causes induction of its own metabolizing enzyme, leading to increased drug clearance and apparent tolerance. Since the body cannot infinitely increase clearance, simply increasing the dose to compensate for the new steady-state amount of metabolic enzyme will circumvent this therapeutic problem. Scheyer et al. [82] give an example of metabolic autoinduction with the antiepileptic medication carbamazepine. Although this qualifies as tolerance, according to our definition, this

PK “tolerance” does not pose an interesting dosing challenge. One simply increases the dosing rate to match the new clearance.

2.1.3 Ideal Kinetic Characteristics of Drugs used in Tolerance Studies

Since one of our larger goals is to determine a “gold-standard” set of dosing guidelines for drugs exhibiting tolerance, we present kinetic characteristics of drugs most likely to lead to successful dosing. *Ideal* PK characteristics are one-compartment disposition, time-invariant parameters, and linear elimination kinetics with a large exit rate constant. One-compartment disposition minimizes distribution effects. Time-invariant PK parameters maintain PK stationarity. Linear elimination kinetics with a large exit rate constant enhances our control of $C(t)$. If the measured physiological effect is continuous and easily measured, the experimental burden is eased.

Ideal pharmacodynamic (PD) characteristics include: instantaneous equilibration between C and *effect*, rate of drug elimination $>$ rate of tolerance disappearance, rate of approach to steady-state drug concentration $>$ rate of tolerance development. Instantaneous equilibration ensures no pre-, at-, or post-receptor delays. The first rate comparison ensures that our dosing regimen is based upon tolerance kinetics and not the drug’s PK. The second rate comparison allows the system to nearly reach its steady-state maximal effect (naïve effect) before tolerance kicks in. If the inequality were reversed, the observer would always see a tolerant state without ever seeing the naïve state.

Although the above “ideal” drug does not exist, the characteristics do help us home in on drugs most likely to be interesting tolerance problems. Like the above “ideal” drug, nitroglycerin shares many favorable PK and PD characteristics.

2.2 Nitroglycerin (GTN)

2.2.1 History and Background

The physico-chemical and pharmacokinetic properties of glycerol trinitrate (GTN), also known as nitroglycerin (NTG) have been well characterized. Technically, GTN ($C_3H_5N_3O_9$, MW = 227.10 g/mol) is not really a nitro compound (C-NO₂); instead it is a nitrate ester (C-O-NO₂) (see Figure 2.1). However, the name nitroglycerin is official and widely used. GTN is a moderately volatile oily liquid; the pure liquid is highly explosive, but can be rendered safe with an inert carrier, such as lactose. The nitrogen in GTN carries an oxidation state of +5; nitrovasodilators must have an oxidation state greater than +1 for significant activity.

In humans, the clearance of GTN is 230 ml/min/kg and the volume of distribution (V_{area}) is 3.3 liters/kg [92]; effective physiological concentration range is 1.2 to 11 ng/ml (5.3 nM to 48 nM). GTN undergoes extensive first-pass metabolism; GTN is metabolized to 1,2- and 1,3-glyceryl dinitrates (1,2-GDN and 1,3-GDN) [31, 32, 34, 81]. When GTN is intravenously given to humans, GTN tolerance develops within 10 to 24 hours [22, 80, 109]. The “Monday headache” frequently experienced by poorly protected workers in explosive manufacturing plants has become a well-known example of GTN tolerance. These munitions workers would develop a headache during the first couple of days of their work week. As the week progressed,

the headaches subsided (tolerance); however, the GTN-free environment over the weekend caused these workers to become resensitized to GTN. Thus, when these workers returned to work on Monday, they again developed “Monday headaches.” [66].

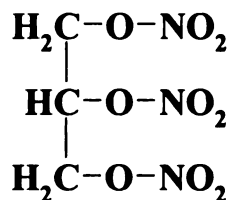


Figure 2.1. Nitroglycerin Chemical Structure

In 1846, Sobrero first synthesized GTN; he also observed that a small amount of GTN placed on the tongue caused a severe headache. In 1857 Brunton hypothesized that lowering blood pressure would relieve recurrent anginal pain; he accomplished this with phlebotomy and amyl nitrite. Although Hering and Davis were carrying out experiments with GTN in humans around 1847, it was William Murrell’s 1879 classic paper in *Lancet* that sparked over a century’s worth of GTN research. In this paper, Murrell connected the beneficial effects of amyl nitrite to GTN; furthermore, he revived the sublingual use of nitrates for anginal pain.

Today we have over one hundred years worth of clinical research and experience that confirm Brunton’s and Murrell’s findings that amyl nitrite and GTN terminate anginal attacks. Yet, a definitive, comprehensive theory encapsulating GTN’s mechanism of action and mechanism of tolerance does not exist. Current theories suggest that GTN is metabolized directly into nitric oxide (NO• or NO) or a nitrosothiol (RSNO) (capable of spontaneously releasing NO•), both of which are

capable of inducing smooth muscle relaxation (See Figure 2.2). Theories regarding GTN tolerance are still debated and unsettled.

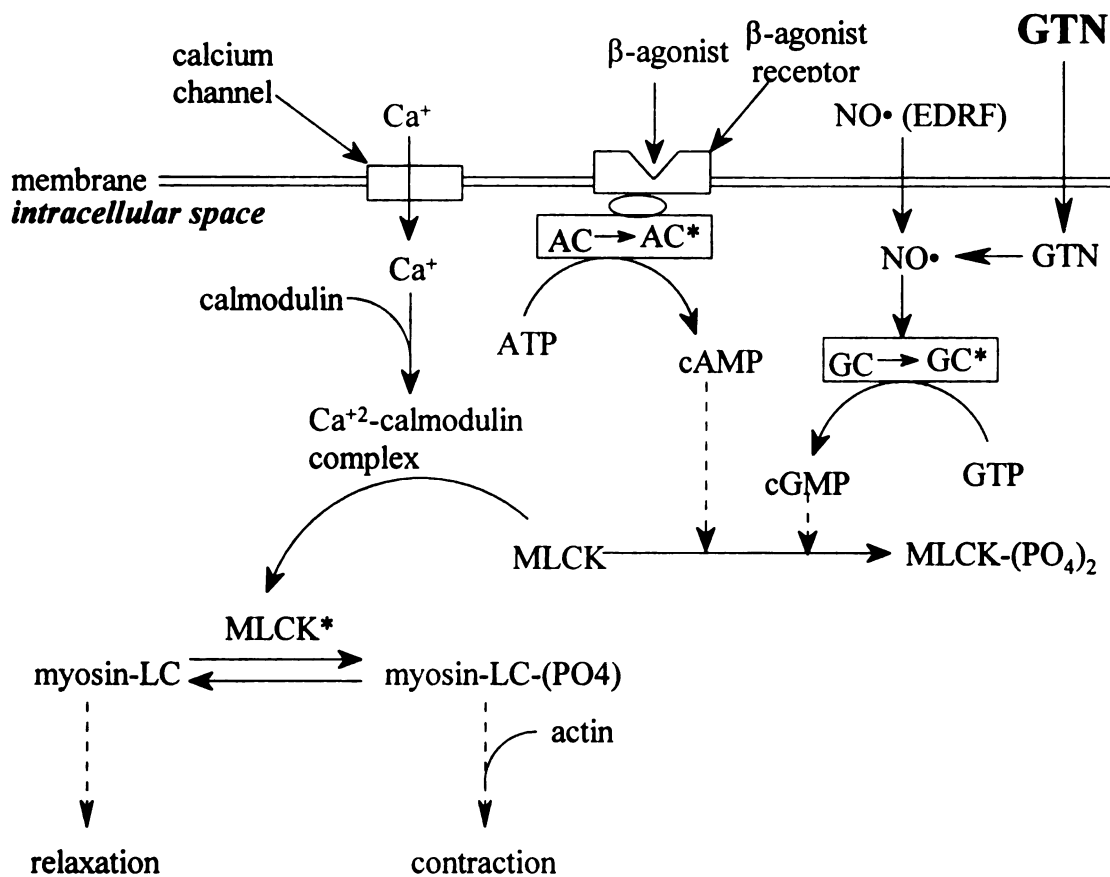


Figure 2.2. Schematic of Smooth Muscle Relaxation. Three general pathways resulting in smooth muscle relaxation are shown above. Nitroglycerin (GTN) readily moves across the cell membrane, where it directly releases NO or transfers one of its NO's to a carrier. Other compound, shown in Table 0.1, can also release their NO on either side of the membrane, which easily diffuses across the membrane. NO stimulates soluble guanylate cyclase (GC), which catalyzes the conversion of GTP into cGMP. The Ca^{2+} -calmodulin complex activates myosin light chain kinase (MLCK), which in turn phosphorylates myosin-light chain (myosin-LC) leading to smooth muscle contraction. NO donors and beta-agonists produce the second messengers cGMP/cAMP that can phosphorylate MLCK into an inactive form. Sequestering of MLCK in its phosphorylated form prevents the phosphorylation of myosin-LC and thus leads to smooth muscle relaxation.

Generally, N-oxide compounds ($\text{NO}\bullet$, NO^+ , NO^-) trigger smooth muscle relaxation via activation of guanylate cyclase (see Figure 2.3). NO activates guanylate cyclase ($\text{GC} \rightarrow \text{GC}^*$), which catalyzes the conversion of GTP into cGMP. Originally, endothelium dependent releasing factor (EDRF) was labeled as the activator of GC [37, 40], and Furchgott [28] first proposed that EDRF might actually be NO. Further studies by Palmer et al. [71] showed pharmacological and chemical evidence supporting that EDRF was NO or a nitroso compound that spontaneously generates NO; for a historical review of EDRF and $\text{NO}\bullet$, the reader is directed to Ignarro [37]. cGMP has been correlated to smooth muscle relaxation (see Figure 2.2 and decreased blood pressure via cGMP-dependent activation of phosphorylating kinases (MLCK), which phosphorylate various proteins in smooth muscle cells. These phosphorylated proteins lead to the loss of the phosphate group on myosin-LC through an undetermined biochemical cascade. It is well known that the dephosphorylated myosin-LC leads to smooth muscle relaxation [65, 103].

Six major chemical classes of NO donors have been studied: organic nitrates and nitrites, ferrous-nitro compounds, sydnonimines, S-nitrosothiols, and nucleophile adducts. $\text{NO}\bullet$, a true chemical radical, is amazingly stable as a radical. Estimates of its half-life range from 3 seconds to 15 seconds [38, 39]. Lancaster's simulations, using a diffusion coefficient of $3300 \mu\text{m}^2/\text{sec}$ from the work of Malinski [58] and the reported half-lives, showed that $\text{NO}\bullet$ could be found several cells away from the cell that produced it. For a comprehensive review on NO donors, the reader is directed to [4, 16, 24, 25, 35, 90]. Although each donor produces $\text{NO}\bullet$, some also produce other

N-oxides: nitrosonium ion (NO^+) and/or nitroxide ion (NO^-). The distinction between the three NO's is more than just chemical; they can have significantly different biological actions [5, 16, 24, 96]. Key characteristics of various NO donors are shown in Table 2.1.

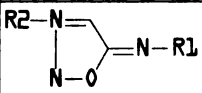
Chemical class	Structure	Example	Oxid. State	$\text{NO}\cdot$	NO^-	NO^+	Mechanism of NO generation
Organic nitrate	RONO_2	GTN, ISDN	+5	+	-	-	Mostly enzymatic
Organic nitrite	RONO	Amyl nitrite	+3	+	?	?	Enzymatic, chemical
Ferrous-nitro compounds	$[(\text{CN})_5\text{Fe}^{+2}]\text{NO}$	Sodium nitroprusside	+3	+	?	+	Chemical, enzymatic
Sydnonimines		SIN-1	+3	+	?	-	Enzymatic w/chemical
S-nitrosothiols	R-SNO	SNAP	+3	+	+	+	Chemical, enzymatic
Nucleophile adducts	$\text{R}_2\text{N}[\text{N}(\text{O})\text{NO}]^-$	DETA, NONOates	+3	+	?	?	Chemical

Table 2.1. Key Characteristics of Various NO Donors. Adapted from [5, 24].

2.2.2 Clinical Use

GTN has been a mainstay therapy for anginal attacks; it has also been used in the treatment of preterm labor [53], congestive heart failure, severe hypertension [1], glaucoma, and even chronic obstructive lung disease [3]. Although Yusuf et al. [108] reported that GTN reduced mortality in acute myocardial infarction (AMI), the recent American Heart Association (AHA) Treatment Guidelines [2] do not recommend GTN for more than 48 hours, and then only for symptomatic relief. The ISIS-4 [41] and GISSI-3 [30] trials did not support the routine use of GTN in AMI.

Long-term GTN has always been fraught with tolerance problems. Further exacerbating the tolerance problem, the FDA approved the GTN zero-order release patches based primarily upon PK data. While these patches delivered GTN as designed, there could not have been a worse regimen to deliver a drug inducing tolerance. Patients rapidly developed tolerance to the patch, usually within 10 to 24 hours [22, 80, 106, 109]. To circumvent tolerance, the patients were instructed to alternate wearing the patch and removing the patch every twelve hours. This strategy was successful in circumventing tolerance, but the patients were not receiving any prophylactic benefit during the drug-free period – leaving them more vulnerable to angina attacks [47, 72]. Although multiple dosage forms for GTN exist, ranging from virtually instantaneous (intravenous and sublingual) to continuous zero-order (transdermal patch), an optimal dosing strategy does not exist for GTN. It is lacking because the tolerance mechanism is not well-understood. Although human studies can provide the most relevant information, they are more difficult and costly to perform. Therefore, mechanistic GTN tolerance research has mainly focused on whole-body animal studies, aortic strips, and cell culture.

2.2.3 Mechanisms of GTN Action and Tolerance

Evidence supports the hypothesis that an enzymatic step bioactivates GTN resulting in NO• or RSNO-induced smooth muscle relaxation, thus making GTN a prodrug. The NO• or RSNO then goes on to activate guanylate cyclase. Haefeli et al. [32] demonstrated that GTN is rapidly metabolized to 1,2- and 1,3-GDN, which can be further reduced to 1- and 2-glyceryl mononitrates (1- and 2-GMN) [31].

Regioselectivity also supports the non-chemical degradation of GTN to its GDN byproducts; the 1,2-/1,3- metabolite ratio is elevated (i.e. greater than 2:1), where chemical degradation predicts 2:1. Furthermore, tolerant vessels tend to have a ratio less than 2:1 [10].

Two enzymes, glutathione S-transferase (GST) [33, 52, 97] and cytochrome P-450 [60, 83, 85], have been identified as capable and available GTN metabolizers/bioinactivators. Although the correlation between GST and GTN metabolism is strong, conflicting findings have cast doubts on this hypothesis. Lau and Benet [51] found that GST did not produce the skewed ratio ($> 2:1$) between the two GDN metabolites. Kenkare and Benet [46] found that ethacrynic acid, a GST inhibitor, decreased relaxation in rabbit aortic strips, yet Li et al. [54] found that ethacrynic acid also inhibited relaxation of other non-metabolized $\text{NO}\cdot$ donors in rat muscle. The exact role of GST in GTN metabolism remains unclear and an area of active research.

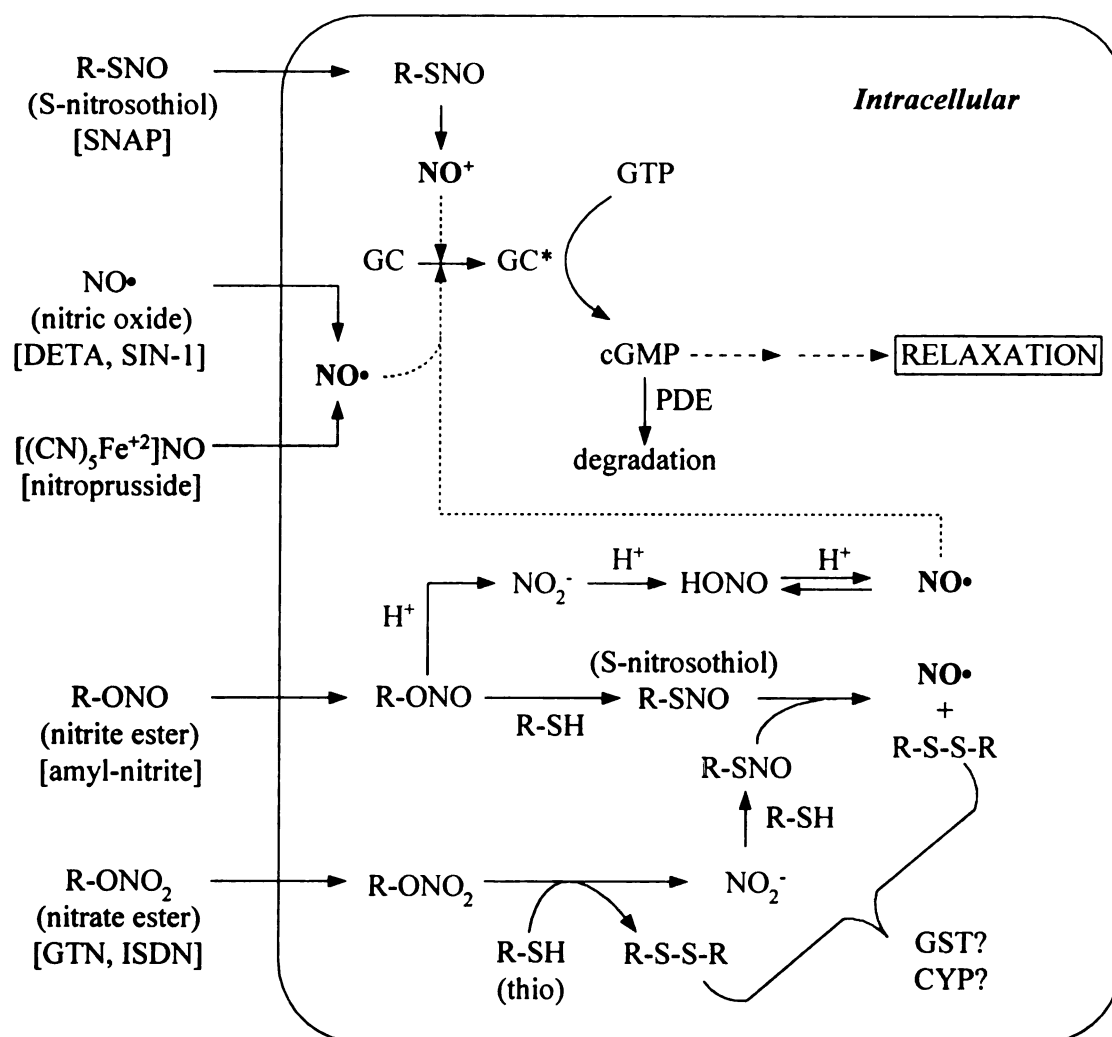


Figure 2.3. Schematic diagram showing proposed mechanisms of action for various NO donors. Nitric oxide easily crosses the cell membrane and activates guanylate cyclase (GC). Activated GC* catalyzes the conversion of GTP to cyclic GMP (cGMP), ultimately leading to muscle relaxation. DETA and SIN-1 undergo spontaneous chemical decomposition to yield NO•. Nitrite and nitrate esters (RONO and RONO₂) are lipophilic and easily enter the cell. Through different pathways, both can generate NO₂⁻ (inorganic nitrite), RSNO (S-nitrosothiol), and NO•. NO₂⁻ can form NO• through a purely chemical, HONO (nitrous acid) pathway. RSNO spontaneously releases NO•. NO• activates GC through an interaction with the GC-heme moiety [96]. Activated GC* catalyzes the conversion of GTP into cGMP (cyclic guanosine monophosphate) initiating a cascade that ultimately ends with muscle relaxation. A phosphodiesterase rapidly degrades cGMP into 5'-GMP preventing the buildup of cGMP. GTN tolerance researchers have focused on four main areas: thio-depletion, GST/CYP down-regulation, GC down-regulation, and PDE activation. Adapted from [37].

In addition to GST metabolism, cytochrome P-450 (CYP) is capable of GTN metabolism. Of the many CYP isozymes, 3A4 shows the highest activity towards GTN [20]. CYP research has also produced somewhat conflicting results, depending on species, organ/tissue type, or cell extract. Aortic strip experiments [9, 56], showing CYP was not necessary for GTN bioactivation, conflict with aortic and liver extract findings [11, 60]. In 1997, Yuan et al. [107] reported the *in vivo* bioactivation of GTN by CYP3A in rats. They suggested that *in vitro* findings might be confounded by uncontrolled O₂ tension. In cell culture models with only CYP2C11 present, Schröder and Schrör [85] and Schröder [83] found bioactivation of GTN by P-450 was inhibited by cimetidine, suggesting CYP2C11 activity. As with GST, CYP's role in GTN bioactivation continues to be an area of active research.

The role of the thiol pool in GTN activation and tolerance continues to evade researchers. The "thiol depletion" theory for GTN tolerance has its roots in the work of Needleman and co-workers [67, 68]. They found that intracellular pools of reduced thiols were depleted by prolonged GTN exposure. Although thiols are generally considered necessary for GTN bioactivation, the "depletion theory" for GTN tolerance lacks convincing support. Fung and co-workers [17, 27] have reviewed both evidence for and against the depletion theory. Other work has concluded that thiol depletion is partially responsible for acute GTN tolerance [12, 13, 27].

Two other proposed tolerance mechanisms include down-regulation of GC and increased phosphodiesterase (PDE) activity. Brandish et al. [15] found that simple dissociation of NO• from soluble guanylate cyclase (sGC) could not account for the *in*

in vivo deactivation time. They also found that thiols, such as GSH, and oxyhemoglobin could decrease the regeneration time, but not enough to match *in vivo* data. Bellamy et al. [7] estimated that deactivation of sGC occurred within a few seconds. Filippov et al.[26] found that NO decreases the stability of mRNA's coding for sGC. Schröder et al. [84] found sGC was desensitized by GTN and suggested tolerance recovery required *de novo* synthesis of sGC. Further evidence of a NO receptor on sGC in rat medullary interstitial cells was presented by Ujiie et al.[100]. Bennett et al. [8] suggested that tolerance might be caused by activation of the PDE rather than down-regulation of sGC. Pagani et al [70] reported that zaprinast, a PDE-V inhibitor, caused tolerance reversal in aortic rings. Although the PDE hypothesis is plausible, most research efforts are focused on the three other mechanisms.

Recently, another mechanism for GTN-induced relaxation has been proposed [14]. This mechanism involves calcitonin gene-related peptide (CGRP); they found that only Piloty's acid and GTN caused the release of CGRP, which contributed to the vasodilatory activity. The significance of this pathway is unknown at this time.

2.3 LLC-PK₁ Epithelial Cell Culture

The LLC-PK₁ (PK₁) cell line (ATCC CL-101, previously CRL-1392) is a well-characterized *Sus scrofa* (male pig, Hampshire) kidney epithelial cell line [18]. In 1958, Hull and coworkers [36] developed and characterized this cell line. This cell line is nontumorigenic, forms domes, and produces plasminogen activator (without renin) [61]. For a detailed history on LLC-PK₁ cells, the reader is directed to Meier and Insel [61]. This cell line possesses the necessary metabolizing complement to

convert GTN into a form of NO that can activate guanylate cyclase, thus leading to increases in cGMP. Similar to human smooth muscle, this cell line not only produces cGMP in response to GTN, but continued exposure to GTN leads to decreased amounts of cGMP or GTN tolerance [8, 85].

The experiments presented in this work used cGMP as a surrogate marker for tolerance to GTN incubations varying in concentration and exposure time. In our hands this cell line produced highly repeatable amounts of cGMP for each set of experimental conditions. In addition, the longevity and consistency of a specific culture from passage to passage was excellent over 8 to 10 passages (corresponding to passage numbers from about 205 to 215).

2.3.1 Cyclic GMP (cGMP) and Phosphodiesterases

The PK1 cells possess phosphodiesterase (PDE) activity capable of degrading cyclic GMP (cGMP). Rassier et al. [79] found all five PDE's known in 1990 in the PK1 cell line. Since 1991, over eleven PDE isozymes families have been discovered. Excellent review articles (1991, [93]; 1995 [6]; 1999 [21]) have rapidly become outdated. Current literature lists at least 11 different isozyme families [23, 57, 95]. Experimentally, these PDE's degrade cGMP so quickly that the levels of intracellular cGMP are below the radioimmunoassay (RIA) detection limit. Montague and Cook [62, 63] used 3-isobutyl-1-methylxanthine (IBMX) to raise intracellular cAMP and determine its effects on insulin release in isolated rat Islets of Langerhans. IBMX appears to only produce a partial PDE blockade [43, 94, 99]. IBMX has a molecular weight of 222.25, is poorly soluble in water, and easily diffuses into cells. We have

data (not shown) indicating that IBMX enters the cell and produces its blockade within 60 seconds. Although IBMX provides only partial antagonism, the blockade effectively amplified the cGMP concentration into the RIA detection range. Tzeng and Fung [98] estimated the cGMP half-life to be ~20 seconds (in the absence of any PDE inhibitor).

2.4 References

- [1] J. Abrams. Beneficial Actions of Nitrates in Cardiovascular Disease. *American Journal of Cardiology*, 1996, 77(13): 31C-37C.
- [2] A. H. A. AHA. The Era of Reperfusion: Section 1: Acute Coronary Syndromes (Acute Myocardial Infarction). *Circulation*, 2000, 102(8 (Supplement I)): I-172-I-203.
- [3] J. Ahlner, R. G. Andersson, K. Torfgard, and K. L. Axelsson. Organic Nitrate Esters: Clinical Use and Mechanisms of Action. *Pharmacological Reviews*, 1991, 43:351-423.
- [4] D. R. Arnelle and J. S. Stamler. NO⁺, NO, and NO⁻ Donation by S-nitrosothiols: Implications for Regulation of Physiological Functions by S-nitrosylation and Acceleration of Disulfide Formation. *Archives of Biochemistry and Biophysics*, 1995, 318(2): 279-285.
- [5] J. A. Bauer, B. P. Booth, and H.-L. Fung, "Nitric Oxide Donors: Biochemical Pharmacology and Therapeutics," in *Nitric Oxide: Biochemistry, Molecular Biology, and Therapeutic Implications*, vol. 34, *Advances in Pharmacology*, L. Ignarro and F. Murad, Eds. San Diego: Academic Press, Inc., 1985, pp. 361-381.
- [6] J. Beavo. Cyclic Nucleotide Phosphodiesterases: Functional Implications of Multiple Isoforms. *Physiological Reviews*, 1995, 75(4): 725-748.
- [7] T. C. Bellamy, J. Wood, D. A. Goodwin, and J. Garthwaite. Rapid Desensitization of the Nitric Oxide Receptor, Soluble Guanylate Cyclase,

- Underlies Diversity of Cellular cGMP Responses. *Proceedings of the National Academy of Sciences*, 2000, 97(6): 2928-2933.
- [8] B. M. Bennett, D. C. Leitman, H. Schröder, J. H. Kawamoto, K. Nakatsu, and F. Murad. Relationship Between Biotransformation of Glyceryl Trinitrate and Cyclic GMP Accumulation in Various Cultured Cell Lines. *Journal of Pharmacology and Experimental Therapeutics*, 1989, 250(1): 316-323.
- [9] B. M. Bennett, B. J. McDonald, R. Nigam, P. G. Long, and W. C. Simon. Inhibition of Nitrovasodilator- and Acetylcholine-induced Relaxation and Cyclic GMP Accumulation by the Cytochrome P-450 Substrate, 7-ethoxyresorufin. *Canadian Journal of Physiology and Pharmacology*, 1992, 70:1297-1303.
- [10] B. M. Bennett, B. J. McDonald, R. Nigam, and W. C. Simon. Biotransformation of Organic Nitrates and Vascular Smooth Muscle Cell Function. *Trends in Pharmacological Sciences*, 1994, 15(July 1994): 245-249.
- [11] B. M. Bennett, B. J. McDonald, and M. J. St. James. Hepatic Cytochrome P-450-mediated Activation of Rat Aortic Guanylyl Cyclase by Glyceryl Trinitrate. *Journal of Pharmacology and Experimental Therapeutics*, 1992, 261:716-723.
- [12] S. Boesgaard. Thio Compounds and Organic Nitrates. *Danish Medical Bulletin*, 1995, 42(5): 473-484.
- [13] S. Boesgaard, J. S. Petersen, J. Aldershvile, H. E. Poulsen, and H. Flachs. Nitrate Tolerance: Effect of Thiol Supplementation during Prolonged

- Nitroglycerin Infusion in an in Vivo Rat Model. *Journal of Pharmacology and Experimental Therapeutics*, 1991, 258(3): 851-856.
- [14] B. P. Booth, M. A. Tabrizi-Fard, and H.-L. Fung. Calcitonin Gene-Related Peptide-Dependent Vascular Relaxation of Rat Aorta. *Biochemical Pharmacology*, 2000, 59(12): 1603-1609.
- [15] P. E. Brandish, W. Buechler, and M. A. Marletta. Regeneration of the Ferrous Heme of Soluble Guanylate Cyclase from the Nitric Oxide Complex: Acceleration by Thiols and Oxyhemoglobin. *Biochemistry*, 1998, 37(48): 16898-16907.
- [16] A. R. Butler, F. W. Flitney, and D. L. H. Williams. NO, Nitrosonium Ions, Nitroxide Ions, Nitrosothiols and Iron-nitrosyls in Biology: A Chemist's Perspective. *Trends in Physical Sciences*, 1995, 16:18-22.
- [17] S. Chong and H.-L. Fung. Biochemical and Pharmacological Interactions Between Nitroglycerin and Thiols. *Biochemical Pharmacology*, 1991, 42(7): 1433-1439.
- [18] A.-A. T. C. Collection. LLC-PK1 Information. : ATCC, 2000.
- [19] N. L. Dayneka, V. Garg, and W. J. Jusko. Comparison of Four Basic Models of Indirect Pharmacodynamic Responses. *Journal of Pharmacokinetics and Biopharmaceutics*, 1993, 21(4): 457-478.
- [20] M. Delaforge, D. Servent, P. Wirsta, C. Ducrocq, D. Mansuy, and M. Lenfant. Particular Ability of Cytochrome P-450 CYP3A to Reduce Glyceryl Trinitrate

- in Rat Liver Microsomes: Subsequent Formation of Nitric Oxide. *Chemical Biological Interactions*, 1993, 86:103-117.
- [21] T. P. Dousa. Cyclic-3',5'-nucleotide Phosphodiesterase Isozymes in Cell Biology and Pathophysiology of the Kidney. *Kidney International*, 1999, 55(1999): 29-62.
- [22] U. Elkayam. Tolerance to Organic Nitrates: Evidence, Mechanisms, Clinical Relevance, and Strategies for Prevention. *Annals of Internal Medicine*, 1991, 114(1991): 667-677.
- [23] L. Fawcett, R. Baxendale, P. Stacey, C. McGrouther, I. Harrow, S. Soderling, J. Hetman, J. A. Beavo, and S. C. Phillips. Molecular Cloning and Characterization of a Distinct Human Phosphodiesterase Gene Family: PDE11A. *Proceedings of the National Academy of Sciences*, 2000, 97(7): 3702-3207.
- [24] M. Feelisch. The Use of Nitric Oxide Donors in Pharmacological Studies. *Naunyn-Schmiedeberg's Archives of Pharmacology*, 1998, 385(1998): 113-122.
- [25] M. Feelisch and J. S. Stamler, "Donors of Nitrogen Oxides.," in *Methods in Nitric Oxide Research*, M. Feelisch and J. S. Stamler, Eds. Chichester: Wiley, 1996, pp. 77-115.
- [26] G. Filippov, D. B. Bloch, and K. D. Bloch. Nitric Oxide Decreases Stability of mRNAs Encoding Soluble Guanylate Cyclase Subunits in Rat Pulmonary

- Artery Smooth Muscle Cells. *Journal of Clinical Investigation*, 1997, 100(4): 942-948.
- [27] H.-L. Fung, S. Chong, E. Kowaluk, K. Hough, and M. Kakemi. Mechanisms for the Pharmacologic Interaction of Organic Nitrates with Thiols. Existence of an Extracellular Pathway for the Reversal of Nitrate Vascular Tolerance by N-Acetylcysteine. *Journal of Pharmacology and Experimental Therapeutics*, 1988, 245(2): 524-530.
- [28] R. F. Furchgott, "Studies on Relaxation of Rabbit Aorta by Sodium Nitrite: The Basis for the Proposal that the Acid-activatable Factor from Bovine Retractor Penis is Inorganic Nitrite and the Endothelium-derived Relaxing factor is Nitric Oxide," in *Mechanisms of Vasodilatation*, P. M. Vanhoutte, Ed. New York: Raven Press, Publishers, 1988, pp. 401-414.
- [29] M. Gardmark, L. Brynne, M. Hammarlund-Udenaes, and M. O. Karlsson. Interchangeability and Predictive Performance of Empirical Tolerance Models. *Clinical Pharmacokinetics*, 1999, 36(2): 145-167.
- [30] GISSI-3. Gruppo Italiano per lo Studio della Sopravvivenza nell'Infarto Miocardico. Six-month Effects of Early Treatment with Lisinopril and Transdermal Glyceryl Trinitrate Singly and Together Withdrawn Six Weeks After Acute Myocardial Infarction: The GISSI-3 Trial. *The American Journal of Cardiology*, 1996, 27:337-344.
- [31] M. Gumbleton, J. R. Cashman, and L. Z. Benet. 1,2- and 1,3-dinitrate Metabolites of Nitroglycerin: Spectroscopic Characterization and Initial

- Administration to Man. *International Journal of Pharmaceutics*, 1991, 71(1991): 175-186.
- [32] W. E. Haefeli, M. Gumbleton, L. Z. Benet, B. B. Hoffman, and T. F. Blaschke. Comparison of Vasodilatory Response to Nitroglycerin and its Dinitrate metabolites in Human Veins. *Clinical Pharmacology and Therapeutics*, 1992, 52(1992): 590-596.
- [33] K. E. Hill, R. W. Hunt, Jr., R. Jones, R. L. Hoover, and R. F. Burk. Metabolism of Nitroglycerin by Smooth Muscle Cells: Involvement of Glutathione and Glutathione s-transferase. *Biochemical Pharmacology*, 1992, 43(3): 561-566.
- [34] J. R. Hodgson and C. C. Lee. Trinitroglycerol Metabolism: Denitration and Glucuronide Formation in the Rat. *Toxicology and Applied Pharmacology*, 1975, 34:449-455.
- [35] J. A. Hrabie, J. r. Klose, D. A. Wink, and L. K. Keefer. New Nitric Oxide-Releasing Zwitterions Derived from Polyamines. *Journal of Organic Chemistry*, 1993, 58:1472-1476.
- [36] R. N. Hull, W. R. Cherry, and W. Weaver. The Origin and Characteristics of a Pig Kidney Cell Strain, LLC-PK. *In Vitro*, 1976, 12:670-677.
- [37] L. J. Ignarro. Biological Actions and Properties of Endothelium-Derived Nitric Oxide Formed and Released From Artery and Vein. *Circulation Research*, 1989, 65(1): 1-21.

- [38] L. J. Ignarro. Endothelium-Derived Nitric Oxide: Pharmacology and Relationship to the Actions of Organic Nitrate Esters. *Pharmaceutical Research*, 1989, 6(8): 651-659.
- [39] L. J. Ignarro. Signal Transduction Mechanisms Involving Nitric Oxide. *Biochemical Pharmacology*, 1991, 41(4): 485-490.
- [40] L. J. Ignarro, R. E. Byrns, and K. S. Wood, "Biochemical and Pharmacological Properties of Endothelium-derived Relaxing Factor and Its Similarity to Nitric Oxide Radical," in *Mechanisms of Vasodilatation*, P. M. Vanhoutte, Ed. New York: Raven Press, Publishers, 1988, pp. 427-435.
- [41] ISIS-4. ISIS-4 (Fourth International Study fo Infarct Survival) Collaborative Oral Mononitrate, and Intravenous Magnesium Sulphate in 58,050 Patients with Suspected Acute Myocardial Infarction. *The Lancet*, 1995, 1995:669-385.
- [42] W. J. Jusko and H. C. Ko. Physiologic Indirect Response Models Characterize Diverse Types of Pharmacodynamic Effects. *Clinical Pharmacology and Therapeutics*, 1994, 56(4): 406-419.
- [43] A. E. Kalderon, J. W. Dobbs, and M. L. Greenberg. Localization of 3',5'-cyclic Adenosine Monophosphate Phosphodiesterase (cAMP-PDEase) Activity in Isolated Bovine Thyroid Plasma Membranes. *Histochemistry*, 1980, 65(3): 277-289.
- [44] B. Katz and S. Thesleff. A Study of the 'Desensitization' Produced by Acetylcholine at Motor End-Plate. *Journal of Physiology*, 1957, 138(1957): 63-80.

- [45] T. P. Kenakin and D. Beek. Measurement of Antagonist Affinity for Purine Receptors of Drugs Producing Concomitant Phosphodiesterase Blockade: The Use of Pharmacologic Resultant Analysis. *Journal of Pharmacology and Experimental Therapeutics*, 1987, 243(2): 482-486.
- [46] S. R. Kenkare and L. Z. Benet. Effect of Ethacrynic Acid, a Glutathione-S-transferase Inhibitor, on Nitroglycerin-Mediated cGMP Elevation and Vasorelaxation of Rabbit Aortic Strips. *Biochemical Pharmacology*, 1993, 46:279-284.
- [47] T. O. Klemsdal and K. Gjesdal. Intermittent or Continuous Transdermal Nitroglycerin: Still an Issue, or Is the Case Closed? *Cardiovascular Drugs and Therapy*, 1996, 10(1996): 5-10.
- [48] G. F. Koob and F. E. Bloom. Cellular and Molecular Mechanisms of Drug Dependence. *Science*, 1988, 242:715-723.
- [49] D. E. Koshland, Jr. Biochemistry of Sensing and Adaptation. *Trends in Biological Science*, 1980, November, 1980): 297-302.
- [50] W. Krzyzanski and W. J. Jusko. Mathematical Formalism and Characteristics of Four Basic Models of Indirect Pharmacodynamic Responses for Drug Infusions. *Journal of Pharmacokinetics and Biopharmaceutics*, 1998, 26(4): 385-408.
- [51] D. T. Lau and L. Z. Benet. Nitroglycerin Metabolism in Subcellular Fractions of Rabbit Liver. Dose Dependency of Glyceryl Dinitrate Formation and

Possible Involvement of Multiple Isozymes of Glutathione S-transferases.

Drug Metabolism and Disposition, 1990, 18:292-297.

- [52] D. T. Lau, E. K. Chan, and L. Z. Benet. Glutathione S-transferase-mediated Metabolism of Glyceryl Trinitrate in Subcellular Fractions of Bovine Coronary Arteries. *Pharmaceutical Research*, 1992, 9:1460-1464.
- [53] C. Lees, S. Campbell, E. Jauniaux, R. Brown, B. Ramsay, D. Gibb, S. Moncada, and J. F. Martin. Arrest of Preterm Labour and Prolongation of Gestation with Glyceryl Trinitrate, a Nitric Oxide Donor. *The Lancet*, 1994, 343(May 28): 1325-1326.
- [54] C. G. Li, S. F. Brosch, and M. J. Rand. Inhibition by Ethacrynic Acid of NO-mediated Relaxations of the Rat Anococcygeus Muscle. *Clinical and Experimental Pharmacology and Physiology*, 1994, 21:293-299.
- [55] V. Licko, "Drugs, Receptors and Tolerance," in *Pharmacokinetics and Pharmacodynamics of Psychoactive Drugs*, G. Barnett and C. N. Chary, Eds. Foster City: Biomedical Publications, 1985, pp. 311-322.
- [56] Z. Liu, J. F. Brien, G. S. Marks, B. E. McLaughlin, and K. Nakatsu. Lack of Evidence for the Involvement of Cytochrome P-450 or other Hemoproteins in Metabolic Activation of Glyceryl Trinitrate in Rabbit Aorta. *Journal of Pharmacology and Experimental Therapeutics*, 1993, 264:1432-1439.
- [57] K. Loughney, P. B. Snyder, L. Uher, G. J. Rosman, K. Ferguson, and V. A. Florio. Isolation and Characterization of PDE10A, a Novel Human 3',5'-cyclic Nucleotide Phosphodiesterase. *Gene*, 1999, 234(1999): 109-117.

- [58] T. Malinski, Z. Taha, S. Grunfeld, S. Patton, M. Kapturczak, and P. Tomboulian. Diffusion of Nitric Oxide in the Aorta Wall Monitored *in situ* by Porphyrinic Microsensors. *Biochemical and Biophysical Research Communications*, 1993, 193(3): 1076-1082.
- [59] J. W. Mandema and D. R. Wada. Pharmacodynamic Model for Acute Tolerance Development to Electroencephalographic Effects of Alfentanil in Rat. *Journal of Pharmacology and Experimental Therapeutics*, 1995, 275(3): 1185-1194.
- [60] B. J. McDonald and B. M. Bennett. Cytochrome P-450 Mediated Biotransformation of Organic Nitrates. *Canadian Journal of Physiology and Pharmacology*, 1990, 68:1552-1557.
- [61] K. E. Meier and P. A. Insel, "Hormone Receptors and Response," in *Tissue Culture of Epithelial Cells*, M. Taub, Ed. New York: Plenum Press, 1985, pp. 152-158.
- [62] W. Montague and J. R. Cook. Adenosine 3':5'-Cyclic Monophosphate and Insulin Release. *Biochemical Journal*, 1970, 120(4): 9P-10P.
- [63] W. Montague and J. R. Cook. The Role of Adenosine 3':5'-cyclic Monophosphate in the Regulation of Insulin Release by Isolated Rate Islets of Langerhans. *Biochemical Journal*, 1971, 122(1971): 115-120.
- [64] G. Movin-Osswald and M. Hammarlund-Udenaes. Prolatin Release after Remoxipride By an Integrated Pharmacokinetic-Pharmacodynamic Model with

- Intra- and Interindividual Aspects. *Journal of Pharmacology and Experimental Therapeutics*, 1995, 274(2): 921-927.
- [65] F. Murad. Cyclic Guanosine Monophosphate as a Mediator of Vasodilation. *Journal of Clinical Investigation*, 1986, 78:1-5.
- [66] Needleman. Organic Nitrate Metabolism. *Annual Review of Pharmacology and Toxicology*, 1976, 16(1976): 81-93.
- [67] P. Needleman, B. Jakschik, and E. M. Johnson. Sulfhydryl Requirement for Relaxation of Vascular Smooth Muscle. *Journal of Pharmacology and Experimental Therapeutics*, 1973, 187:324-331.
- [68] P. Needleman and E. M. J. Johnson. Mechanism of Tolerance Development to Organic Nitrates. *Journal of Pharmacology and Experimental Therapeutics*, 1973, 184:324-331.
- [69] D. M.-C. Ouellet and G. M. Pollack. Pharmacodynamics and Tolerance Development During Multiple Intravenous Bolus Morphine Administration in Rats. *Journal of Pharmacology and Experimental Therapeutics*, 1997, 281(2): 713-720.
- [70] E. D. Pagani, G. S. VanAller, B. O'Connor, and P. J. Silver. Reversal of Nitroglycerin Tolerance In Vitro by the cGMP-phosphodiesterase Inhibitor Zaprinast. *European Journal of Pharmacology*, 1993, 243(1993): 141-147.
- [71] R. M. J. Palmer, A. G. Ferrige, and S. Moncada. Nitric Oxide Release Accounts for the biological Activity of Endothelium-derived Relaxing Factor. *Nature*, 1987, 327:524-526.

- [72] J. D. Parker. Potential Problems with Intermittent Nitrate Therapy. *Canadian Journal of Cardiology*, 1996, 12(Suppl. C): 22C-24C.
- [73] A. Peper and C. A. Grimbergen. Letter to the Editor: Preliminary Results of Simulations with an Improved Mathematical Model of Drug Tolerance. *Journal of Theoretical Biology*, 1999, 199(1999): 119-123.
- [74] A. Peper, C. A. Grimbergen, J. W. Kraal, and J. H. Engelbart. An approach to the Modeling of the Tolerance Mechanism in the Drug Effect. I: The Drug Effect as a Disturbance of Regulations. *Journal of Theoretical Biology*, 1987, 127(1987): 413-426.
- [75] A. Peper, C. A. Grimbergen, J. W. Kraal, and J. H. Engelbart. An Approach to the Modeling of the Tolerance Mechanism in the Drug Effect. II: On the Implications of Compensatory Regulation. *Journal of Theoretical Biology*, 1988, 132(1988): 29-41.
- [76] H. C. Porchet, N. L. Benowitz, and L. B. Sheiner. Pharmacodynamic Model of Tolerance: Application to Nicotine. *Journal of Pharmacology and Experimental Therapeutics*, 1988, 244(1): 231-236.
- [77] H. C. Porchet, N. L. Benowitz, L. B. Sheiner, and J. R. Copeland. Apparent Tolerance to the Acute Effect of Nicotine Results in Part from Distribution Kinetics. *Journal of Clinical Investigation*, 1987, 80(November 1987): 1466-1471.
- [78] H. P. Rang and J. M. Ritter. On the Mechanism of Desensitization at Cholinergic Receptors. *Molecular Pharmacology*, 1970, 6(1970): 357-382.

- [79] M. E. Rassier, S. J. McIntyre, M. Yamaki, S. Takeda, J.-T. Lin, and T. P. Dousa. Isozymes of Cyclic-3',5'-nucleotide Phosphodiesterases in Renal Epithelial LLC-PK₁ Cells. *Kidney International*, 1992, 41(1992): 88-99.
- [80] N. Reichel, C. Preist, D. Zimrin, T. Chandler, N. Berger, P. Douglas, and M. S. J. Sutton. Antianginal Effect of Nitroglycerin Over 24 Hours: Role of the Method of Administration. *Circulation*, 1984, 70(Supplement II): II-190.
- [81] D. Salvemini, A. Pistelli, and E. Anggard. Vascular and Anti-platelet Actions of 1,2- and 1,3-glyceryl dinitrate. *British Journal of Pharmacology*, 1993, 110(1993): 937-942.
- [82] R. D. Scheyer, J. A. Cramer, and R. H. Mattson. A Pharmacodynamic Approach to the Estimate of Carbamazepine Autoinduction. *Journal of Pharmaceutical Sciences*, 1994, 83(4): 491-494.
- [83] H. Schröder. Cytochrome P-450 Mediates Bioactivation of Organic Nitrates. *Journal of Pharmacology and Experimental Therapeutics*, 1992, 262(1): 298-302.
- [84] H. Schröder, D. C. Leitman, B. M. Bennett, S. A. Waldman, and F. Murad. Glyceryl Trinitrate-induced Desensitization of Guanylate Cyclase in Cultured Rat Lung Fibroblasts. *Journal of Pharmacology and Experimental Therapeutics*, 1988, 245(2): 413-418.
- [85] H. Schröder and K. Schrör. Inhibitors of Cytochrome P-450 Reduce Cyclic GMP Stimulation by Glyceryl Trinitrate in LLC-PK₁ Kidney Epithelial Cells.

Naunyn-Schmiedeberg's Archives of Pharmacology, 1990, 342(1990): 616-618.

- [86] L. A. Segel, A. Goldbeter, P. N. Devreotes, and B. E. Knox. A Mechanism for Exact Sensory Adaptation Based on Receptor Modification. *Journal of Theoretical Biology*, 1986, 120(1986): 151-179.
- [87] A. Sharma, W. F. Ebling, and W. J. Jusko. Precursor-dependent Indirect Pharmacodynamic Response Model for Tolerance and Rebound Phenomena. *Journal of Pharmaceutical Sciences*, 1998, 87(12): 1577-1584.
- [88] L. B. Sheiner. Clinical Pharmacology and the Choice Between Theory and Empiricism. *Clinical Pharmacology and Therapeutics*, 1989, 46(6): 605-615.
- [89] J. Shi, N. L. Benowitz, C. P. Denaro, and L. B. Sheiner. Pharmacokinetic-Pharmacodynamic Modeling of Caffeine: Tolerance to Pressor Effects. *Clinical Pharmacology and Therapeutics*, 1993, 53(1): 6-14.
- [90] J. S. Stamler, D. J. Singel, and J. Loscalzo. Biochemistry of Nitric Oxide and Its Redux-Activated Forms. *Science*, 1992, 258:1898-1902.
- [91] Y.-N. Sun, L. I. McKay, D. C. DuBois, W. J. Jusko, and R. R. Almon. Pharmacokinetic/Pharmacodynamic Models for Corticosteroid Receptor Down-Regulation and Glutamine Synthetase Induction in Rat Skeletal Muscle by a Receptor/Gene-Mediated Mechanism. *Journal of Pharmacology and Experimental Therapeutics*, 1999, 288(2): 720-728.

- [92] U. Thadani and T. Whitsett. Relationship of Pharmacokinetic and Pharmacodynamic Properties of the Organic Nitrates. *Clinical Pharmacokinetics*, 1988, 15:32-43.
- [93] W. J. Thompson. Cyclic Nucleotide Phosphodiesterases: Pharmacology, Biochemistry, and Function. *Pharmacology and Therapeutics*, 1991, 51(1991): 13-33.
- [94] C. Tomes, S. Rossi, and S. Moreno. Isobutylmethylxanthine and Other Classical Cyclic Nucleotide Phosphodiesterase Inhibitors Affect cAMP-dependent Protein Kinase Activity. *Cellular Signalling*, 1993, 5(5): 615-621.
- [95] T. J. Torphy and C. Page. Phosphodiesterases: The Journey Towards Therapeutics. *Trends in Pharmacological Sciences*, 2000, 21(May): 157-159.
- [96] C.-M. Tseng, M. A. Tabrizi-Fard, and H.-L. Fung. Differential Sensitivity among Nitric Oxide Donors toward ODQ-Mediated Inhibition of Vascular Relaxation. *Journal of Pharmacology and Experimental Therapeutics*, 2000, 292(2): 737-742.
- [97] S. Tsuchida, T. Maki, and K. Sato. Purification and Characterization of Glutathione Transferases with an Activity Towards Nitroglycerin from Human Aorta and Heart. *The Journal of Biological Chemistry*, 1990, 265:7150-7157.
- [98] T.-B. Tzeng and H.-L. Fung. Pharmacodynamic Modeling of the *In Vitro* Vasodilating Effects of Organic Mononitrates. *Journal of Pharmacokinetics and Biopharmaceutics*, 1992, 20(3): 227-251.

- [99] J. A. Uchizono and R. A. Siegel. Kinetics of Nitroglycerin-induced cGMP Accumulation in LLC-PK1 Epithelial Cells at Multiple Nitroglycerin Concentrations. Part 1: Transient, Acute Kinetics. *in prep*, 2001,
- [100] K. Ujiie, L. Hogarth, R. Danziger, J. G. Drewett, P. S. Yuen, I. H. Pang, and R. A. Star. Homologous and Heterologous Desensitization of Guanylyl Cyclase-linked Nitric Oxide Receptor in Cultured Rat Medullary Interstitial Cells. *Journal of Pharmacology and Experimental Therapeutics*, 1994, 270(2): 761-767.
- [101] P. Veng-Pedersen and N. B. Modi. A System Approach to Pharmacodynamics. Input-Effect Control System Analysis of Central Nervous System Effect of Alfentanil. *Journal of Pharmaceutical Sciences*, 1993, 82(3): 266-272.
- [102] M. Wakelkamp, G. Alván, J. Gabrielsson, and G. Paintaud. Pharmacodynamic Modeling of Furosemide Tolerance After Multiple Intravenous Administration. *Clinical Pharmacology and Therapeutics*, 1996, 1996(60): 75-88.
- [103] T. D. Warner, J. A. Mitchell, H. Sheng, and F. Murad. Effects of Cyclic GMP on Smooth Muscle Relaxation. *Advances in Pharmacology*, 1994, 26:171-94.
- [104] D. R. Waud. Pharmacological Receptors. *Pharmacological Reviews*, 1968, 20(2): 49-88.
- [105] G. Weiland, B. Georgia, S. Lappi, C. F. Chignell, and P. Taylor. Kinetics of Agonist-Mediated Transitions in State of the Cholinergic Receptor. *The Journal of Biological Chemistry*, 1977, 252(21): 7648-7656.

- [106] A. Wiegand, K. Bauer, R. Bonn, D. Trenk, and E. Jähnchen. Pharmacodynamic and Pharmacokinetic Evaluation of a New Transdermal Delivery System with a Time-Dependent Release of Glyceryl Trinitrate. *Journal of Clinical Pharmacology*, 1992, 32(1992): 77-84.
- [107] R. Yuan, M. Sumi, and L. Z. Benet. Investigation of Aortic CYP3A Bioactivation of Nitroglycerin *In Vivo*. *Journal of Pharmacology and Experimental Therapeutics*, 1997, 281(3): 1499-1505.
- [108] S. Yusuf, S. MacMahon, R. Collins, and R. Peto. Effect of Intravenous Nitrates on Mortality in Acute Myocardial Infarction: An Overview of the Randomised Trials. *The Lancet*, 1988, 1988(May 14): 1088-1092.
- [109] D. Zimrin, N. Reichel, B. K. T., G. Aurigemma, P. Douglas, B. Berko, and H.-L. Fung. Antianginal Effects of Intravenous Nitroglycerin over 24 Hours. *Circulation*, 1988, 77(6): 1376-1384.

3 Kinetics of Nitroglycerin-induced cGMP Accumulation in LLC-PK₁ Epithelial Cells at Multiple Nitroglycerin Concentrations. Part 1: Acute, Transient Kinetics.

James A. Uchizono^{1,3} and Ronald A. Siegel²

¹Department of Biopharmaceutical Sciences, University of California, San Francisco,
CA 94143

²Departments of Pharmaceutics and Biomedical Engineering, University of
Minnesota, Minneapolis, MN 55455

³Current Address: Department of Pharmaceutics and Medicinal Chemistry, University
of the Pacific, Stockton, CA 95211.

Corresponding author: Ronald A. Siegel, Department of Pharmaceutics, WDH 9-177,
University of Minnesota, 308 Harvard St. SE, Minneapolis, MN 55455; Telephone:
(612) 624-6164; E-mail: siege017@tc.umn.edu

3.1 Abstract

In this work we characterize and model the acute transient kinetic behavior of nitroglycerin-induced cGMP accumulation in cultured LLC-PK₁ cells in which isobutylmethyl xanthine (IBMX) is added to inhibit phosphodiesterase activity. Intracellular accumulation of cGMP is mapped kinetically in response to five nitroglycerin (GTN) concentrations ranging from 10⁻⁸ M to 10⁻⁴ M applied to the cells over durations ranging from 15 seconds to 600 seconds. A mathematical model is formulated to account for three major characteristics seen in the data: 1) the initial rate of cGMP accumulation increases with increased [GTN]; 2) 10⁻⁵ M GTN produces a higher cGMP peak than 10⁻⁴ M or 10⁻⁶ M GTN; and 3) GTN concentrations > 10⁻⁶ M produce cGMP curves that reach a maximum and then decrease. Estimates of model parameters are determined by non-linear least squares fitting applied simultaneously to cGMP data from the three highest GTN concentrations. Simulations show that an essential element in our model is the saturable production of cGMP. Our data also support the finding (Bennett et al., 1989) that IBMX only partially blocks PDE degradation of cGMP. The latter observation is corroborated by the decay of cGMP produced in response to the NO donor SNAP (s-nitroso-n-acetylpenicillamine). Simulations provided stronger support for a cofactor depletion model than for models which identify tolerance with rapid desensitization of GC, (c.f. [4]), and do not support GTN-modulated PDE activity. This work provides the foundation for rechallenge assays used in further experiments in which the development of tolerance to GTN, and recovery from such tolerance, is determined in the LLC-PK₁ cell system [18].

KEY WORDS: LLC-PK₁ epithelial cells, nitroglycerin, GTN, cyclic GMP, transient kinetics, tolerance kinetics, tolerance, IBMX, modeling, simulations, SNAP, nitric oxide.

3.2 Introduction

Organic nitrates are smooth muscle relaxants which have received much study due to the hypothesis that their actions are mediated via nitric oxide (NO), and because tolerance is developed after prolonged exposure. Because of tolerance, administration of the most well known of these drugs, nitroglycerin (glyceryl trinitrate, or GTN) via skin patches for prophylaxis against angina must be performed intermittently [12].

The biochemical mechanism of action of GTN and the mechanism underlying tolerance to this drug have been studied by numerous groups using *in vitro* cell culture and *in vivo* whole animal methods. Despite the widespread interest in GTN as a drug exhibiting tolerance, which is a time-dependent phenomenon, there have been few kinetic studies mapping the time course of development of tolerance to GTN and recovery of sensitivity after GTN is removed. An exception is the work of Bauer et al.[3] with the rat model of congestive heart failure.

The present paper constitutes the first of two studies concerning tolerance kinetics in a model cell culture system derived from the LLC-PK₁ porcine kidney epithelial cell line. Although this cell line is not directly relevant to the smooth muscle-relaxant action of GTN, it is a convenient model for biochemical studies due

to its durability [5], which is important in studies of tolerance kinetics which may require long term exposure, and because a simple assay based on cGMP accumulation has been developed by previous researchers for this cell line. The involvement of cGMP in the relaxing action of GTN in smooth muscle cells provides a plausible link between LLC-PK₁ results and those that might be obtained in smooth muscle.[10]

In the assay for tolerance in LLC-PK₁ developed by Bennett et al. [5], the cell line is exposed to GTN at a fixed chosen concentration for a fixed period of time. Following that, the original GTN is removed and the cells are rechallenged for a short period of time with a relatively high dose of GTN, and the accumulation of cGMP in the cells is assayed. Just prior to GTN rechallenge the cells are treated with isobutylmethyl xanthine (IBMX), a phosphodiesterase inhibitor which prevents cGMP degradation and hence boosts cGMP concentration in the cells, increasing assay sensitivity. In the second of these two papers we utilize this rechallenge assay to study the kinetics of tolerance development and the kinetics of recovery from tolerance, as a function of dose, duration of exposure, and time after withdrawal of GTN.

Since Bennett's rechallenge assay involves exposing cells to a high concentration of GTN over a short but finite period of time, a number of kinetic and dynamic questions need to be settled. First, how rapidly do the cells respond to rechallenge? Second, does an acute tolerance to GTN develop during the course of rechallenge? Third, does the duration of pretreatment with IBMX have a significant effect on measurements? Fourth, how effective is IBMX in suppressing

phosphodiesterase activity? The answers to these questions impinge on the experimental design of any study which utilizes this assay.

We first present our experimental results in which the acute response of LLC-PK₁ cells to GTN is mapped kinetically as a function of dose and duration of exposure. We then introduce a kinetic model that can account for many of the features observed in this acute data. This model can be used as a means for calibrating responses in studies using Bennett's assay, and serves as a starting point for modeling that will be presented in the second paper.

In addition to the extensive experiments using GTN as the stimulus, we also present the results of a less detailed experiment in which the cGMP response after exposure to S-nitroso-N-Acetylpenicillamine (SNAP), a direct NO donor, is followed in time.

3.3 Materials and Methods

3.3.1 Materials.

Fetal bovine serum (heat-inactivated), penicillin-streptomycin, Fungizone, HEPES buffer, trypsin (STV), phosphate buffer solution (PBS, Ca⁺², Mg⁺² free), Dulbecco's Modified Eagle's Media/F-12 [50:50 mixture] (DME) [GibcoBRL], and glutamine were obtained from the UCSF Cell Culture Facility (CCF). PK₁ epithelial cells (ATCC CL-101, LLC-PK₁) were also obtained from the UCSF CCF. Nitroglycerin (GTN) was a gift from Professor Dr. Henning Schröder of Department of Toxicology and Pharmacology, Martin Luther University (Halle, Germany); the GTN formulation used was "Perlinganit" solution manufactured by Schwarz Pharma

AG. 3-isobutyl-1-methyl-xanthine (IBMX) [CAS: 28822-58-4] was ultra high purity and was obtained from Sigma Chemical (Cat. No.: I-7018). S-nitroso-acetylpenicillamine (SNAP) [CAS:79032-48-7] was obtained from Research Biochemicals International, Natick, MA, (Cat No: N-152). The H₂O used in the RIA determination was ultra-pure [$> 1 \times 10^9$ ohm], DI water produced from a Millipore de-ionizer/filter. The cGMP[³H] radioimmunoassay (RIA) was obtained from Amersham (Cat. No.: TRK500). All other chemicals used were at least reagent grade and were obtained from multiple sources.

3.3.2 Cell Culture.

LLC-PK₁ (PK₁) cells were maintained in (DME) with 10% FBS, 2.5 µg/ml Fungizone, 100U:100 µg/ml penicillin-streptomycin, 2 mM glutamine. The cells were incubated at 37° C in a humidified atmosphere of 95% air and 5% CO₂. Four day old, confluent cultures were used in all of the experiments. The passage number for these cultures was about 200. Cells were washed twice with 2.0 ml DME just prior to their use in subsequent experiments.

3.3.3 Solution Preparation.

A 10⁻³ M GTN stock solution was prepared by dissolving 2.27 ml of Perlinganit GTN into 7.73 ml DME. Desired GTN concentrations were produced by serial dilution of the stock GTN solution with DME. The IBMX solution was prepared by dissolving 22.22 mg of IBMX into a beaker with 198.0 ml DME and 2.0 ml 1.0 M HEPES buffer to produce a 0.5 mM IBMX/10 mM HEPES/DME solution; this solution was stirred for ~1 hour or until fully dissolved.

3.3.4 Acute GTN/cGMP Kinetics.

This slightly modified procedure is derived from Bennett et al. [5]; we shortened the IBMX incubation and used a different cell lysis protocol. In prepared cultures, 0.9 ml of the IBMX solution was added to each well and allowed to incubate at 37° C for 3 minutes. Then, 0.1 ml of an appropriate GTN solution was added to the well to produce a total volume of 1.0 ml and plate-well GTN concentrations of 10^{-8} , 10^{-7} , 10^{-6} , 10^{-5} , 10^{-4} M, or control, respectively. The cells were then incubated with the appropriate GTN concentration for 15, 30, 45, 60, 90, or 180 seconds. At each prescribed incubation time the GTN/IBMX solution was aspirated from selected wells and the cellular reaction was terminated in those wells by immediately adding 1.0 ml 100% denatured-ethanol according to Friedl et al. [8] and Schröder [13]. After the ethanol had evaporated, 1.0 ml TRIS buffer was added to each well. To insure complete disruption of the cell membrane, the plates were frozen at -80° C for at least 1 hour and then thawed at room temperature. After the samples had fully thawed, each sample was appropriately diluted with TRIS to fall within the RIA limits (anywhere from 1:1 to 1:5). This experiment was repeated four times over a 3-year period with nearly identical results, and results from only one experimental run are shown.

3.3.5 SNAP/cGMP degradation kinetics.

Confluent cultures were washed and incubated in 0.9 ml of 0.5 mM IBMX/10mM HEPES/DME for 5 min. 0.1 ml of 10^{-5} M SNAP/DME was added to each well and allowed to incubate for 4.5 min. At the end of the incubation period a

high intensity; halogen desk lamp was placed over the plates for 60 sec to inactivate any remaining SNAP. At prescribed times, the cells were lysed and assayed for cGMP as described previously. Each time point contained six samples.

3.4 Experimental Results

Figures 3.2A-E summarize the time course of cGMP response of IBMX-treated PK₁ cells exposed to GTN at various concentrations and for various durations. Symbols represent raw data and curves represent the best fit, simultaneously fitting all five concentrations, based on the five, six, or seven--parameter mathematical model to be described below. Figures 3.2D-E have magnified ordinate scales. Figure 3.2F compiles the curves from Figures 3.2A-E for easier comparison. For the lowest concentration (10^{-8} M) the raw data response can be characterized as increasing to plateau, whereas the two highest doses (10^{-5} and 10^{-4} M) yield a response that first increases but ultimately decreases. The raw data for 10^{-6} and 10^{-7} M also show slight biphasic behavior.

An immediate consequence of the data in Figure 3.2 is that cGMP is eliminated after it is formed. Otherwise, all curves would be monotonically increasing. Either IBMX is not completely effective in blocking phosphodiesterase activity, or cGMP is lost through alternative pathways.

Of particular interest is the comparative behavior at GTN concentrations 10^{-4} M and 10^{-5} M. While the initial slope is greater for 10^{-4} M GTN, the peak value is reached earlier than for 10^{-5} M GTN, and the peak cGMP value is actually lower at the

higher concentration of GTN. This behavior proved key in differentiating the models tested.

Figure 3.3 displays the decay of cGMP after 4.5 minutes exposure to the NO donor SNAP, with IBMX present as before. SNAP was inactivated at time zero in this graph by application of intense UV light. Since cGMP formation is activated by NO which is rapidly degraded *in vivo* after formation (Ignarro, 1989) and SNAP-produced NO does not produce tolerance (Tseng et al., 2000; Shaffer, 1992), the decay seen in Figure 3.3 must be attributed to elimination of cGMP alone and not a decrease in its formation rate. Due to experimental difficulties, only three time points were obtained. The half-life between the first two points is ~245 sec. The half-life between the last two points is ~18 min.

3.5 Modeling

To interpret and model the kinetic data in Figure 3.1 we adopt and modify a mechanistic scheme proposed by Tzeng and Fung [16, 17] to account for the relaxation response of arterial strips to various nitrates, and modified that scheme according to considerations based on the work of Bennett et al.[5], who correlated the buildup of tolerance to GTN in LLC-PK₁ cells with metabolism of GTN.

The proposed scheme is shown in Figure 3.1. It is assumed that GTN is metabolized to an intermediate, N, which may correspond to NO [16, 17] or a nitrosothiol [2]. The rate of metabolism is proportional to the concentrations of cofactors, F₁ and F₂, which are also depleted in the metabolic reaction. The intermediate N subsequently experiences first order degradation. During its lifetime N

converts inactive guanylate cyclase, GC, to an activated form, GC*. For simplicity activation is assumed to be due to rapid [14] and saturable single-site binding of N to GC[15], so a Langmuirian function relates [GC*] to [GC] and [N]. GC* catalyzes the formation of cGMP from GTP, and cGMP is removed in a first order manner by pathways that are partially blocked by IBMX.

The scheme in Figure 3.1 is summarized by the differential equations

$$\frac{df_1}{dt} = -k_1[GTN]f_1 \quad (3.1)$$

$$\frac{df_2}{dt} = -k_2[GTN]f_2 \quad (3.2)$$

$$\frac{dn}{dt} = (k_1f_1 + k_2f_2)[GTN] - k_3n \quad (3.3)$$

$$\frac{d[cGMP]}{dt} = \frac{\alpha_2 n}{\alpha_1 + n} - k_4[cGMP] \quad (3.4)$$

where k_3 and k_4 are first-order rate constants representing degradation of N and cGMP, respectively, and k_1 and k_2 are, respectively, apparent second-order rate constants accounting for depletion of F_1 and F_2 in the presence of GTN. The term α_1 is the apparent binding constant of N to GC, while α_2 represents the maximal rate of conversion of GTP to cGMP by GC* given the total amount of GC and the availability of GTP in the cell, i.e. $\alpha_2 = \text{constant} \times [GTP] \times [GC]_{total}$. We assume that the GTP and GC pools in the cells are not significantly depleted during the experiment.

Because we do not observe either F or N in our experiments, absolute units cannot be assigned to these quantities. To make the model and its parameters identifiable, we set $f_1 = [F_1]/([F_1]_0 + [F_2]_0)$ and $f_2 = [F_2]/([F_1]_0 + [F_2]_0)$, dimensionless,

where $[F_1]_0$ and $[F_2]_0$ are the intercellular concentrations of F_1 and F_2 , respectively, in cells that have not been exposed by GTN. The initial relative molar abundance of the two factors is specified by $f_1(0)$. We also let a dimensionless variable n represent N and the “binding constant” α_1 is also rendered dimensionless.

To obtain the optimal set of parameters $[k_1, k_2, k_3, k_4, \alpha_1, \alpha_2, f_1(0)]$ for the model, a least squares minimization was performed simultaneously for the five data sets corresponding to $[GTN] = 10^{-4}, 10^{-5}, 10^{-6}, 10^{-7},$ and 10^{-8} M. Three optimizations corresponding to five, six, and seven-parameter models were performed. For reasons to be discussed later, we fixed $f_1(0)=0.598$, which is based on the degree to which cells are able to recover their responsiveness to GTN after chronic exposure, as determined in the second paper in this series. Estimates of the other parameters with 95% chi-square-based confidence intervals, are listed in Table 3.1. The confidence intervals for all parameters are tight and symmetrical, with only k_2 exhibiting a coefficient of variation greater than 10%. Moreover, correlation coefficients for the parameter estimates (not shown) are never so high as to cast doubt on parameter identifiability.

Fits of this model to the data are shown as solid lines in Figure 3.2A-E. These fits are satisfactory at $[GTN]=10^{-4}$ M and 10^{-5} M. A hint of model misspecification appears when $[GTN]=10^{-6}$ M, insofar as the model predictions do not “tip over” as fast as the data. This type of model misspecification is more pronounced at $[GTN]=10^{-7}$ M and 10^{-8} M. Therefore, the model cannot be said to fit the data well at all levels of GTN pre-exposure.

A reduced variant of this model, in which only one cofactor is present, was also considered by eliminating Eq. (3.2), fixing $k_2=0$, and fixing $f_1(0)=1$. This model reduction was rejected on statistical grounds (Akaike Information Criterion), but the resulting fits are shown as dashed curves in Figure 3.2A-E. The reduced model predictions differ little from those of the six-parameter model when $[GTN]=10^{-4}$ M and 10^{-5} M. It is inferior, however, at tracking the early rise of $[cGMP]$ at the lower GTN concentrations. The inclusion of a high affinity (“fast”), low capacity pathway in the full model is the source of its superior performance during the rise phase at these low GTN concentrations, although it must be recognized that the more complex model still has its shortcomings. At the higher GTN concentrations, the “fast” pathway depletes its factor very rapidly, and the measured response tracks the lower affinity, higher capacity, “slow” pathway. Since the “capacity” of GC, α_2 is adjustable, the elimination or inclusion of the fast pathway can be compensated for at the stage of formation of cGMP.

As mentioned before, when $f_1(0)$ is allowed to freely roam its parameter space, the optimal fit estimates its value at 0.916. This fit is also shown in Figure 3.2 as the dash-dot-dash lines. Clearly, both visually and by AIC, this fit is best. However, the high value for $f_1(0)$ needed for this fit eliminates it as a reasonable choice when modeling the chronic tolerance kinetics (fit shown in second paper).

Other model variants were studied, and rejected either because they provided poorer fits to the data, or because improvement in fit was not sufficiently great to offset the added complexity, based on the Akaike Information Criterion [1]. In the

first variant, Eq. (3.3) was eliminated in favor of the assumption that N is at quasi-steady state. This variant led to rise-times that were too small. In the second variant, activation of GC by N was not considered to be saturable. In this case the significantly smaller peak in response at $[GTN]=10^{-4}$ M compared to $[GTN]=10^{-5}$ M was not predicted. In the third variant, a $[GTN]$ -dependent term was included in the expression for the rate of elimination of cGMP, as suggested by Bennett et al. [5]. The improvement in fit in this case was marginal, so the augmented model was rejected on grounds of simplicity. Finally, we considered a model based on down regulation of GC by NO [4, 7, 19, 20]. Fits of this model to our data were not as good as those of the model of Figure 3.1.

3.6 Discussion

In order to map chronic GTN kinetics, a clear understanding and model of the transient cGMP response kinetics is needed. Curve fitting and modeling: i) do not support linear, GTN-modulation of PDE activity; ii) support the simultaneous production from GTN and cellular factors of an activator (N) of GC, and depletion of these factors; iii) support rapid kinetics of removal of N; and iv) support saturable activation of GC and hence saturable production of cGMP. Bennett et al. [5] suggested the hypothesis that PDE activity was being altered which caused the non-monotonic $[GTN]$ vs. cGMP curve. This hypothesis was difficult to test with the present experimental design, since there is substantial blockage of the PDE pathway due to the use of IBMX.

Since we have identified tolerance with the depletion of the hypothetical cellular factors F_1 and F_2 , we note that these hypothetical factors could be enzymes, helper proteins, enzyme co-factors, etc. Whatever these factors may be, they must be rapidly depleted relative to their long-term constitutive production and degradation. The long-term production and degradation aspects are unidentifiable under the current experimental design, but are identifiable under the design used in the second paper of this series, in which longer term experiments are carried out.

The rapid n degradation kinetics that we observed ($t_{1/2} = 11$ sec) are consistent with reported range for the nitric oxide half-life [6, 9-11]. Tzeng and Fung [16] reported ~15 sec for the NO half-life ($k = 2.74 \text{ min}^{-1}$). Although the literature tends to more strongly support n being NO vs. s-nitrosothiol, Arnelle and Stamler [2] present kinetic evidence for a nitrosothiol hypothesis. Although our data and modeling are unable to reconcile the identity of n , the modeling does support its presence.

Prior to the experiment, cells are conditioned in media without GTN, so levels of N (actually n) and cGMP are essentially zero, and we may assume that F_1 and F_2 are at their maximal levels. These are the initial conditions assumed in our model. In the second paper of this series, we shall use the present protocol as a probe to test the tolerant state of cells after longer term exposure to GTN at various levels and over various durations. Specifically, the probe consists of the present protocol, with $[\text{GTN}] = 10^{-5}$ M for 180 sec. It is reasonable to question whether the above initial conditions will still hold under these circumstances.

Since no IBMX is applied during the initial exposure and washout periods, we may safely assume that n and [GTN] are close to zero at the time the probe is applied, and the initial conditions used above are valid. However, the levels of F_1 and F_2 (i.e. f_1 and f_2) at the start of the probe are expected to be lower than their values in the naïve cell system, reflecting tolerance developed over time.

Since the data are most consistent with more than one pathway for development of tolerance, it should be noticed immediately that a single probe measurement cannot be used to determine the levels of F_1 and F_2 uniquely. This point is illustrated in Figure 3.4, in which it is shown that a continuum of combinations of f_1 and f_2 at the start of the probe can lead to the same predicted value of [cGMP]. Nevertheless, the probe can be used to make estimates of parameters that determine the time course of development of tolerance in each of the pathways, as will be discussed in the next paper.

Perhaps the most delicate modeling issue surrounds the choice of $f_i(0)$ used in the fits. When we allowed this parameter to vary freely, its optimum value was about 0.9. This fit, while superior, was not an appropriate choice in the second paper. With the six-parameter model, we found, upon comparing the predictions with the data, that the resulting model was virtually indistinguishable from the reduced model at high GTN concentrations, as would be expected since most of the cellular factors are associated with the low affinity, “slow” pool. Fits were much less satisfactory at the lower GTN concentrations, however. We suspect that the greater amount of absolute variance that needs to be explained at high GTN levels forced the fits to pay closer

attention to these cases. While this biasing of the fits could be prevented by a well specified variance model at the different GTN levels, we have at present not attempted to formulate such a variance model. Instead, we simply chose information, to be obtained in the next paper, on the fractional degree to which cells recover their sensitivity after prolonged exposure to GTN. In using this procedure, we assume that only the “slow” pathway recovers.

In conclusion, this work underscores the importance, when testing for drug tolerance, of understanding the transient kinetics of the naïve system while exploring its chronic kinetic behavior. Our model demonstrates that even a minimal model could be used to describe fairly complex, transient behavior of a system experiencing input over a 5-orders of magnitude range. In our models we assume that depletion of cellular factors by GTN outweighs any endogenous production and turnover of these factors during the time scale of the experiments. These processes will be the focus of the next paper. Lastly, this work demonstrates how apparent nonmonotonic concentration *versus* effect curves can be caused by sampling time choice of a dynamic process.

3.7 References

- [1] H. Akaike. A New Look at the Statistical Model Identification. *IEEE Transactions on Automatic Control*, 1974, AC-19(6): 716-723.
- [2] D. R. Arnelle and J. S. Stamler. NO⁺, NO, and NO⁻ Donation by S-nitrosothiols: Implications for Regulation of Physiological Functions by S-nitrosylation and Acceleration of Disulfide Formation. *Archives of Biochemistry and Biophysics*, 1995, 318(2): 279-285.
- [3] J. A. Bauer and H.-L. Fung. Concurrent Hydralazine Administration Prevents Nitroglycerin-induced Hemodynamic Tolerance in Experimental Heart Failure. *Circulation*, 1991, 84(1): 35-39.
- [4] T. C. Bellamy, J. Wood, D. A. Goodwin, and J. Garthwaite. Rapid Desensitization of the Nitric Oxide Receptor, Soluble Guanylate Cyclase, Underlies Diversity of Cellular cGMP Responses. *Proceedings of the National Academy of Sciences*, 2000, 97(6): 2928-2933.
- [5] B. M. Bennett, D. C. Leitman, H. Schröder, J. H. Kawamoto, K. Nakatsu, and F. Murad. Relationship Between Biotransformation of Glyceryl Trinitrate and Cyclic GMP Accumulation in Various Cultured Cell Lines. *Journal of Pharmacology and Experimental Therapeutics*, 1989, 250(1): 316-323.
- [6] T. M. Cocks, J. A. Angus, J. H. Campbell, and G. R. Campbell. Release and Properties of Endothelium-derived Relaxing Factor (EDRF) from Endothelial Cells in Culture. *Journal of Cellular Physiology*, 1985, 123(3): 310-20.

- [7] G. Filippov, D. B. Bloch, and K. D. Bloch. Nitric Oxide Decreases Stability of mRNAs Encoding Soluble Guanylate Cyclase Subunits in Rat Pulmonary Artery Smooth Muscle Cells. *Journal of Clinical Investigation*, 1997, 100(4): 942-948.
- [8] A. Friedl, C. Harmening, B. Schuricht, and B. Hamprecht. Rat Atrial Natriuretic Peptide Elevates the Level of Cyclic GMP in Astroglia-rich Brain Cell Cultures. *European Journal of Pharmacology*, 1985, 111(1985): 141-142.
- [9] Y. Henry, C. Ducrocq, J.-C. Drapier, D. Servent, C. Pellat, and A. Guissani. Nitric Oxide, A Biological Effector: Electron Paramagnetic Resonance Detection of Nitrosyl-iron-protein Complexes in Whole Cells. *European Biophysics Journal*, 1991, 20(1991): 1-15.
- [10] L. J. Ignarro. Endothelium-Derived Nitric Oxide: Pharmacology and Relationship to the Actions of Organic Nitrate Esters. *Pharmaceutical Research*, 1989, 6(8): 651-659.
- [11] M. Kelm, R. Dahmann, D. Wink, and M. Feelisch. The Nitric Oxide/Superoxide Assay. *The Journal of Biological Chemistry*, 1997, 272(15): 9922-9932.
- [12] T. O. Klemsdal and K. Gjesdal. Intermittent or Continuous Transdermal Nitroglycerin: Still an Issue, or Is the Case Closed? *Cardiovascular Drugs and Therapy*, 1996, 10(1996): 5-10.

- [13] H. Schröder. Cytochrome P-450 Mediates Bioactivation of Organic Nitrates. *Journal of Pharmacology and Experimental Therapeutics*, 1992, 262(1): 298-302.
- [14] J. R. Stone and M. A. Marletta. Spectral and Kinetic Studies on the Activation of Soluble Guanylate Cyclase by Nitric Oxide. *Biochemistry*, 1996, 35(4): 1093-1099.
- [15] C.-M. Tseng, M. A. Tabrizi-Fard, and H.-L. Fung. Differential Sensitivity among Nitric Oxide Donors toward ODQ-Mediated Inhibition of Vascular Relaxation. *Journal of Pharmacology and Experimental Therapeutics*, 2000, 292(2): 737-742.
- [16] T.-B. Tzeng and H.-L. Fung. Pharmacodynamic Modeling of the *In Vitro* Vasodilating Effects of Organic Mononitrates. *Journal of Pharmacokinetics and Biopharmaceutics*, 1992, 20(3): 227-251.
- [17] T.-B. Tzeng and H.-L. Fung. Pharmacokinetic/Pharmacodynamic Relationship of the Duration of Vasodilating Action of Organic Mononitrates in Rats. *Journal of Pharmacology and Experimental Therapeutics*, 1992, 261(2): 692-700.
- [18] J. A. Uchizono and R. A. Siegel. Kinetics of Nitroglycerin-induced cGMP Accumulation in LLC-PK1 Epithelial Cells at Multiple Nitroglycerin Concentrations. Part 2: Chronic, Tolerance Kinetics. , 2001,
- [19] K. Ujiie, L. Hogarth, R. Danziger, J. G. Drewett, P. S. Yuen, I. H. Pang, and R. A. Star. Homologous and Heterologous Desensitization of Guanylyl Cyclase-

linked Nitric Oxide Receptor in Cultured Rat Medullary Interstitial Cells.

Journal of Pharmacology and Experimental Therapeutics, 1994, 270(2): 761-767.

- [20] S. A. Waldman, R. M. Rapoport, R. Ginsberg, and F. Murad. Desensitization to Nitroglycerin in Vascular Smooth Muscle in Rat and Human. *Biochemical Pharmacology*, 1986, 35:3525.

3.8 Figure and Table Captions

Table 3.1. Table showing optimal parameter estimates and confidence statistics. The confidence regions were calculated using the Chi-squared statistic.

Figure 3.1. Scheme on which model of GTN tolerance is based.

Figure 3.2. Response of LLC-PK1 cells exposed to GTN at different concentrations and different durations. Raw data are indicated by symbols and model fits by solid lines (full model) and dashed lines (reduced model). Each panel shows a different GTN concentration. Panel F combines the fit curves for comparison. These fits are based upon the five-parameter model shown in Figure 1 ($k_5 = 0$).

Figure 3.3. Degradation of cGMP in the presence of IBMX. Symbols indicate raw data ($n=6$). The solid line connects the average value at each time point. PK₁ cells were exposed to SNAP (NO donor) in the presence of IBMX for 4.5 minutes. The SNAP was then inactivated by 60 seconds of UV exposure.

Figure 3.4. Surface plot displaying the relationship between f_1 and f_2 initial conditions for the 7-parameter model and the cGMP value it predicts from a single, fixed concentration and exposure challenge. Initial condition for $n = 0$ (see text) and $\text{cGMP}_{t=0} = 0$ (see Figure 5). Initial conditions for f_{10} and f_{20} are shown on the x and y-axes, respectively. For a given initial condition pair, $(f_1, f_2)_{t=0}$, the z-axis shows the

expected value for cGMP in response to a 180 second, 10^{-5} M GTN challenge.

Given any $(f_1, f_2)_{t=0}$ pair, the model predicts an appreciable, stable response.

Parameter	Optimal value	95% Likelihood Profile Confidence Region			
		Lower Bound	Upper Bound	Lower Bound %	Upper Bound %
α_1 (M sec ⁻¹)	0.000289	0.000284	0.000295	-1.8	2.0
α_2	10.9	10.8	11.0	-1.4	1.3
k_1 (M ⁻¹ •sec ⁻¹)	1252	1227	1278	-2.0	2.1
k_2 (sec ⁻¹)	0.0675	0.0663	0.0687	-1.8	1.8
k_3 (sec ⁻¹)	0.00278	0.00269	0.00288	-3.3	3.6
k_4 (M ⁻¹ •sec ⁻¹)	5905	5264	6654	-10.9	12.7

Table 3.1. Optimal Parameters and 95% Likelihood Profile Confidence Intervals

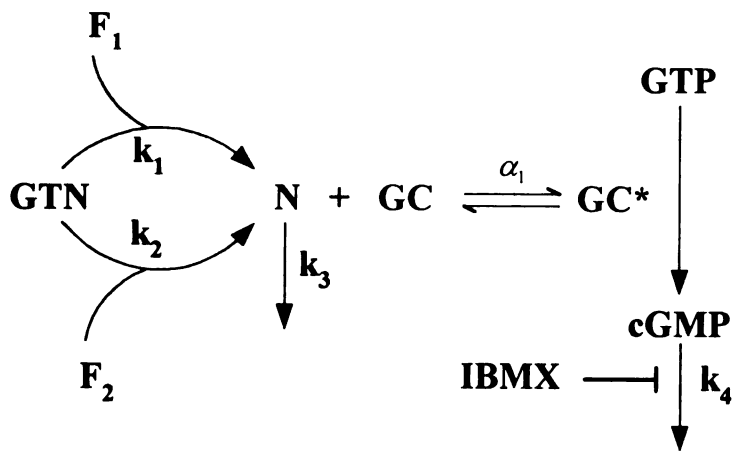


Figure 3.1 Diagram showing transient model

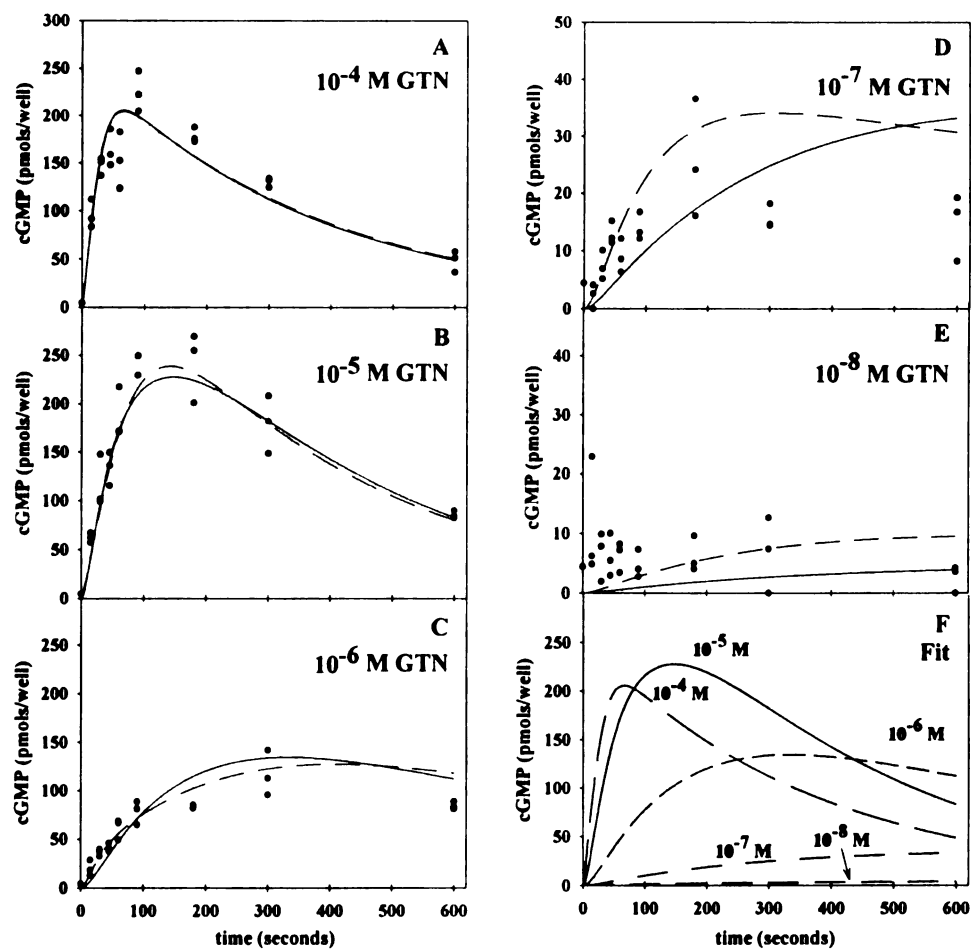


Figure 3.2. Transient kinetic behavior at multiple GTN concentrations

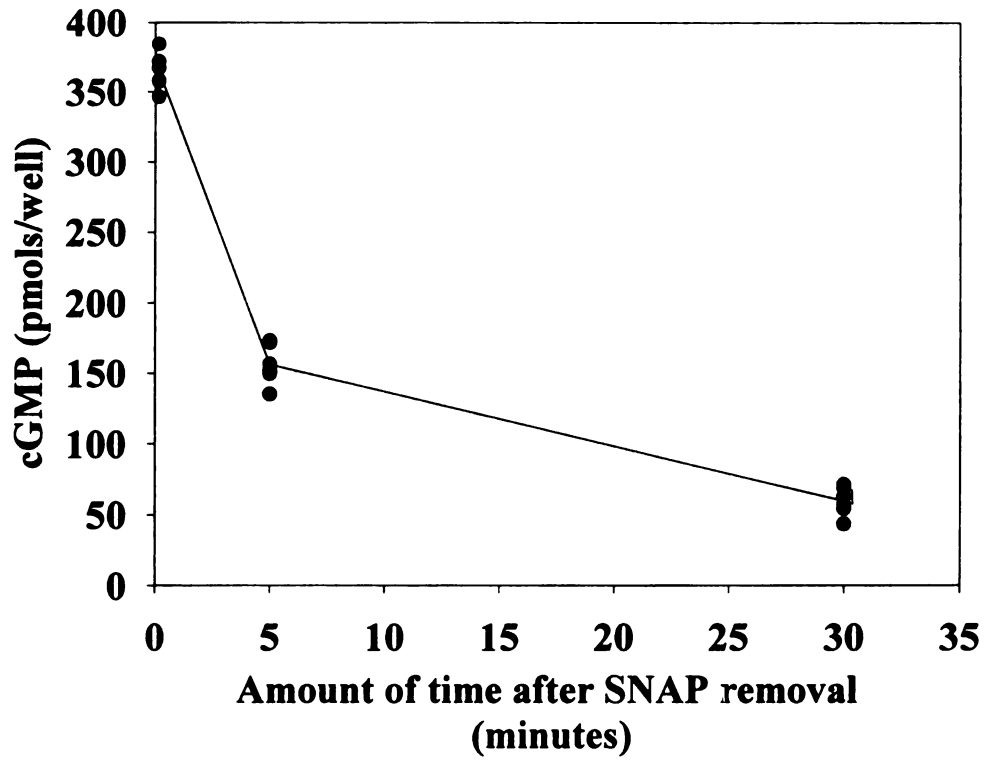


Figure 3.3. Degradation of cGMP

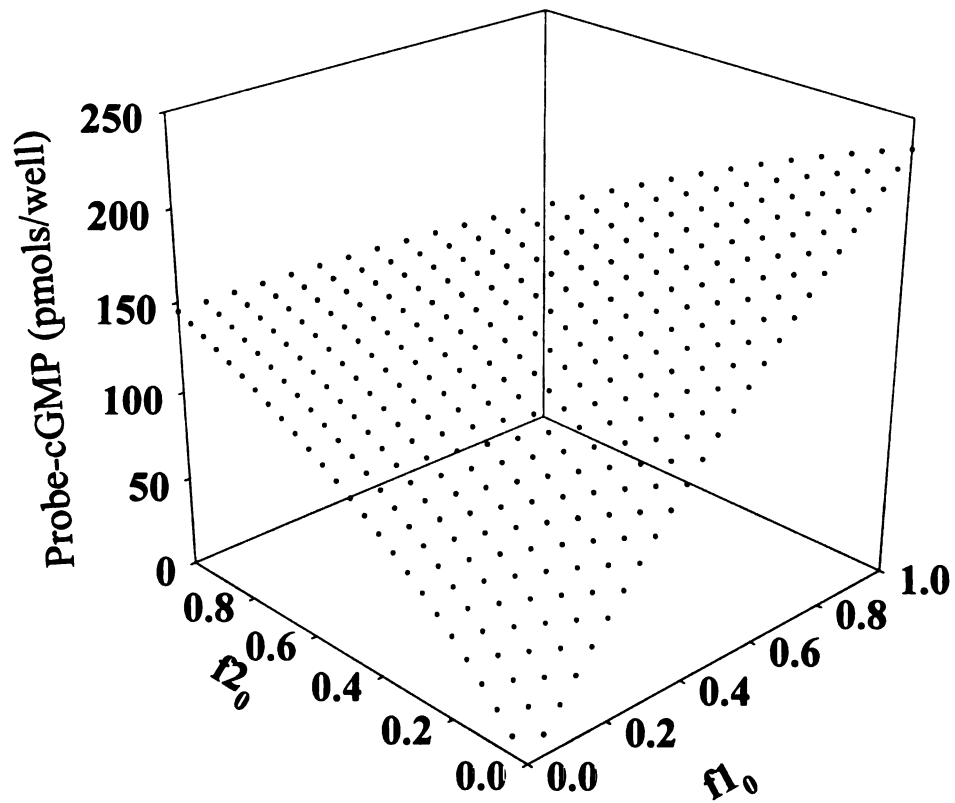


Figure 3.4. Surface plot showing relationship between initial conditions of f_1 and f_2 and cGMP accumulation

4 Kinetics of Nitroglycerin-induced cGMP Accumulation in LLC-PK₁ Epithelial Cells at Multiple Nitroglycerin Concentrations. Part 2: Chronic, Tolerance Kinetics.

James A. Uchizono^{1,3} and Ronald A. Siegel²

¹Department of Biopharmaceutical Sciences, University of California, San Francisco,
CA 94143

²Departments of Pharmaceutics and Biomedical Engineering, University of
Minnesota, Minneapolis, MN 55455

³Current Address: Department of Pharmaceutics and Medicinal Chemistry, University
of the Pacific, Stockton, CA 95211.

Corresponding author: Ronald A. Siegel, Department of Pharmaceutics, WDH 9-177,
University of Minnesota, 308 Harvard St. SE, Minneapolis, MN 55455; Telephone:
(612) 624-6164; E-mail: siege017@tc.umn.edu

4.1 Abstract

In this work we characterized the rate and extent of tolerance development and recovery to nitroglycerin (GTN)-induced cGMP accumulation in LLC-PK₁ (PK1) epithelial cells. To measure tolerance development, PK1 cells were incubated with GTN solutions of varying concentrations (5×10^{-8} , 10^{-7} , 2.5×10^{-7} , 5×10^{-7} , 10^{-6} M) for varying amounts of time (1, 5, 10, 15, 30, 60, 90, 120 minutes). At the specified times, cells were rechallenged with a GTN probe (10^{-5} M, 180 sec.) in the presence of the phosphodiesterase inhibitor 3-isobutyl-1-methylxanthine (IBMX). Tolerance recovery was measured by inducing tolerance with varying concentrations (10^{-7} , 2.5×10^{-7} , 5×10^{-7} M) of GTN for 2 hours, and then allowing the cells to recover in GTN-free media. At specified times (1 min, 6, 12, 20, 30 hours), cells were rechallenged with the GTN probe. GTN causes these cells to produce cyclic GMP (cGMP), and cGMP was measured by radioimmunoassay. We found that tolerance development occurred rapidly (< 2 hours). The extent and rate of tolerance development was concentration dependent. The tolerant cells never fully recovered, only reaching approximately 60% of their naïve control response. The data were not sufficient to support conclusions regarding the rate of tolerance recovery, but they do indicate that a majority of recovery occurred within 12 hours after induction ceased. The mathematical model presented here builds on a previous model [34] designed for GTN's transient kinetic behavior by adding an additional parameter to account for the chronic, long-term constitutive turnover of a cellular factor mediating the response to GTN.

KEY WORDS: LLC-PK₁ epithelial cells, nitroglycerin, GTN, cyclic GMP, tolerance kinetics, tolerance, kinetics of response, IBMX, modeling, simulations, SNAP, nitric oxide

4.2 Introduction

The mechanism of nitroglycerin (GTN) tolerance has eluded researchers for over a century. While the debate over GTN's mechanisms of action and tolerance actively continues, the rate of GTN tolerance development and recovery has drawn increasing attention [3, 5, 8, 9, 29, 32]. Tolerance can be defined as the reversible loss or lessening of drug effect while maintaining a constant drug concentration.

Many believe that GTN elicits its pharmacologic action through the release or bioactivation, in the presence of thiols, of nitric oxide (NO) [10, 11, 15, 16, 27, 28] or S-nitrosothiol (RSNO) [22]. NO or RSNO activates soluble guanylate cyclase (sGC) which catalyzes the conversion of GTP to cGMP. cGMP is subsequently degraded by a phosphodiesterase (PDE). Four hypotheses have been proposed to explain GTN tolerance: 1) thiol pool depletion [19, 24], 2) down-regulation of a bioactivating enzyme [18], 3) down-regulation of sGC [2, 4, 26, 29, 35], and 4) up-regulation of PDE [1, 7].

In this work, we examined the rate and extent of tolerance development at five GTN concentrations (10^{-8} , 10^{-7} , 2.5×10^{-7} , 5×10^{-7} , 10^{-6} M) and the rate and extent of tolerance recovery at three GTN concentrations (10^{-7} , 2.5×10^{-7} , 5×10^{-7} M). We

measured the accumulation of cGMP as the surrogate marker. Previously, we characterized and modeled the transient kinetics of a GTN challenge probe, of fixed concentration and duration [34], used in this work to assess the cells' cGMP-production tolerance state.

4.3 Materials and Methods

4.3.1 Materials

Fetal bovine serum (heat-inactivated), penicillin-streptomycin, Fungizone, HEPES buffer, trypsin (STV), phosphate buffer solution (PBS, Ca⁺², Mg⁺² free), Dulbecco's Modified Eagle's Media/F-12 [50:50 mixture] (DME) [GibcoBRL], and glutamine were obtained from the UCSF Cell Culture Facility (CCF). PK₁ epithelial cells (ATCC CL-101, LLC-PK₁) were also obtained from the UCSF CCF. Nitroglycerin (GTN) was a gift from Professor Dr. Henning Schröder of Department of Toxicology and Pharmacology, Martin Luther University (Halle, Germany); the GTN formulation used was "Perlinganit" solution manufactured by Schwarz Pharma AG. 3-isobutyl-1-methyl-xanthine (IBMX) [CAS: 28822-58-4], ultra high purity, and was obtained from Sigma Chemical (Cat. No.: I-7018). S-nitroso-acetylpenicillamine (SNAP) [CAS:79032-48-7] was obtained from Research Biochemicals International, Natick, MA, (Cat No: N-152). Deionized, ultra-pure H₂O used in the RIA determination was [$> 1 \times 10^9$ ohm] produced from a Millipore de-ionizer/filter. The cGMP[³H] radioimmunoassay (RIA) was obtained from Amersham (Cat. No.: TRK500). All other chemicals used were at least reagent grade and were obtained from multiple sources.

4.3.2 Cell Culture

LLC-PK₁ (PK₁) cells were maintained in (DME) with 10% FBS, 2.5 µg/ml Fungizone, 100U:100 µg/ml penicillin-streptomycin, 2 mM glutamine. The cells were incubated at 37° C in a humidified atmosphere of 95% air and 5% CO₂. Four day old, confluent cultures were used in all of the experiments. The passage number for these cultures was about 200. Cells were washed twice with 2.0 ml DME just prior to their use in subsequent experiments.

4.3.3 Solution Preparation

Solutions were prepared as previously reported [34]. Additional IBMX and GTN solutions were prepared for the tolerance recovery experiments due to the length of the experiments; solutions older than 6 hours were discarded. Newly prepared solutions were exposed to incubator conditions for at least one hour prior to use.

4.3.4 Rechallenge Probe

The rechallenge probe tested the tolerance state of the cell system. The rechallenge probe was as follows: 0.9 ml of IBMX was added to each well for 5 minutes, then 0.1 ml of 10⁻⁴ M GTN (final concentration of 10⁻⁵ M) was added for 3 minutes. The IBMX/GTN mixture was removed and the cells were immediately lysed and assayed for cGMP. Details of the probe are provided in ref. [34].

4.3.5 Tolerance Development

Four-day old cells were washed and 1.0 ml of GTN (1x10⁻⁸, 1x10⁻⁷, 2.5x10⁻⁷, 5x10⁻⁷, or 1x10⁻⁶ M) was added to each well. At prescribed times (shown on the left hand side of the abscissa of Figure 4.2), the incubating solution was aspirated and the

cells were washed twice. The rechallenge probe was used to measure the state of tolerance.

4.3.6 Tolerance Recovery

Four-day old cells were washed and 1.0 ml of GTN (1×10^{-7} , 2.5×10^{-7} , or 5×10^{-7} M) was added to each well and allowed to incubate for 2 hours. Upon removal of the incubating solution, cells were washed twice and 2.0 ml GTN-free and FBS-free media were added to each well to allow the cells to recover. At prescribed times (shown on the right-hand side of the abscissa in Figure 4.2) the GTN-free media was removed and the cells were washed twice. The cells were then rechallenged with the probe.

4.4 Experimental Results

Figures 4.2-4.5 show the averages of the raw data, shown as symbols. The raw data show that tolerance recovery was incomplete, with GTN response returning to approximately 60% of its value in the control or naïve state. Our control experiments (shown as open circles in Figures 4.2B) did not show significant loss of function over time, and the 60% recovery was virtually independent of degree of GTN exposure, so the lack of full recovery probably cannot be simply explained as the loss of activity due to mechanical manipulations (washing of cells, etc.) or cell death due to age.

The raw data shown in Figure 4.2 indicate that rate and extent of tolerance development increases with increasing GTN concentrations. At 10^{-6} M GTN, tolerance appears to reach a steady-state within 60 minutes. Other data (not shown) indicates that the curves for the smaller GTN concentrations do not significantly

change after the 120 minute time point, suggesting that these concentrations have also reached their steady-state at 120 minutes of GTN exposure. Five concentrations were studied for tolerance development, but only three were used in the recovery experiments due to experimental complexity.

Figures 4.2-4.5 show an open triangle (t=30 hours). Even though the standard deviation bars are relatively small, this point was considered an outlier and was not used in the fitting procedures.

4.5 Modeling

We used two different approaches to modeling the chronic kinetics. In the first approach, we used a phenomenological model to determine if the tolerance development kinetics could be explained by a simple GTN concentration-dependent model and the recovery kinetics by a simple concentration independent model. Tolerance development and recovery were modeled by the following two equations, respectively.

$$cGMP = C_0 e^{-k_2 t} + \frac{R_0}{r} e^{-(k_1[GTN]+r)t} + \frac{R_0}{(k_1[GTN]+r)} (1 - e^{-(k_1[GTN]+r)t}) \quad (4.1)$$

$$cGMP = \frac{R_0}{(k_1[GTN]+r)} + \left(\frac{R_0}{r} - \frac{R_0}{(k_1[GTN]+r)} \right) (1 - e^{-rt}) \quad (4.2)$$

C_0 is the cGMP lost to a secondary mechanism which is never regained. This feature needed to be added because the tolerance recovery is incomplete. R_0 is a zero-order production term and k_1 , k_2 , and r are first-order degradation rate constants. These equations are based on the simple phenomenon of a system going from one steady-state value to a second in response to a change in input ([GTN]).

This model shows that the recovery rate can be modeled by a single, concentration-independent rate constant. It also shows that the tolerance development rate is concentration dependent. The GTN concentration also is key in determining the steady-state tolerance level. Since our previous work shows the mapping between cofactors, F_1 and F_2 , and cGMP-accumulation is monotonic and nearly linear, we expected this model to reasonably model the chronic behavior (i.e. any depletion in F_1 and F_2 results in a near linear reduction in cGMP).

In the second approach, we have chosen to model the system based on a mechanism [34], in which the cGMP response to GTN is mediated by two cellular factors, F_1 and F_2 , which react with GTN to form an intermediate, N, (probably nitric oxide or S-nitrosothiol), which in turn activates guanylate cyclase, GC, which catalyzes the conversion of cellular GTP to cGMP. cGMP is then removed by a phosphodiesterase. This mechanism is illustrated in Figure 4.1. As described previously [34], tolerance development is associated with the consumption of F_1 and F_2 . Recovery from tolerance must therefore be due to replenishment processes for these factors. Since recovery is incomplete, we assume that only F_1 is replenished, and we choose a simple model in which a constant rate of synthesis of F_1 is postulated. The steady level of F_1 that is present in the absence of GTN stimulation is assumed to result from the balance of this zero order synthesis with a first order constitutive degradation process.

The model based on this mechanism is an extension of the model used previously to describe the transient, or short term response of the cells, and involves four ordinary differential equations:

$$\frac{df_1}{dt} = a \cdot r - (r + k_1[GTN])f_1 \quad (4.3)$$

$$\frac{df_2}{dt} = -k_2[GTN]f_2 \quad (4.4)$$

$$\frac{dn}{dt} = (k_1f_1 + k_2f_2)[GTN] - k_3n \quad (4.5)$$

$$\frac{d[cGMP]}{dt} = \frac{\alpha_2 n}{\alpha_1 + n} - k_4[cGMP] \quad (4.6)$$

where f_1 , f_2 and n are nondimensionalized concentrations of F_1 , F_2 , and N , respectively. Model parameters include k_3 and k_4 , which are first-order rate constants representing degradation of N and $cGMP$, respectively, and k_1 and k_2 which are, respectively, apparent second-order rate constants accounting for depletion of F_1 and F_2 in the presence of GTN . The term α_1 is the apparent binding constant of N to GC , while α_2 represents the maximal rate of conversion of GTP to $cGMP$ by GC^* given the total amount of GC and the availability of GTP in the cell, i.e. $\alpha_2 = \text{constant} \times [GTP] \times [GC]_{total}$. We assume that the GTP and GC pools in the cells are not significantly depleted during the experiment.

In Figure 4.1 the constitutive production of F_1 (or f_1) is represented by the zero-order rate constant, R_0 , and the constitutive degradation of F_1 is represented by the first order rate constant, r . For naïve cells that have had no exposure to GTN , these processes are balanced, and it may be seen that $f_1 = R_0/r$. In Eq. (4.3) we denote this

ratio by a , which is equivalent to the initial condition parameter $f_1(0)$ in [43], and should also be equal to the fractional degree of recovery that is achieved, assuming the model is correct.

Values of all parameters except r and a are fixed by results from our previous paper, in which the transient response of the cells to short term stimuli was characterized and modeled. To obtain estimates of r and a , we performed nonlinear least-squares (NLS) fitting, in which the GTN exposure, recovery (when appropriate), and probe phases were all included in the integrations of Eqs. (4.3)-(4.6). During the exposure and recovery phases, only Eqs. (4.3) and (4.4) were relevant. During the washout period before the probe phase, both n and [cGMP] were expected to drop to near-vanishing levels [43], so these variables were both set to 0 at the beginning of the probe phase.

In the best case, a should have the same value in the transient and chronic fits. However, we were not able to achieve this internal consistency in our fits. In order to obtain the fits shown in Figures 4.4A-B and 4.4A-B, we had to fit the data in stages, where the chronic and transient data were fit separately.

In Figure 4.4A-B, the transient and chronic data were fit independent of each other. First, a seven-parameter fit to the transient data was performed. The optimal parameters from this fit, except for a , were used as fixed values in the chronic model. In the second stage, the chronic data were fit to two parameters, a and r , results shown in Table 4.5 and as predicted curves (solid/dashed lines) in Figure 4.4A-B.

In Figure 4.5A-B, two additional fits were based upon the chronic parameter estimates from Figure 4.4A-B. In an attempt to preserve self-consistence integrity, the value for a , 0.598, obtained in fit 4.4A-B was carried over into another fit of the transient model. This fit fixed $a = 0.598$, then estimated the other six transient parameters. This newly obtained transient parameters were then used as fixed values in a second chronic fit, 4.5A-B. In fit 4.5A-B, a and r were fit with the transient parameters fixed. The 4.5A-B fit is shown in Table 4.6 and Figure 4.5A-B. If our modeling was self-consistence, we would have obtained a value near 0.6 for a . However, as Table 4.6 shows, a was estimated to be 0.373.

The data show a half-life of recovery of approximately 4 to 6 hours. When the data is fit to the model shown in Figure 4.4 (Table 4.4), the model overshoots tolerance development, but estimates a recovery half-life of approximately 9.6 hours. However, if we are willing allow more mis-fitting in tolerance recovery, where data is limited, then we can get reasonable tolerance development trajectories (see Figure 4.5). This is at the cost of poorly fitting tolerance recovery trajectories, which estimate the recovery half-life at approximately 0.68 hours.

A similar balance between the development and chronic fits was also seen with the phenomenological model. The better fitting recovery parameter estimates a half-life of 10.2 hours, whereas the poorer fitting model estimates 0.51 hours. Again the trade-off is clear; a better recovery fit leads to a poorer development fit.

4.6 Discussion

The intent of this work was to characterize and model the chronic kinetics of GTN-induced cGMP accumulation. Other workers have studied the transient behavior in PK1 cells [5], rat-lung fibroblasts (RLF) [5, 29], rat aortic smooth muscle [17], rat aortic strips [25], guinea-pig ileum smooth muscle, and *in vivo* rat aortic [12]. Among these, some have reported GTN chronic tolerance as a binary phenomenon (i.e. naïve or tolerance state) in cell culture [5, 14, 30, 31], *in vivo* rat [6] and rat aortic strips [21, 23], rabbit aortic strips [18], bovine coronary arteries [20], and human [9, 37]. Others have reported and/or modeled GTN tolerance as a more continuous phenomenon – providing information on the rate of tolerance formation and/or recovery in smooth muscle cells [36], rats [3, 33], and rat [32] and bovine aortic strips [13]. In this work, we linked our chronic tolerance model to our previously reported transient model [34] to simultaneously model both transient and chronic behavior.

Our results show that the extent and rate of tolerance development depends on GTN concentration. GTN exposures beyond 120 minutes (data not shown) do not significantly increase the extent of tolerance. Even our highest GTN concentration, 10^{-6} M, did not cause 100% tolerance (i.e. no cGMP produced in response to the GTN rechallenge); a finding consistent with Bennett et al. [5], who found PK1 cells still responsive to 10^{-5} M GTN rechallenge after a three hour incubation with 10^{-4} M GTN. Their cells showed approximately 89% tolerance; at 10^{-6} M, our cells showed approximately 87% tolerance when compared to the control. Hinz and Schröder [14] also found, in PK1 cells, less than 100% tolerance for a 5-hour, 10^{-6} M GTN

incubation. Schröder et al. [29] found 89% tolerance with 10^{-4} M GTN and 3 hour incubation in RLF cells. We find that tolerance develops rapidly, as do others. Henry et al. [13] found that GTN concentrations of 10^{-6} , 10^{-5} , and 10^{-4} M produced tolerance at 10 minutes and further tolerance at 60 minutes. Their analysis also supported previous findings that the extent of tolerance depends on GTN concentration, duration of GTN exposure, and the subsequent duration of the GTN-free period. In addition to confirming their results, we find that the rate of tolerance development is also concentration dependent and tolerance occurs at concentrations lower than previously reported. While other workers have used higher concentrations ($>10^{-6}$ M, typically in the 10^{-4} to 10^{-5} M range) to induce tolerance, we find tolerance at concentrations (5×10^{-7} to 10^{-8} M) closer to the physiological range (5.3×10^{-9} to 4.8×10^{-8} M).

Besides the “binary” GTN tolerance literature, there is little published work on the recovery kinetics of GTN – and what works there are do not agree. Zhang et al. [36] reported a full recovery 72 hours after ending a 1-hour, 10^{-4} M GTN pre-exposure in smooth muscle cells. Our rechallenge probe (10^{-5} M GTN) was nearly identical to theirs, except they used 10^{-4} M GTN. Henry et al. [13] saw only a partial recovery from 10 minute-, 10^{-6} , 10^{-7} , and 10^{-8} M pre-exposures when measured 30, 60, and 120 minutes after the pre-exposure. Bennett et al. [5] reported incomplete recovery (22% of naïve control) when PK1 cells were measured 18 hours after a 3-hour, 10^{-4} M GTN pre-exposure. Our data, while limited due to experimental complexity, do not appear to support full recovery from tolerance even at 30 hours. Instead, recovery appears to

plateau at approximately 60% of naïve control. Our 40 hour time points (not shown) are not statistically different from the 20 or 30 hour time points. Schröder et al. [29] showed that *de novo* synthesis of sGC, using cycloheximide – an inhibitor of sGC production, maybe necessary for tolerance recovery in RLF cells.

The lack of sufficient recovery data from the beginning of recovery to 12 hours lead to imprecise estimates of the rate of tolerance recovery. More importantly, why is recovery incomplete? While our data cannot answer this question, we did create a model to account for it. According to our transient model, f_1 and f_2 are rapidly inactivated or consumed in the conversion of GTN to NO and even further reduced during tolerance development. However, our model only allows for f_1 to recover. The 40% missing from complete recovery is attributed to the irreversible loss of f_2 . Bennett and coworkers [5, 31] reported findings that suggest regioselectivity at low GTN concentrations, but not at higher GTN concentrations. This finding led them to hypothesize that GTN is metabolized via at least two different routes: a high affinity-low capacity and a low affinity-high capacity pathway. These two pathways could be represented by our f_1 and f_2 variables. Both share the necessary characteristics [34] regarding affinity and capacity mentioned by Bennett et al. [5].

In this work we have attempted to couple the transient and the chronic, tolerance behavior of GTN-induced cGMP accumulation through a single, mechanistic-based mathematical model. Although the chronic and transient data are not fit well with a single rate of tolerance recovery, the joint model does manage to capture the magnitude of recovery. Further work should encompass a simultaneous fit

of the transient and chronic data to better discern a value of a that better balances the transient and chronic kinetics. The phenomenological model suggests a mechanism that has concentration-dependent development kinetics and concentration-independent recovery kinetics. More recovery data within the first 10 to 12 hours of recovery are needed. This work does show that reasonably simple models characterizing complex biological responses to multiple drug concentrations and over time scales ranging from seconds to days can be developed from simple mechanisms.

4.7 Figure and Table Captions

Figure 4.1. Diagram showing tolerance model. Two additional parameters have been added R_0 and r , zero-order endogenous production and degradation for F_1 , respectively. A key characteristic is the absence of a production term for F_2 ; therefore, F_2 is depleted upon GTN exposure, but is not regenerated.

Figures 4.2A-B and 4.3A-B. Phenomenological Fits. The dashed lines indicate no recovery data available, but tolerance development data ($\nabla = 5 \times 10^{-8}$ M, $\diamond = 10^{-6}$ M) was included in fit. Solid symbols indicate development and recovery data also used in the curve fitting ($\bullet = 5 \times 10^{-7}$ M, $\blacktriangle = 2.5 \times 10^{-7}$ M, $\blacksquare = 10^{-7}$ M). Tolerance recovery time is the length of the GTN-free period prior to GTN rechallenge. Both figures represent five parameter fits. In Figure 4.2, three of the five parameters were determined using the recovery data and the two remaining parameters were determined using the development data. In Figure 4.3, all five parameters were determined using the development data. The recovery plots are based upon the parameters determined from the development fit. The open triangle represents a data point considered an outlier that was not used in fitting procedures.

Figures 4.4A-B and 4.5A-B. Mechanistic Fits. Rate and extent of tolerance development and recovery. The dashed lines indicate no recovery data available, but tolerance development data ($\nabla = 5 \times 10^{-8}$ M, $\diamond = 10^{-6}$ M) was included in fit. Solid symbols indicate development and recovery data also used in the curve fitting ($\bullet = 5 \times 10^{-7}$ M, $\blacktriangle = 2.5 \times 10^{-7}$ M, $\blacksquare = 10^{-7}$ M). Tolerance recovery time is the length of the GTN-free period prior to GTN rechallenge. Figure 4.4A-B shows the results of

placing greater weight on the transient value of a (0.913). Figure 4.5A-B shows the results of shifting greater weight on the chronic value of a (0.598). The AIC supports the model used in Figure 4.5.A-B (see Table 4.4). All data points have s.d. < 15% (error bars not shown for plot clarity) and have an $n = 3$. The open triangle represents a data point considered an outlier that was not used in fitting procedures.

Table 4.4. Comparison of Modeling Fits. The fits in Figures 4.4 and 4.5 were accomplished by independently fitting the transient and chronic data. The three AIC columns correspond to the transient fit, the chronic fit, and a composite (transient AIC + chronic AIC). The Akaike Information Criterion (AIC) identifies Panel A as the better model for the transient data and Panel B for the chronic and combined model.

Table 4.5. The optimal parameter estimates for r and a are shown. In this fit, the seven parameter transient model was used to model the rechallenge probe. As Table 4.4 shows, this fit favors a better transient fit.

Table 4.6. This table shows the optimal parameter estimates from the second fit described in the text. In the transient model was refit with $fI(0)$ fixed at 0.598 (from 4.4A-B).

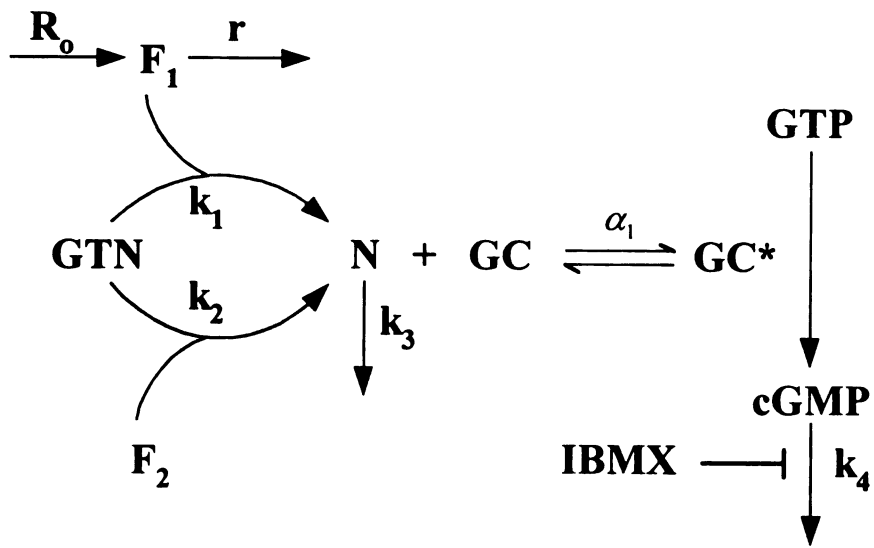
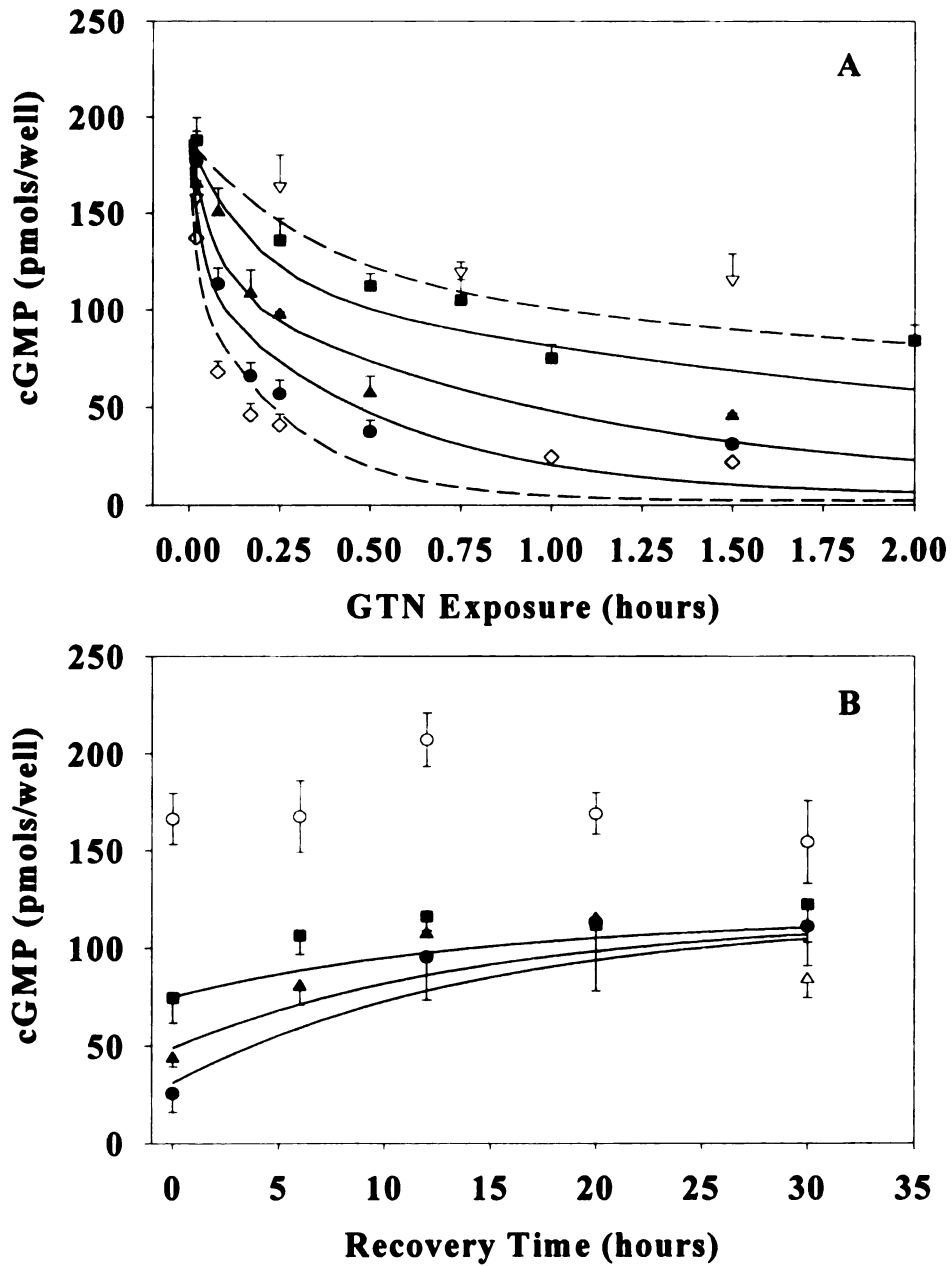


Figure 4.1. Diagram showing tolerance model



Figures 4.2A-B. Phenomenological Fit – 2 parameter development fit and 3 parameter recovery fit.

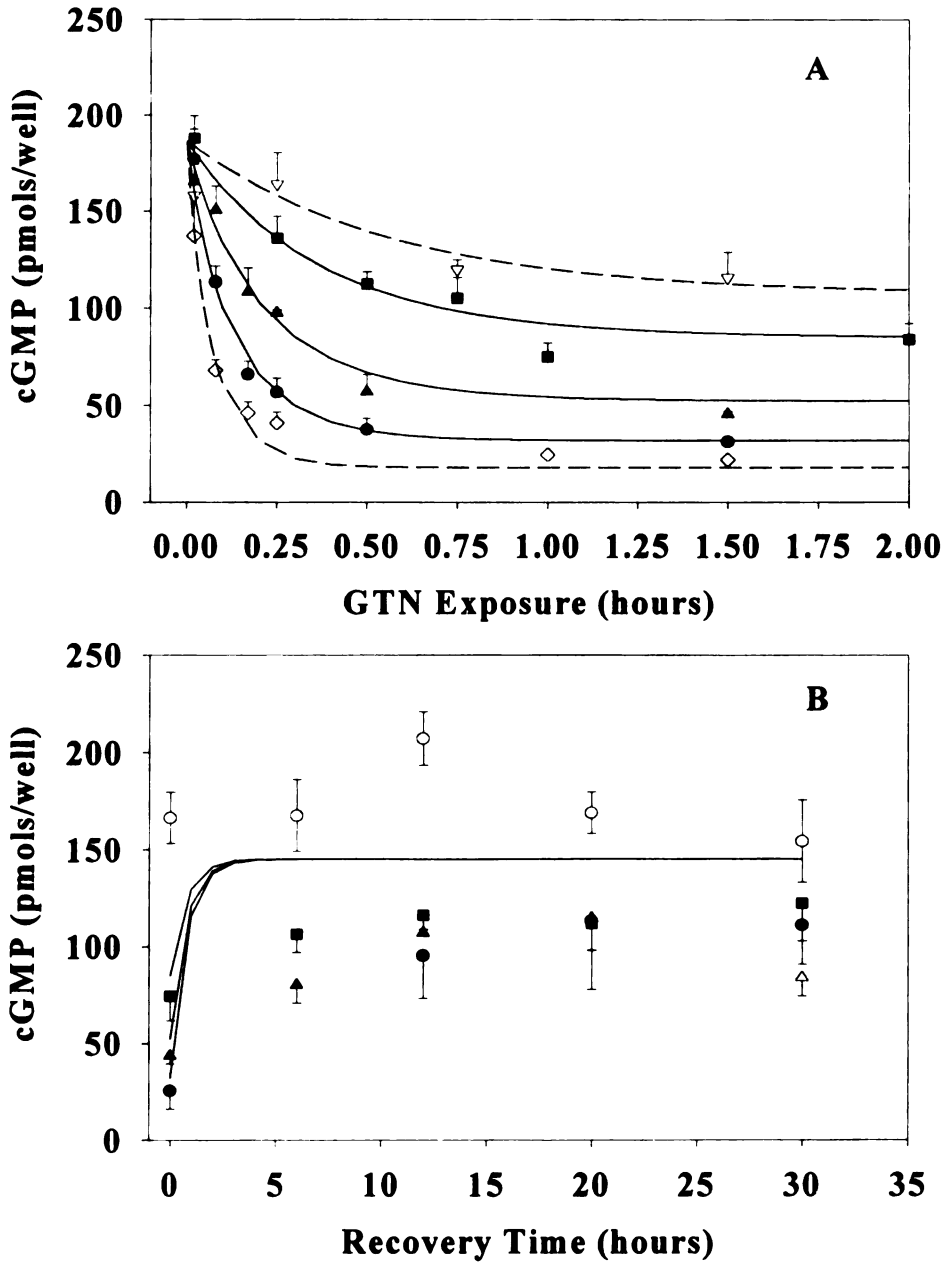


Figure 4.3A-B. Phenomenological Fit – 5 parameter development fit and recovery trajectories using development parameters.

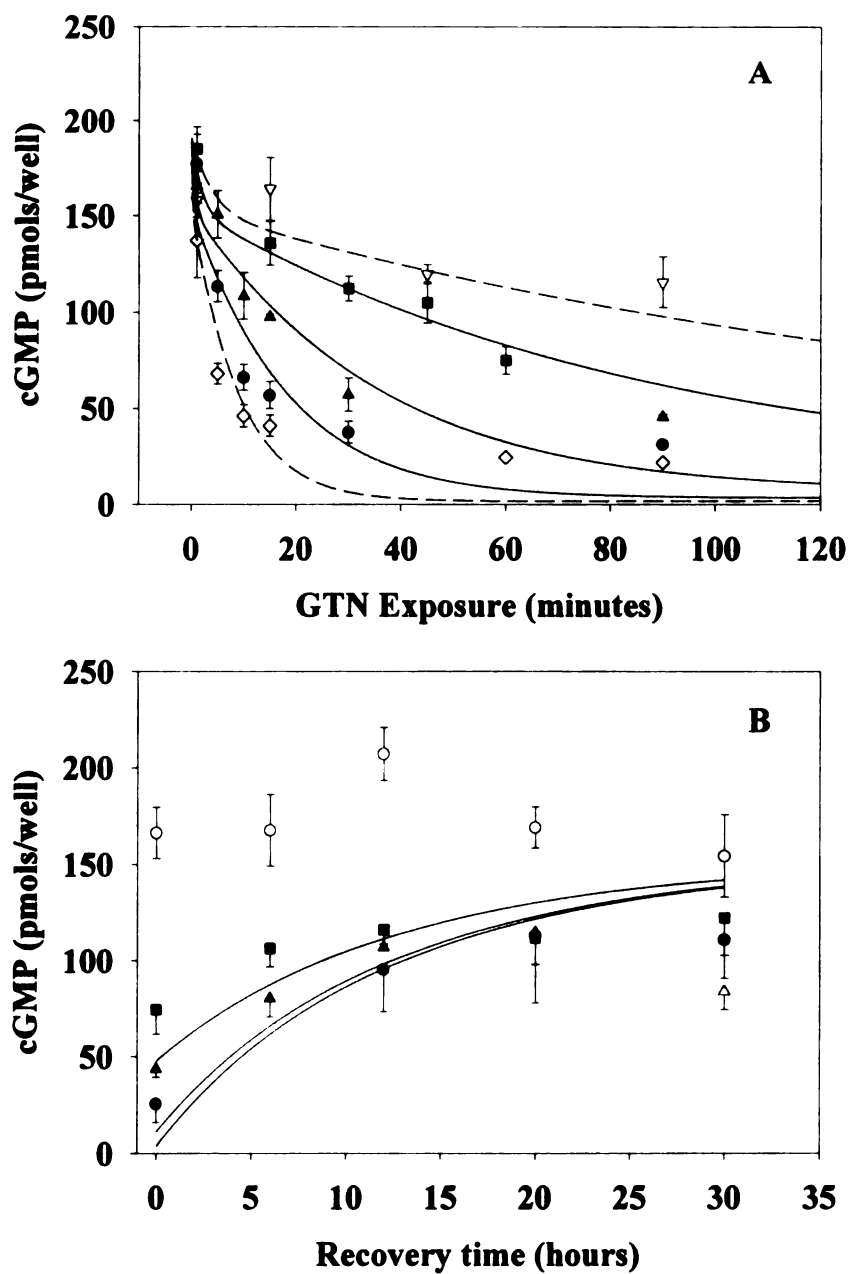


Figure 4.4A-B. Mechanistic Fit – 2 parameter chronic fit and 7 parameter transient fit.

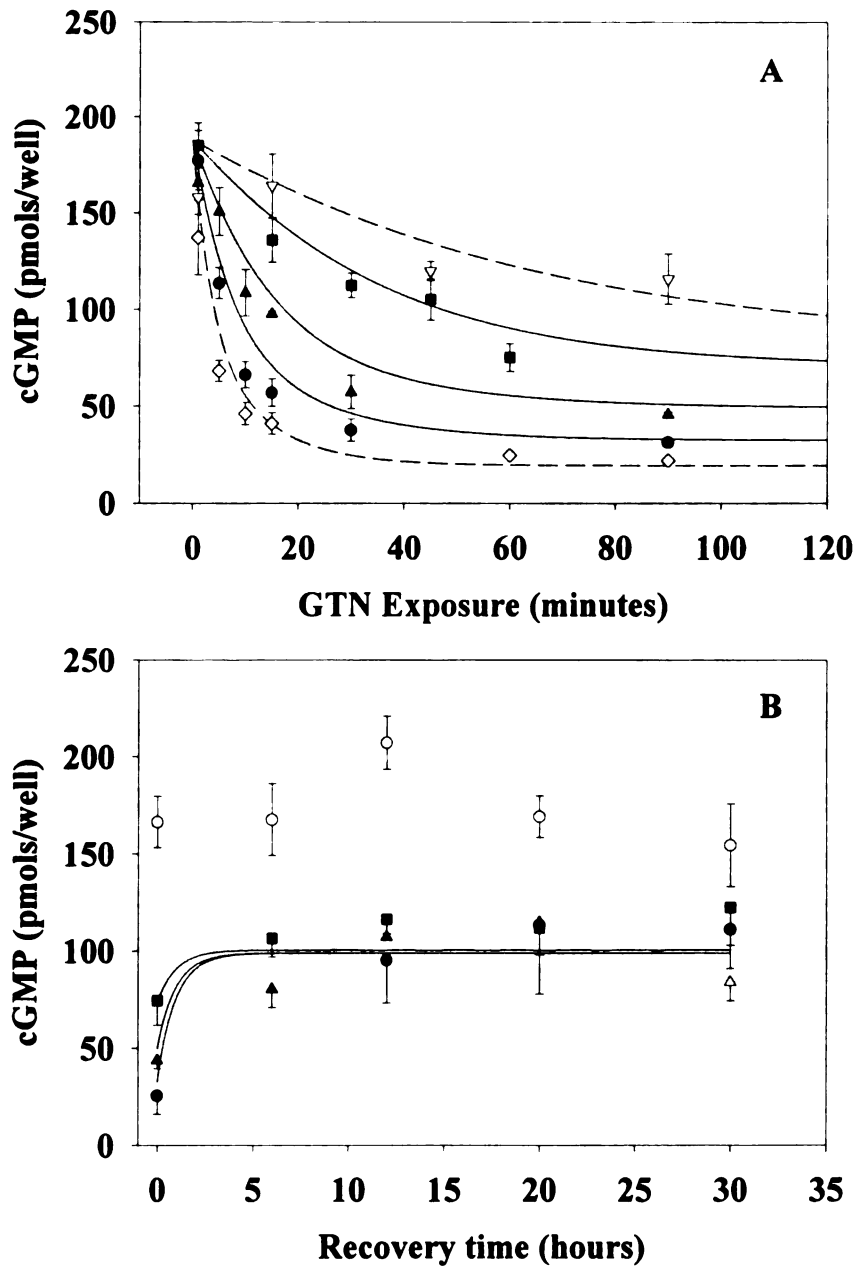


Figure 4.5A-B. Mechanistic Fit – 2 parameter chronic fit and 6 parameter transient fit.

Parameter	Estimate	Lower CI	Upper CI	Lower CI%	Upper CI%
C_0	72.59084	46.28085	98.90084	-36.24%	36.24%
k_2	5.833161	-0.80618	12.47251	-113.82%	113.82%

Table 4.1. Parameter Estimates for 2-parameter development fit shown in Figure 4.2A

Parameter	Estimate	Lower CI	Upper CI	Lower CI%	Upper CI%
R_0	7.826727	1.925327	13.72813	-75.40%	75.40%
r	0.067666	0.01139	0.123942	-83.17%	83.17%
k_1	0.03677	0.007404	0.066137	-79.86%	79.86%

Table 4.2. Parameter Estimates for 3 parameter recovery fit shown in Figure 4.2.B

Parameter	Estimate	Lower CI	Upper CI	Lower CI%	Upper CI%
k_1	0.962237	0.714987	1.209486	-25.70%	25.70%
k_2	3.546717	0.157104	6.93633	-95.57%	95.57%
R_0	196.4961	112.9027	280.0896	-42.54%	42.54%
r	1.353881	0.583873	2.12389	-56.87%	56.87%
C_0	41.37752	9.26507	73.48997	-77.61%	77.61%

Table 4.3. Parameter Estimates for 5 parameter development fit shown in Figures 4.3A-B

Panel ID Figure	Num. Of Params. Trans/Chr	Transient -2 log likelihood	Chronic -2 log likelihoo d	AIC transient	AIC chronic	AIC combined
4.4A-B	7/2	10.70	9.42	1309	371	1680
4.5A-B	6/2	10.81	9.01	1320	356	1676

Table 4.4. AIC values for Mechanistic Fits

Parameter	Optimal value	Lower Bound	Upper Bound	Lower Bound %	Upper Bound %
<i>r</i>	2.03E-05	1.76E-05	2.35E-05	-13.3	15.8
<i>a</i>	0.598	0.579	0.617	-3.2	3.2

Table 4.5 – Optimal parameters for Figure 4.4A-B

Parameter	Optimal value	Lower Bound	Upper Bound	Lower Bound %	Upper Bound %
<i>r</i>	0.000285	0.0002	0.000385	-29.8	35.1
<i>a</i>	0.373	0.355	0.39	-4.8	4.6

Table 4.6. Optimal parameters for Figure 4.5A-B

4.8 References

- [1] J. Ahlner, R. G. G. Andersson, K. L. Axelsson, U. Dahlstrom, and E. L. Rydell. Development of Tolerace to Glyceryl Trinitrate in an Isolated Human Peripheral Vein and Its Relation to Cyclic GMP Metabolism. *ACTA Pharmacology and Toxicology*, 1986, 59:123.
- [2] K. L. Axelsson and J. Ahlner. Nitrate Tolerance from a Biochemical Point of View. *Drugs*, 1987, 33:63.
- [3] J. A. Bauer, J. P. Balthasar, and H.-L. Fung. Application of Pharmacodynamic Modeling for Designing Time-Variant Dosing Regimens to Overcome Nitroglycerin Tolerance in Experimental Heart Failure. *Pharmaceutical Research*, 1997, 14(9): 1140-1145.
- [4] T. C. Bellamy, J. Wood, D. A. Goodwin, and J. Garthwaite. Rapid Desensitization of the Nitric Oxide Receptor, Soluble Guanylate Cyclase, Underlies Diversity of Cellular cGMP Responses. *Proceedings of the National Academy of Sciences*, 2000, 97(6): 2928-2933.
- [5] B. M. Bennett, D. C. Leitman, H. Schröder, J. H. Kawamoto, K. Nakatsu, and F. Murad. Relationship Between Biotransformation of Glyceryl Trinitrate and Cyclic GMP Accumulation in Various Cultured Cell Lines. *Journal of Pharmacology and Experimental Therapeutics*, 1989, 250(1): 316-323.
- [6] S. Boesgaard, J. S. Petersen, J. Aldershvile, H. E. Poulsen, and H. Flachs. Nitrate Tolerance: Effect of Thiol Supplementation during Prolonged

- Nitroglycerin Infusion in an in Vivo Rat Model. *Journal of Pharmacology and Experimental Therapeutics*, 1991, 258(3): 851-856.
- [7] M. Bohyn, G. Berkenboom, and J. Fontaine. Effect of Nitrate Tolerance and Dipyridamole on the Response of SIN1 in the Human Isolated Saphenous Vein. *Cardiovascular Drugs and Therapy*, 1991, 5:457.
- [8] L. Cloarec-Blanchard, C. Funck-Brentano, A. Carayon, and P. Jaillon. Rapid Development of Nitrate Tolerance in Healthy Volunteers: Assessment Using Spectral Analysis of Short-term Blood Pressure and Heart Rate Variability. *Journal of Cardiovascular Pharmacology*, 1994, 24(1994): 266-273.
- [9] U. Elkayam. Tolerance to Organic Nitrates: Evidence, Mechanisms, Clinical Relevance, and Strategies for Prevention. *Annals of Internal Medicine*, 1991, 114(1991): 667-677.
- [10] M. Feelisch. Biotransformation to Nitric Oxide of Organic Nitrates in Comparison to Other Nitrovasodilators. *European Heart Journal*, 1993, 14(Supplement I): 123-132.
- [11] M. Feelisch and M. Kelm. Biotransformation of Organic Nitrates to Nitric Oxide by Vascular Smooth Muscle and Endothelial Cells. *Biochemical and Biophysical Research Communications*, 1991, 180(1): 286-293.
- [12] A. I. Haj-Yehia and L. Z. Benet. Dissociation of Tissue Thiols Content from Nitroglycerin-Induced Cyclic-3',5'-Guanosine Monophosphate and the State of Tolerance: *In Vivo* Experiments in Rats. *Journal of Pharmacology and Experimental Therapeutics*, 1995, 273(1): 94-100.

- [13] P. J. Henry, J. D. Horowitz, and W. J. Louis. Determinants of In Vitro Nitroglycerin Tolerance Induction and Reversal: Influence of Dose Regimen, Nitrate-free Period, and Sulfhydryl Supplementation. *Journal of Cardiovascular Pharmacology*, 1989, 14(1989): 31-37.
- [14] B. Hinz and H. Schröder. Vitamin C Attenuates Nitrate Tolerance Independently of Its Antioxidant Effect. *Federation of European Biochemical Societies Letters*, 1998, 428(1998): 97-99.
- [15] L. J. Ignarro. Biological Actions and Properties of Endothelium-Derived Nitric Oxide Formed and Released From Artery and Vein. *Circulation Research*, 1989, 65(1): 1-21.
- [16] L. J. Ignarro. Endothelium-Derived Nitric Oxide: Pharmacology and Relationship to the Actions of Organic Nitrate Esters. *Pharmaceutical Research*, 1989, 6(8): 651-659.
- [17] R. A. Keith, A. M. Burkman, T. D. Sokoloski, and R. H. Fertel. Vascular Tolerance to Nitroglycerin and Cyclic GMP Generation in Rat Aortic Smooth Muscle. *Journal of Pharmacology and Experimental Therapeutics*, 1982, 221(3): 525-531.
- [18] S. R. Kenkare and L. Z. Benet. Tolerance to Nitroglycerin in Rabbit Aorta. *Biochemical Pharmacology*, 1996, 51(10): 1357-1363.
- [19] G. Kojda, M. Wilfried, and E. Noack. Influence of Endothelium and Nitrovasodilators on Free Thiols and Disulfides in Porcine Coronary Smooth Muscle. *European Journal of Pharmacology*, 1993, 250:385-394.

- [20] W. Kukovetz and S. Holzmann, "Tolerance to Nitric Oxide in Bovine Coronary Arteries," in *Endothelium-Derived Relaxing Factors*, vol. 1990, G. Rubanyi and P. Vanhoutte, Eds. Switzerland: S. Karger, Basel, 1990, pp. 213-220.
- [21] E. Malta. Studies of the Biphasic Relaxant Curve of Glyceryltrinitrate in Rat Aorta: Role of GTN Metabolites. *Clinical and Experimental Pharmacology and Physiology*, 1989, 16(1989): 829-835.
- [22] W. R. Mathews and S. W. Kerr. Biological Activity of S-nitrosothiols: The Role of Nitric Oxide. *Journal of Pharmacology and Experimental Therapeutics*, 1993, 267(3): 1529-1537.
- [23] M. J. Mihm, C. M. Coyle, L. Jing, and J. A. Bauer. Vascular Peroxynitrite Formation during Organic Nitrate Tolerance. *Journal of Pharmacology and Experimental Therapeutics*, 1999, 291(1): 194-198.
- [24] P. Needleman and E. M. J. Johnson. Mechanism of Tolerance Development to Organic Nitrates. *Journal of Pharmacology and Experimental Therapeutics*, 1973, 184:324-331.
- [25] A. I. Patel and J. Diamond. Activation of Guanosine 3',5'-Cyclic Monophosphate (cGMP)-Dependent Protein Kinase in Rabbit Aorta by Nitroglycerin and Sodium Nitroprusside. *Journal of Pharmacology and Experimental Therapeutics*, 1997, 283(2): 885.

- [26] C. Romanin and W. R. Kukovetz. Tolerance to Nitroglycerin is Caused by Reduced Guanylate Cyclase Inactivation. *Journal of Molecular and Cellular Cardiology*, 1989, 21:1.
- [27] D. Salvemini, V. Mollace, A. Pistelli, E. Anggard, and J. Vane. Metabolism of Glyceryl Trinitrate to Nitric Oxide by Endothelial Cells and Smooth Muscle Cells and Its Induction by *Escherichia coli* Lipopolysaccharide. *Proceedings of the National Academy of Sciences*, 1992, 89(1992): 982-986.
- [28] H. Schröder, "Molecular Mode of Action of Organic Nitrates and Their Bioactivation via Cytochrome P-450," in *Frontiers in Biotransformation: Medicinal Implications in Cytochrome-P450 Catalyzed Biotransformations*, vol. 8, K. Ruckpaul and H. Rein, Eds. Berlin: Akademie-Verlag, 1993, pp. 234-245.
- [29] H. Schröder, D. C. Leitman, B. M. Bennett, S. A. Waldman, and F. Murad. Glyceryl Trinitrate-induced Desensitization of Guanylate Cyclase in Cultured Rat Lung Fibroblasts. *Journal of Pharmacology and Experimental Therapeutics*, 1988, 245(2): 413-418.
- [30] H. Schröder, D. C. Leitman, L. D. Hayward, B. M. Bennett, and F. Murad. Cultured rat lung fibroblasts as a model for organic nitrate-induced cyclic GMP accumulation and activation of guanylate cyclase. *Journal of Applied Cardiology*, 1987, 2(4): 301-311.
- [31] H. Schröder and K. Schrör. Inhibitors of Cytochrome P-450 Reduce Cyclic GMP Stimulation by Glyceryl Trinitrate in LLC-PK₁ Kidney Epithelial Cells.

- Naunyn-Schmiedeberg's Archives of Pharmacology*, 1990, 342(1990): 616-618.
- [32] T.-B. Tzeng and H.-L. Fung. Pharmacodynamic Modeling of the *In Vitro* Vasodilating Effects of Organic Mononitrates. *Journal of Pharmacokinetics and Biopharmaceutics*, 1992, 20(3): 227-251.
- [33] T.-B. Tzeng and H.-L. Fung. Pharmacokinetic/Pharmacodynamic Relationship of the Duration of Vasodilating Action of Organic Mononitrates in Rats. *Journal of Pharmacology and Experimental Therapeutics*, 1992, 261(2): 692-700.
- [34] J. A. Uchizono and R. A. Siegel. Kinetics of Nitroglycerin-induced cGMP Accumulation in LLC-PK1 Epithelial Cells at Multiple Nitroglycerin Concentrations. Part 1: Transient, Acute Kinetics. *in prep*, 2001,
- [35] S. A. Waldman, R. M. Rapoport, R. Ginsberg, and F. Murad. Desensitization to Nitroglycerin in Vascular Smooth Muscle in Rat and Human. *Biochemical Pharmacology*, 1986, 35:3525.
- [36] L.-M. Zhang, M. R. Castresana, and W. H. Newman. Tolerance to Nitroglycerin in Vascular Smooth Muscle Cells: Recovery and Cross-tolerance to Sodium Nitroprusside. *Anesthesia Analgesic*, 1994, 78(1994): 1053-1059.
- [37] D. Zimrin, N. Reichel, B. K. T., G. Aurigemma, P. Douglas, B. Berko, and H.-L. Fung. Antianginal Effects of Intravenous Nitroglycerin over 24 Hours. *Circulation*, 1988, 77(6): 1376-1384.

5 Conclusions

In the work presented, we characterized and modeled the GTN-induced cGMP accumulation in PK1 cells from their transient response, occurring in seconds, to their development of tolerance, occurring in minutes, to their recovery from tolerance, occurring in hours. Initially, our focus was primarily on the development and recovery tolerance kinetics. However, a solid understanding of the transient kinetics was foundational to understanding the long-term chronic kinetics.

In Chapter 3, we carefully detailed the transient time-course of cGMP accumulation in response to multiple GTN concentrations for varying exposure durations. Our goals were two-fold: to gain more insight into the non-monotonic behavior of the concentration versus effect curve and to fully characterize the transient kinetic behavior of the rechallenge probe needed to determine the cells' state of tolerance in the chronic experiments. The non-monotonic concentration versus effect behavior occurs primarily as a combination of sampling artifact and incomplete PDE blockade by IBMX. In classic concentration versus effect experiments, one usually chooses an exposure time sufficient to observe the steady-state effect, which in a non-tolerance drug does not disappear with constant stimulation. In our system, tolerance develops from the outset of drug exposure. Thus, the choice of sampling time (or length of incubation) will always introduce a timing artifact. Secondly, since IBMX only partially blocks the PDE, each transient curve will naturally have a rising and declining portion, as seen in Chapter 3, Figure 3.2F. If PDE blockade were complete, the time versus effect curves would be monotonically increasing, thus leading to a

monotonic concentration versus effect curve. The importance of understanding the transient kinetics, especially when the effect is not stationary, cannot be emphasized enough.

A reasonably complete understanding of our GTN rechallenge probe was necessary for interpretation of our chronic tolerance data. After reviewing data from repeated experiments, we selected a concentration and exposure duration giving us a repeatable and high signal/noise ratio response: GTN concentration of 10^{-5} M and a duration of 180 seconds. We modeled the probe's transient kinetics with a system involving the consumption of two factors, F_1 and F_2 , and the formation of an intermediate, n . Although the transient kinetics were reasonably modeled with a single F , we added F_2 to account for one transient and one chronic phenomenon. The addition of F_2 significantly improved (AIC) the fit to the low concentration transient data ($< 10^{-6}$ M); it also provided a mechanism for the incomplete tolerance recovery obtained in the chronic experiments. The parameter, n or (NO or nitrosothiol), was necessary for a reasonable fit to the data. n acts like a high-frequency filter by capping the infinite derivative change that occurs when GTN is stepped up or down; it also causes a slight delay between the concentration change and the new response – as seen in the data.

In Chapter 4, we addressed the issue of chronic tolerance development and recovery. Two important questions were asked for both phases, tolerance development and tolerance recovery, “To what extent does the system exhibit tolerance or return to its naïve state?” and “How quickly does tolerance develop or

dissipate?” Using the probe from Chapter 3, we created a map showing the state of tolerance for a given concentration at given times (see Chapter 4, Figure 4.2). The tolerance mapping shows that as GTN concentration increases, so does the extent and the rate of tolerance development. However, even the highest concentration fails to produce 100% loss of effect. The extent of tolerance, shown as the plateauing region of each curve, is reached more quickly by the higher GTN concentrations, indicating a greater rate of tolerance development. The plateau region does indicate that whatever the tolerance mechanism is, the system is actively regenerating itself, even in the continued presence of GTN, and has reached its steady-state tolerance level.

Our recovery data is far less conclusive. Although a recovery rate constant is identifiable, its utility is limited by sparse data in the 0 to 12 hour region. However, two key aspects can be seen from our data: recovery is incomplete and extent of recovery is independent of the GTN concentration used to induce tolerance; both are easily seen in Chapter 4, Figure 4.2A-B. One possible reason for the incomplete recovery is the irreversible loss of an enzyme or co-factor (or it is replaced very slowly). The loss of cells due to age or GTN oxidative stress (including $\text{NO}\bullet$) is not supported by these data. Our naïve control cells (not shown for plotting clarity) are the same age as tested cells, yet they still fully respond to the probe rechallenge. Cell loss due to GTN or $\text{NO}\bullet$ would be plausible under two conditions: a) the lowest GTN concentration (i.e. 10^{-7} M) fully saturates this mechanism of cell loss, and b) full saturation of this mechanism can only cause 40% cell loss. Without these two conditions, one would expect different recovery plateaus for each concentration.

Rather than developing such a model, we chose to use the irreplaceable loss of f_2 as our mechanism for dealing with incomplete recovery. Since f_2 is a low capacity-high affinity protein, enzyme, or co-factor, its concentration approaches zero even at very low concentrations (10^{-8} M). In either explanation for the lack of full recovery, both are based on unsubstantiated assumptions: either assume a saturable cell death mechanism which only kills 40% of the cells or assume some factor, f_2 , exists, which accounts for 40% of the cultures' naïve response, and is irreplaceably lost (for the time-span of our experiments).

The joint model for transient plus chronic kinetics shows that simple models can possess robust descriptive and predictive capabilities over data with considerable breadth. Our input data, GTN concentration, ranged from 10^{-4} to 10^{-8} M with response measurements made in the seconds, minutes, hours, and days time-scales. Given this breadth of input and output data, we are reasonably satisfied with this model.

We suspect that future tolerance models will have to include well-defined transient kinetic models or at the minimum data supporting the exclusion of transient kinetics. Cross-tolerance studies stand to gain the most from detailed transient kinetic studies of each substance being tested. For example, using Drug A and B, typical cross-tolerance protocols would give A for t_1 minutes, washout for t_2 minutes, and then give B for t_3 minutes (usually $t_1=t_3$). Then the reverse is applied: give B for t_1 , washout for t_2 , then give A for t_3 (again $t_1=t_3$). When investigating cross-tolerance we ask ourselves, is it more important to have t_1 the same, but use different concentrations of A and B or have the same concentrations of A and B and have

different t_1 's? When inducing tolerance with A and rechallenging with B, what fraction of the rechallenge response is lost due to B's transient kinetics versus the tolerance developed from A? For a completely rigorous cross-tolerance study, the transient kinetics of A and B, for each cross-tolerance concentration being used, should be performed on the same day as the cross-tolerance experiment as a control.

Drug tolerance is difficult to fully grasp and even more difficult to measure. This thesis puts forward one attempt to develop some of the tools needed for studying and better understanding the phenomenon called drug tolerance. Although GTN tolerance has been studied for years, we add our contribution to help solve the "The 100 Year Old Mystery" [1]. Hopefully, we will one day have enough understanding of tolerance to provide patients with dosing strategies for drugs rendered useless by tolerance.

- [1] M. Packer. What Causes Tolerance to Nitroglycerin?: The 100 Year Old Mystery Continues. *Journal of the American College of Cardiology*, 1990, 16(4): 932-935.

6 Future Work

Our plans for future GTN research build upon two areas presented in this work: the characterization and modeling of GTN tolerance kinetics. Future tolerance recovery studies will focus on the initial 10 hours of recovery. The lack of information in this region led to limited quantitative conclusions regarding the rate of recovery. Furthermore, improved resolution of early recovery time points should decrease model misspecification and/or guide the selection of a better fitting model. In a larger context, we plan to continue working on models that link a system's transient kinetics to its chronic behavior, especially in non-stationary systems.

7 Appendix A

Detailed Experimental Procedures and Materials

7.1 Lysis, Extraction, RIA Preparation, and Miscellaneous Procedure

7.1.1 Cell Lysis and Intracellular cGMP Extraction

The cell lysis and cGMP extraction procedure were taken from Freidl, et. al.[1]. We altered their procedure by performing only one ethanol extraction and we re-dissolved the residue with TRIS buffer rather than water. The TRIS buffer was used to match the control solution (Solution #1, Amersham TRK500 RIA Kit) of the ^3H -cGMP RIA Kit. This procedure has several advantages over other cell lysis techniques: 1) the ethanol instantly halts all cellular metabolism; 2) the ethanol disrupts the cell membrane allowing access to the intracellular compartment; 3) the intracellular contents are easily separated from the ethanol by simply letting the ethanol evaporate; and 4) the ethanol lysis and TRIS reconstitution of the intracellular reconstitution can be performed in the cell culture plate (i.e. the culture plates are not susceptible to ethanol degradation). The rapid freeze/thawing steps were included to insure that the cell membrane was fully disrupted.

The cell lysis and intracellular cGMP extraction procedure was as follows:

1. The incubating media was aspirated and 1.0 ml of ethanol was added to each well.

2. The ethanol was allowed to evaporate and 1.0 ml of TRIS buffer was added.
3. The plates were covered and then placed into a -80°C freezer, and the TRIS buffer was allowed to fully freeze. In a -80°C freezer the TRIS solution will freeze in approximately 20 to 30 minutes. Our samples were left in the freezer for at least 90 minutes to insure complete freezing.
4. The plates were removed from the freezer and allowed to thaw at room temperature. The plates covers were left on to prevent fungal contamination (this contamination occurred in early experiments).
5. The contents from each well were placed into separate vials (1.6 ml micro-centrifuge vials) for storage.
6. For short-term storage, the vials were placed in the standard -20°C freezer. For long-term storage, the vials were placed into a -80°C freezer.

7.1.2 RIA Sample Preparation and Dilutions

Since the ^3H -cGMP RIA kit could only reliably measure the amount of cGMP between 0.5 to 8 pmol, our intracellular cGMP samples had to be diluted. The optimal ratio for cell systems was 4:1 (TRIS:sample). The following procedure was used to dilute our samples:

7. If the samples were frozen, the samples were allowed to thaw and allowed to warm up to room temperature.
8. The vial to contain the diluted sample was filled to 800 μl of TRIS buffer.
9. 200 μl of the appropriate sample was added to its respective vial.

10. Each vial was capped and vigorously shaken to mix its contents.
11. A 100 μ l aliquot was used for the cGMP RIA (as per directions enclosed with the RIA kit).

7.2 Cell Culture Procedures

7.2.1 Preparation for Media Used in Cell Culture Maintenance

Materials (See Appendix 7.6 for details): DME-H21/F-12 Media, Fetal Bovine Serum (FBS) [if possible heat-inactivated], penicillin-streptomycin (PCN/SM), Fungizone, 5, 10, 25 ml disposable pipets.

The following procedure was done in a sterilized Laminar-flow hood.

1. If the FBS was not heat-inactivated, then the FBS was heated to 37° C to thaw. The FBS was then placed into a 56° C water bath for about 45 minutes.
2. All other solutions were thawed and placed into the 37° C water bath until each solution reached 37° C.
3. After warming, all bottles were sterilized with 70% ethanol/water and placed into the laminar hood.
4. 5 ml of Fungizone, 5 ml of PCN/SM, and 50 ml of FBS were added to each 500 ml bottle of DME-H21/F-12.
5. Bottles were wiped clean, capped, and stored in the refrigerator. Each bottle was labeled: "COMPLETE" DME-H21/F-12/10%FBS and dated.

6. Any unused “COMPLETE” media was discarded 2 weeks after being made to maintain media consistency and to reduce the probability of contamination growth.

7.3 Cell Passaging

7.3.1 Maintenance of Cell Pool Reservoir: T-150 or T-75 Flasks

Materials (See Appendix 7.6 for details): PBS Ca^{+2} Mg^{+2} , Corning T-150 flasks [or Falcon T-75 flasks], “COMPLETE” DME-H21/F-12/10%FBS media, trypsin, 5, 10, 25 ml disposable pipets, 50 ml centrifuge tubes, centrifuge.

The following procedure was done in a sterilized Laminar-flow hood.

1. Sterilize the laminar air-flow hood.
2. Stock hood with 5, 10, 25 ml pipets, Pasteur pipets, 50 ml centrifuge tubes.
3. The trypsin was removed from the freezer and placed into a 37°C water bath.
4. The DME-H21/F-12/10%FBS and PBS Ca^{+2} Mg^{+2} , were removed from the refrigerator and placed into a 37°C water bath.
5. After warming the above solutions to 37°C, each bottle was wiped down with 70% ethanol/water; the cleaned bottles were placed into the laminar hood.
6. The LLC-PK₁ cells were removed from the incubator and placed into the sterile laminar hood.
7. Using a six-inch disposable glass pipet, the growth media from each flask of cells was aspirated.

8. Each flask of cells was washed twice with 25 ml (20 ml for T-75 flasks) of PBS Ca^{+2} Mg^{+2} : 25 ml of the PBS was added to each flask, gently agitated, and then aspirated.
9. 10 ml of 0.25% trypsin was added to each flask, gently agitated, and allowed to incubate in the hood for 3 to 10 minutes.
10. After the cells have incubated for several minutes, the flask was jarred to help free the cells from the bottom of the flask.
11. Using a 10 ml pipet, the cell suspension was rapidly drawn in and out of the pipet to break up any residual aggregates of cells.
12. The aggregate-free cell suspension was then placed into a 50 ml centrifuge tube containing 20 ml of DME-H21/F12/10%FBS.
13. The centrifuge tubes were placed into the centrifuge and spun for 10 minutes at 2000 RPM and 10°C (approximately 800-1000G).
14. While centrifuging the cell suspension, the new T-150 flasks were placed into the hood and 50 ml of "COMPLETE" media was added to each flask.
15. After removing the tubes from the centrifuge, the supernatant was carefully aspirated as to not disturb the pellet.
16. The pellet was resuspended with 15 ml of DME-H21/F-12/10%FBS.
17. 2.5 ml of the cell suspension was added to each Corning T-150 flask containing 50 ml of DME-H21/F-12/10%FBS.
18. The flask was gently agitated and then placed into the incubator.

7.3.2 Plating for Experiments: Falcon 6-well Plates

Materials (See Appendix 7.6 for details): PBS Ca^{+2} Mg^{+2} , Falcon 3046 6-well tissue culture plates, “COMPLETE” DME-H21/F-12/10%FBS media, trypsin, 5, 10, 25 ml disposable pipets, 50 ml centrifuge tubes, centrifuge.

The following procedure was done in a sterilized Laminar-flow hood.

1. Sterilize the laminar air-flow hood.
2. Stock hood with 5, 10, 25 ml pipets, Pasteur pipets, 50 ml centrifuge tubes.
3. The trypsin was removed from the freezer and placed into a 37° C water bath.
4. The DME-H21/F-12/10%FBS and PBS Ca^{+2} Mg^{+2} were removed from the refrigerator and placed into a 37° C water bath.
5. After warming the above solutions to 37° C, each bottle was wiped down with 70% ethanol/water; the cleaned bottles were placed into the laminar hood.
6. The LLC-PK₁ cells were removed from the incubator and placed into the sterile laminar hood.
7. Using a 6 inch disposable glass pipet, the growth media from each flask of cells was aspirated.
8. Each flask of cells was washed twice with 25 ml of PBS Ca^{+2} Mg^{+2} : 25 ml of the PBS was added to each flask, gently agitated, and then aspirated.
9. 10 ml of 0.25% trypsin was added to each flask, gently agitated, and allowed to incubate in the hood for 3 to 10 minutes.

10. After the cells have incubated for several minutes, the flask was jarred to help free the cells from the bottom of the flask.
11. Using a 10 ml pipet, the cell suspension was rapidly drawn in and out of the pipet to break to break up any residual aggregates of cells.
12. The aggregate-free cell suspension was then placed into a 50 ml centrifuge tube containing 20 ml of DME-H21/F-12/10%FBS.
13. The centrifuge tubes were placed into the centrifuge and spun for 10 minutes at 2000 RPM and 10° C (approximately 800-1000 G).
14. After removing the tubes from the centrifuge. the supernatant was carefully aspirated as to not disturb the pellet.
15. While centrifuging the cell suspension, the new 6-well plates were removed from their sterile wrapping and placed into the hood; 2.0 ml of “COMPLETE” media was added to each well of the plate.
16. The pellet was resuspended with 15 ml of DME-H21/F-12/10%FBS.
17. 600 μ L of the cell suspension was added to each well containing 2.0 ml of DME-H21/F-12/10%FBS.
18. The plates were gently agitated and then placed into the incubator.

7.4 Cell Counting

7.4.1 Cell Counting for T-150 and T-75 Flasks and 6-well Plate Seeding

This procedure was used to determine the cell density of seeding solutions used for the T-150, T-75 flask and the 6-well plates used in experiments. Once the seeding density was determined, an appropriately sized aliquot was chosen to give the

cells the appropriate space to become confluent for a given flask/plate size and desired maturity date.

Materials (See Appendix 7.6 for details): hemocytometer with cover slip, optical light microscope, counter, 200 μ L pipetor, trypsin, FBS, trypan blue.

1. The cell suspension (from A.2.2, Maintenance of Cell Pool Reservoir: T-150 or T-75 Flasks, Step 16) was appropriately diluted with “COMPLETE” media (adjusted to give 25 to 40 cells per grid square).
2. A 100 μ L aliquot of cell suspension (from Step 1) was placed into a 1.0 ml microcentrifuge tube.
3. 200 μ L of trypan blue was added to this tube.
4. The microcentrifuge tube was capped and lightly shaken to mix the contents.
5. The 200 μ L pipet was used to draw up some of the cell/trypan blue suspension.
6. A clean cover slip was placed onto the hemocytometer.
7. The hemocytometer was filled up with the cell/trypan blue suspension contained in the 200 μ L pipet.
8. Using a light microscope, the number of cells in each grid was counted. (The hemocytometer gives the most accurate readings when the cell density is between 25 to 40 cells per grid square).
9. Each side of the hemocytometer contained ten counting squares. All ten counting squares were counted and averaged. After using this average cell count and dilution factors, the actual cell density of the original cell

suspension (from A.2.2, Maintenance of Cell Pool Reservoir: T-150 or T-75 Flasks, Step 16 was calculated.

10. The size of the seeding aliquot was then based upon the average cell density determined in Step 9.

7.4.2 Cell Counting for 6-well Plates Used in Experiments

This procedure was used to determine the number of cells per well of the 6-well plates used in experiments. Although we used this procedure for confluent cultures, it can be used in cultures that are not confluent.

Materials (See Appendix 7.6 for details): hemocytometer with cover slip, optical light microscope, counter, 200 μ L pipetor, trypsin, FBS, trypan blue.

1. In experiments where this cell counting procedure was used, the 6-well plates were randomly chosen from the 6-well plates to be used for the experiments.
2. 1.0 ml of 0.25% trypsin was added to each well that was to be counted. The plate and trypsin were incubated for 3 to 10 minutes. As the cells detached from the bottom of the well, the cell suspension was mixed with a 1.0 ml pipet by drawing the cell suspension in and out of the pipet.
3. Once the cells were fully removed from the plate, 0.1 ml of FBS was added to inactivate the trypsin.
4. 0.9 ml of "COMPLETE" or DME-H21/F-12 was added to each well to give a (1:1) dilution.
5. The cell suspension was mixed several times with a 1.0 ml pipet.
6. Immediately, a 100 μ L aliquot of cell suspension (from Step 5) was placed into a 1.0 ml microcentrifuge tube.

7. 200 μL of trypan blue were added to this tube.
8. The microcentrifuge tube was capped and lightly shaken to mix the contents.
9. The 200 μL pipet was used to draw up some of the cell/trypan blue suspension.
10. A clean cover slip was placed onto the hemocytometer.
11. The hemocytometer was filled up with the cell/trypan blue suspension contained in the 200 μL pipet.
12. Using a light microscope, the number of cells in each grid were counted. (The hemocytometer gives the most accurate readings when the cell density is between 25 to 40 cells per grid square).
13. Each side of the hemocytometer contained ten counting squares. All ten counting squares were counted and averaged. Using a dilution factor of 2, the number of cells per well was calculated.

7.5 Preparation of Commonly Used Solutions

7.5.1 Nitroglycerin Solutions

This general procedure was used to create the GTN solutions in the Concentration vs. Response, Probe Kinetics, Tolerance Development/Recovery, and Cross-tolerance experiments.

Materials (See Appendix 7.6 for details): All GTN used was Perlinganit Lösung. This formulation of nitroglycerin was (10 mg/10 ml) GTN, which corresponded to 4.4 mM. The base media was dependent upon the experiment: Earle's Balanced Salt Solution, PBS, Ham's/F-12, DME-H21, and PBS Ca^{+2} , Mg^{+2} . The GTN solutions were prepared just prior to each experiment. In the Tolerance Recovery experiments

all the beakers, glass vials, lids, stirbars, and any other equipment had to be sterilized; these solutions were made in the sterile laminar airflow hood.

1. 2.27 ml of 4.4mM Perlinganit Lösung GTN was dissolved into 7.73 ml of base media to produce a 1.0×10^{-3} M GTN solution. This solution was vortexed for ≈ 5 seconds.
2. Using the above solution, the appropriate dilutions were performed to make the desired concentrations of GTN.
3. All solutions were discarded after the completion of the experiment.

7.5.2 IBMX Solutions

This general procedure was used to create the IBMX solutions in the Concentration vs. Response, Probe Kinetics, Tolerance Development/Recovery, and Cross-tolerance experiments.

Materials (see Appendix 7.6 for details): IBMS, HEPES buffer, base media. The base media was dependent upon the experiment. In most experiments the base media was DME-H21/F-12. Other base media used were: Earle's Balanced Salt Solution, PBS, Ham's/F-12, DME-H21, and PBS Ca^{+2} , Mg^{+2} . In the Tolerance Recovery experiments all the beakers, glass vials, lids, stirbars, and any other equipment had to be sterilized; these solutions were made in the sterile laminar hood.

The procedure below was used to produce 200 ml of a 0.5 mM IBMX solution.

1. 22.22 mg of IBMX was carefully weighed out and placed into a 250 ml Pyrex beaker.
2. 198.0 ml of base media was added to the beaker, and a stirbar was placed into the beaker.
3. 2.0 ml of HEPES buffer was added.

4. The solution was stirred for \approx 1 hour or until the solid IBMX was fully dissolved.
5. The IBMX solutions were prepared approximately 1 to 1-1/2 hours prior (to allow the IBMX to fully dissolve) to the beginning of the experiment.

7.5.3 SNAP Solutions

This general procedure was used to create the SNAP solutions in the Concentration vs. Response and Cross-Tolerance experiments.

Materials (See Appendix 7.6 for details): SNAP, base media. The base media was dependent upon the experiment. In most experiments the base media was DME-H21/F-12. Other base media used were: Earle's Balanced Salt Solution, DME-H21, and PBS Ca^{+2} , Mg^{+2} .

1. Due to the light sensitive degradation of SNAP, all vials and beakers were wrapped with foil or ducting tape.
2. The following steps were done in a room with reduced lighting to prevent the degradation of SNAP.
3. 44.0 mg of SNAP was carefully weighed out and placed into a 20 ml scintillation vial.
4. 20.0 ml of base media was added to the vial and the vial was vortexed for \approx 5 seconds. This snap solution was $1.0 \times 10^{-2}\text{M}$.
5. Using the above solution, the appropriate dilutions were performed to make the desired SNAP concentrations.
6. All SNAP solutions were discarded after the experiment was completed.

7.5.4 DETA-NONO Solutions

This general procedure was used to create the DETA-NONO (DETA) solutions in the Concentration vs. Response and Cross-tolerance experiments.

Materials (See Appendix 7.6 for details): DETA-NONO, base media. The base media was dependent upon the experiment, The base media was either DME-H21/F-12 or PBS Ca^{+2} , Mg^{+2} .

1. Since the rate of degradation was pH sensitive, the pH of the base media was recorded prior to the addition of DETA-NONO.
2. Due to the extreme heat sensitive degradation of DETA-NONO, the following steps were done as rapidly as possible.
3. 32.60 mg of base media was carefully weighed and placed into a 20 ml scintillation vial.
4. 20.0 ml of base media was added to the vial and the vial was vortexed for ≈ 5 seconds. This DETA solution was $1.0 \times 10^{-2}\text{M}$.
5. Using the above solution, the appropriate dilutions were performed to make the desired DETA concentrations.
6. All DETA-containing vials were immediately placed on ice.
7. All DETA solutions were discarded after the experiment was completed.

7.5.5 Buffer Solutions

This procedure was used to make the TRIS/EDTA buffer. This buffer was used to reconstitute the cell contents after being lysed with ethanol.

Materials (See Appendix 7.6 for details): TRIS, EDTA, ultra pure water, 1 N HCl.

1. 6.06 g of TRIS and 1.49 g of EDTA were carefully weighed out and placed into a 600 ml Pyrex beaker.

2. 300 ml of water was added to the 600ml beaker and mixed until the TRIS and EDTA fully dissolved.
3. The solution was then titrated to a pH of 7.5 with HCl.
4. The solution was then transferred to a 1000 ml volumetric flask.
5. Water was added to the 1000 ml mark and the solution was well mixed.
6. The solution was transferred to a 1000 ml Pyrex bottle and stored in the refrigerator.
7. This solution was discarded after 6 months.

7.6 Materials and Equipment

7.6.1 Cell Culture

1. **Fetal Bovine Serum (FBS):** FBS, refiltered 0.1 μm sterile filtered, 100 ml Hyclone brand, UCSF-CCF No: IA300.
2. **Fetal Bovine Serum (FBS):** heat-inactivated, 100 ml, 0.1 μm sterile filtered, Gibco brand, UCSF-CCF No: IC310.
3. **Penicillin/Streptomycin (PCN/SM):** PCN/SM 100x (10,000 Units/ml PCN-G, 10,000 $\mu\text{g}/\text{ml}$ SM), 100 ml, UCSF-CCF No: FM200.
4. **Fungizone:** 250 $\mu\text{g}/\text{ml}$, 100x, 25 ml, sterile, UCSF-CCF No: FD200.
5. **HEPES buffer:** 1.0 M, 100 ml, 0.1 μm sterile filtered, in 0.9% normal saline with 13.5 g/L NaOH.
6. **Dulbeco's Modified Eagle's Media/F-12 (DME-H21/F-12):** without HEPES, GibcoBRL brand (11320-033), 0.1 μm sterile filtered, 2.483 g/L

- NaHCO₃, 3.15 g/L glucose, 0.055 g/L NaPyruvate, 0.365 g/L L-glutamine, UCSF-CCF No: VA850.
7. **Dulbeco's Modified Eagle's Media (DME-21 4.5 g/L glucose):** 0.1 µm sterile filtered with 0.584 g/L glutamine, 3.7 g/L NaHCO₃, 500 ml, UCSF-CCF No: AA400.
 8. **Media-199 (M-199) with Earle's Balance Salt Solution (EBSS) with glutamine:** 500 ml, 2.2 mg/L NaHCO₃, Gibco brand (11150-059), UCSF-CCF No: VG100.
 9. **Trypsin (STV) 0.05%, versene 0.02% in saline A:** 0.1 µm sterile filtered, 100 ml, 0.5 g/l trypsin, 0.2 g/L EDTA, 1.0 g/L glucose, 58 g/L NaHCO₃.
 10. **Phosphate Buffer Solution (PBS), Ca⁺², Mg⁺² free:** 0.1 µm sterile filtered, 500 ml, 0.2 g/L KH₂PO₄, 2.16 g/L Na₂HPO₄·7H₂O, 0.2 g/L KCl, 8.0 g/L NaCl, UCSF-CCF No: BG200.
 11. **Phosphate Buffer Solution (PBS):** 0.1 µm filtered, 0.1 g/L CaCl₂, 0.1 g/L MgCl₂·6H₂O, 0.2 g/L KCl, 0.2 g/L KH₂PO₄, 8.0 g/L NaCl, 2.16 g/L Na₂HPO₄·7H₂O, UCSF-CCF No: BG100.
 12. **Earle's Balanced Salt Solution (EBSS):** 6.8 g/L NaCl, 0.4 g/L KCl, 0.2 g/L CaCl₂, 0.1 g/L MgSO₄·7H₂O, 0.125 g/L NaH₂PO₄·H₂O, 1.0 g/L glucose, 0.05 g/L phenol red, 2.2 g/L NaHCO₃.
 13. **Trypan blue 0.4%:** membrane filtered, prepared in 0.85% saline, Gibco brand (15250-012), 100 ml, UCSF-CCF No: WH570.

14. **F-12/Ham's Mix:** 450 ml, 1.802 g/L glucose, 0.11 g/L NaPyruvate, 0.146 g/L L-glutamine, 1.176 g/L NaHCO₃, UCSF-CCF No: AC200. Used in early experiments.
15. **Glutamine 100x, 0.2M:** 0.1 μ m sterile filtered, 25 ml, 29.2 g/L L-glutamine, UCSF-CCF No: ED200. Used in early experiments.
16. **Insulin 1.0 mg/ml:** 2.0 ml, UCSF-CCF No: EW200. Used in early experiments.
17. **Micro pipets:** Pipetman 200 μ l and 1000 μ L with disposable tips.
18. **5, 10, 25 ml pipets:** Fisher brand, polystyrene, serological disposable pipets.
19. **Culture plates:** Falcon (3046) 6-well culture plates, flat-bottom with low evaporation lid, polystyrene.
20. **T-75 culture flasks:** Falcon T-75 (3110), vented tissue culture flasks, 75 cm², sterile/gamma irradiated.
21. **T-150 culture flasks:** Corning T150 (430825), tissue culture treated flasks, 150 cm², polystyrene, 0.2 μ m vented cap.
22. **Centrifuge:** Beckman GS-6 Series centrifuge with 50 ml centrifuge tube holders.
23. **Incubator:** Napco 6100-R incubator. Settings: 37° C, 5% CO₂.
24. **Pipet aid:** Drummond Scientific Inc. Pipet-aid. This device is absolutely essential.

7.6.2 Chemicals, Solvents, and Miscellaneous

1. **Nitroglycerin (GTN):** “Perlinganit Lösung zur i.v. Infusion, 5 Ampullen”, 1 Ampulle a 10 ml enthält: 10 mg Glyceroltrinitrat in 10 ml isotonischer Glucoselösung. (10 mg GTN/10 ml isotonic glucose/ethanol). [**Manufacturer:** Schwarz Pharma AG Mittelstr. 11-13, 4019 Monheim]. All GTN used was generously donated by Prof. Dr. rer. nat. Henning Schröder, Martin-Luther-Universität Halle-Wittenberg.
2. **IBMX:** 3-isobutyl-1-methyl-xanthine (IBMX) ($C_{10}H_{14}N_4O_2$), FW: 222.2, ultra high purity grade. [CAS: 28822-58-4] [**Vendor:** Sigma Chemical Cat No: I-7018].
3. **TNM:** tetranitromethane (TNM), [CAS: 509-14-8], FW: 196.0, [**Vendor:** Sigma Chemicals, Cat No: T-5752].
4. **SNAP:** S-nitroso-penicillamine (SNAP), MW: 220.2, [CAS: 79032-48-7], [**Vendor:** Research Biochemicals International, Natick, MA, Cat No: N-152].
5. **DETA-NONO (DETA or diethylenetriamine NONOate):** Ethanamine, 2,2'-(hydroxynitrosohydrozono)bis- ($C_4H_{13}N_5O_2$), [CAS: 146724-94-9], FW: 163.2. [**Vendor:** Cayman Chemical, Ann Arbor, MI, Cat No: 82120].
6. **TRIS:** GibcoBRL brand (15504-012), ultrapure 500g, MW: 121.14, purity $\geq 99\%$, [CAS: 77-86-1].
7. **EDTA:** GibcoBRL brand (15576-028), ultrapure 500g, MW: 372.24, purity $> 99\%$, [CAS: 6381-92-6].

8. **Ethanol:** Reagent grade, 200 proof, denatured. [**Vendor:** UCSF School of Pharmacy Stockroom].
9. **Scintillation Cocktail:** Beckman Biodegradable counting scintillant (BCS). [**Vendor:** Amersham, Cat No: NBCS104].
10. **DI H₂O:** UCSF De-ionized water on tap.
11. **Ultra-pure DI H₂O:** Ultra-high purity, de-ionized ($\geq 1,000,000$ ohm) with a Millipore de-ionizer/filter.

7.6.3 Radioimmunoassay

1. **RIA cGMP kit:** Amersham cyclic GMP [³H] RIA Assay System. [**Vendor:** Amersham, Cat No: TRK500].
2. Test tubes for standard preparations: 12 x 75mm.
3. **Test tubes for RIA assay:** 13 x 100mm, must be able to withstand high G force centrifugation, polystyrene.
4. **Scintillation vials:** 20 ml disposable glass vials.
5. **Multi-pipetor:** Eppendorf multi-pipetor and 1.25 ml, 2.50 ml, 5.0 ml, and 50.0 ml tips.
6. **Cotton balls:** Fisher brand, used for removing residual (NH₄)₃SO₄ from the insides of the test tubes, Cat No: 07-886.
7. **Ice chest:** Coleman ice chest.
8. **Vortex mixer:** Thermodyne vortex/mixer, type: 16700.
9. **Centrifuge:** Beckman centrifuge with holders for 13 x 100mm test tubes.
10. **Scintillation counter:** Beckman Liquid Scintillation Counter.

7.6.4 Experimental Apparatus and Equipment

1. Laminar airflow hood: 3' width minimum.
2. Aspiration apparatus: Simple vacuum system with trap.
3. Water bath: Capable of heating to 37° C. The bath should be able to hold six-500 ml bottles.
4. Beakers: Pyrex beakers – assorted sized with polypropylene lids (100 ml, 250 ml, and 1000ml) for GTN, IBMX, SNAP, TNM, DETA-NONO solutions. Beakers and lids must be able to withstand autoclaving.
5. Stopwatches: Fisher brand, digital stopwatches.
6. Freezers: -80° C freezer (for RIA freeze/thaw step, storage of DETA-NONO, and long-term storage); -20° C freezer (for short term sample storage, trypsin, PCN/SM, FBS, Fungizone, IBMX, SMAP, RIA kits).
7. Refrigerators: Storage of cell culture media, opened RIA kits, GTN, TRIS buffer, HEPES buffer.

7.7 References

- [1] A. Friedl, C. Harmening, B. Schuricht, and B. Hamprecht. Rat Atrial Natriuretic Peptide Elevates the Level of Cyclic GMP in Astroglia-rich Brain Cell Cultures. *European Journal of Pharmacology*, 1985, 111(1985): 141-142.

8 Appendix B

Technique for estimating the Chi-squared statistic and the Variance/Covariance/Correlation matrix

8.1 Chi-squared statistic

The Chi-squared values were given by

$$\chi_{opt}^2 = \chi^2_{([GTN], time | \hat{\mathbf{p}}_{opt})} = \frac{\sum_i \sum_j (cGMP_{i,j} - \widehat{cGMP}_{i,j})^2}{S_{pooled}^2}$$

$$\chi_{test}^2 = \chi^2_{([GTN], time | \hat{\mathbf{p}}_{test})} = \frac{\sum_i \sum_j (cGMP_{i,j} - \widetilde{cGMP}_{i,j})^2}{S_{pooled}^2}$$

where,

$$cGMP_{i,j} = cGMP([GTN]_i, t_j)_{observed}$$

$$\widehat{cGMP}_{i,j} = cGMP([GTN]_i, t_j | \hat{\mathbf{p}}_{opt})$$

$$\widetilde{cGMP}_{i,j} = cGMP([GTN]_i, t_j | \hat{\mathbf{p}}_{test})$$

and the pooled variance is given by

$$S_{pooled}^2 = \frac{\sum_i \sum_j \nu_{i,j} s_{i,j}^2}{\sum_i \sum_j \nu_{i,j}}$$

$\hat{\mathbf{p}}_{opt}$ is the optimal parameter set; $\hat{\mathbf{p}}_{test}$ is the test parameter set; $\nu_{i,j} = (n_{i,j} - 1)$ is the number of statistical degrees of freedom; and $s_{i,j}^2$ is the variance for each respective $[GTN]_i$ and time point, t_j .

8.2 Correlation Matrix

We determined the correlation matrix (**COR**) by applying a frequently used, but seemingly infrequently described [1] technique for approximating the variance-covariance matrix (**COV**). First, the Hessian matrix (**H**), or second derivative matrix, was approximated by calculating the change in the objective function, J , per change in two parameters, p_n^o and p_m^o , where $\Delta p_n = p_n^o / 1000$ and $\Delta p_m = p_m^o / 1000$. If we approximate J with a second-order Taylor series, and let $\tilde{p}_1 = p_1^o + \Delta p_1$, $\tilde{p}_2 = p_2^o + \Delta p_2$

$$J(\tilde{p}_1, \tilde{p}_2) \approx J(p_1^o, p_2^o) + \frac{1}{1!} \left[\frac{\partial J}{\partial p_1} (\tilde{p}_1 - p_1^o) + \frac{\partial J}{\partial p_2} (\tilde{p}_2 - p_2^o) \right] + \frac{1}{2!} \left[\frac{\partial^2 J}{\partial p_1^2} (\tilde{p}_1 - p_1^o)^2 + 2 \frac{\partial^2 J}{\partial p_1 \partial p_2} (\tilde{p}_1 - p_1^o)(\tilde{p}_2 - p_2^o) + \frac{\partial^2 J}{\partial p_2^2} (\tilde{p}_2 - p_2^o)^2 \right] \quad (\text{B.1})$$

At (p_1^o, p_2^o) , $\partial J / \partial p_1 = \partial J / \partial p_2 = 0$ and using the Hessian operator, **H**, J becomes

$$J(\tilde{p}_1, \tilde{p}_2) \approx J(p_1^o, p_2^o) + \frac{1}{2} \left[\frac{\partial^2 J}{\partial p_1 \partial p_1} (\tilde{p}_1 - p_1^o)^2 + 2 \frac{\partial^2 J}{\partial p_1 \partial p_2} (\tilde{p}_1 - p_1^o)(\tilde{p}_2 - p_2^o) + \frac{\partial^2 J}{\partial p_2 \partial p_2} (\tilde{p}_2 - p_2^o)^2 \right] \quad (\text{B.2})$$

$$= J(p_1^o, p_2^o) + \frac{1}{2} \left[H_{11} (\tilde{p}_1 - p_1^o)^2 + 2 H_{12} (\tilde{p}_1 - p_1^o)(\tilde{p}_2 - p_2^o) + H_{22} (\tilde{p}_2 - p_2^o)^2 \right]$$

where

$$\mathbf{H} = \frac{\partial^2 J}{\partial p_i \partial p_j} = \begin{bmatrix} H_{11} & H_{12} \\ H_{21} & H_{22} \end{bmatrix} \quad (\text{B.3})$$

The diagonal elements were determined by setting $\tilde{p}_j = p_j^o$ in Equation (B.2) and solving for either H_{11} or H_{22}

$$H_{ii} = 2 \frac{J(\tilde{p}_i, p_j^o) - J(p_i^o, p_j^o)}{(\tilde{p}_i - p_i^o)^2} \quad (\text{B.4})$$

and off-diagonal elements were calculated by substituting H_{11} and H_{22} from Equation (B.4) into (B.2) and solving for H_{12}

$$\begin{aligned}
 J(\tilde{p}_1, \tilde{p}_2) - J(p_1^o, p_2^o) &= J(\tilde{p}_1, p_2^o) - J(p_1^o, p_2^o) + J(\tilde{p}_2, p_1^o) - J(p_1^o, p_2^o) \\
 &\quad + H_{12}(\tilde{p}_1 - p_1^o)(\tilde{p}_2 - p_2^o) \tag{B.5} \\
 \Rightarrow H_{12} = H_{21} &= \frac{J(\tilde{p}_1, \tilde{p}_2) + J(p_1^o, p_2^o) - J(\tilde{p}_1, p_2^o) - J(\tilde{p}_2, p_1^o)}{(\tilde{p}_1 - p_1^o)(\tilde{p}_2 - p_2^o)}
 \end{aligned}$$

Since the Hessian matrix is symmetric, only the upper or lower triangular elements need to be determined to obtain all the off-diagonal elements.

If given \mathbf{H} , we can calculate the **COV** and **COR** matrices

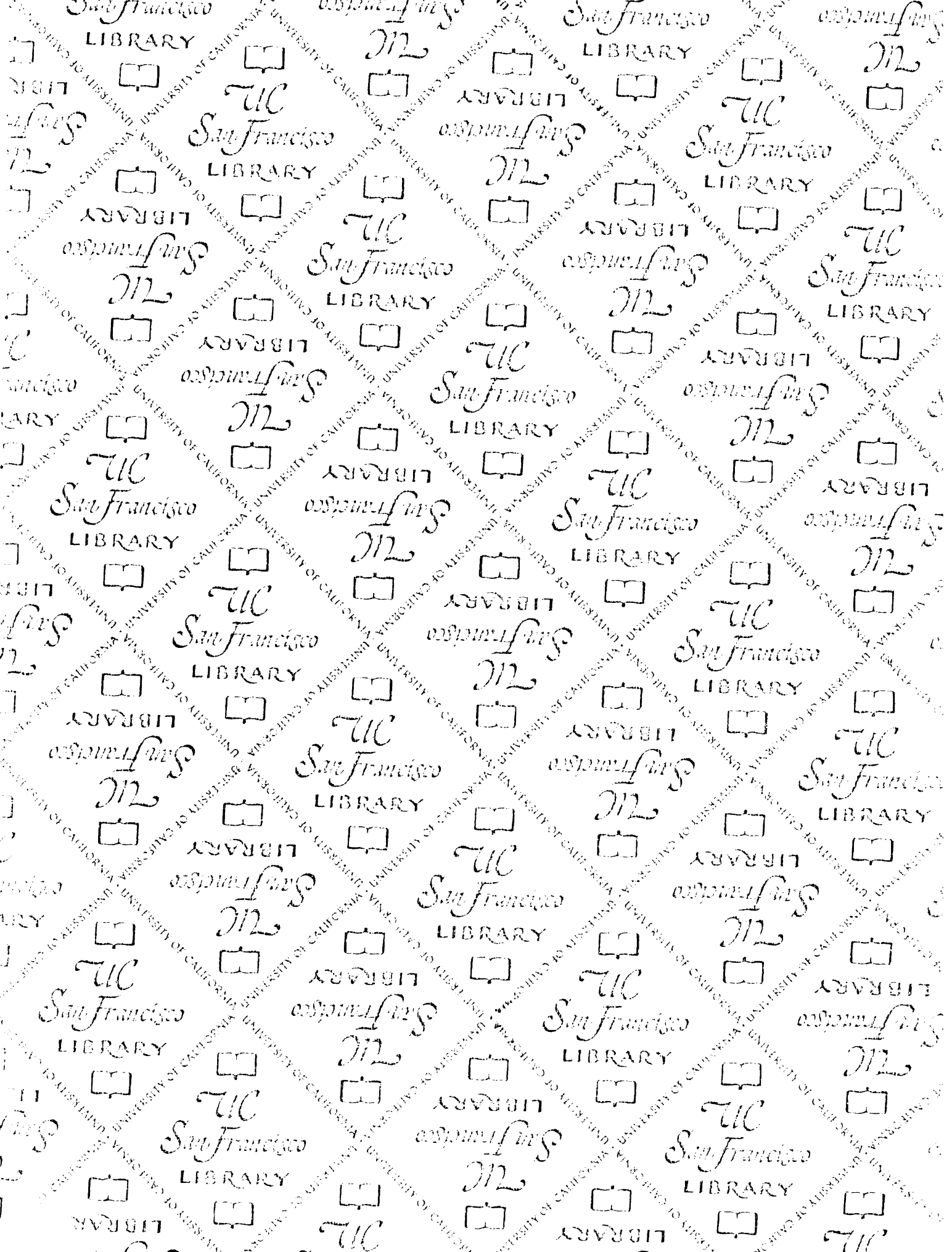
$$\mathbf{H}^{-1} \approx \mathbf{COV} = \begin{bmatrix} s_{11}^2 & s_{12}^2 & \cdots & s_{18}^2 \\ s_{21}^2 & s_{22}^2 & \cdots & \vdots \\ \vdots & \vdots & \ddots & \vdots \\ s_{81}^2 & \cdots & \cdots & s_{88}^2 \end{bmatrix} \tag{B.6}$$

The inverse of the standard deviation matrix ($\mathbf{V}^{1/2}$) is given by

$$(\mathbf{V}^{1/2})^{-1} = \begin{bmatrix} \frac{1}{\sqrt{s_{11}^2}} & 0 & \dots & 0 \\ 0 & \frac{1}{\sqrt{s_{22}^2}} & \dots & 0 \\ \vdots & \vdots & \ddots & \vdots \\ 0 & 0 & \dots & \frac{1}{\sqrt{s_{88}^2}} \end{bmatrix} \quad (\text{B.7})$$

Given $\mathbf{V}^{-1/2}$ and \mathbf{COV} , the \mathbf{COR} matrix is given by

$$\mathbf{COR} = (\mathbf{V}^{1/2})^{-1} \mathbf{COV} (\mathbf{V}^{1/2})^{-1} = \begin{bmatrix} \frac{s_{11}^2}{\sqrt{s_{11}^2} \sqrt{s_{11}^2}} & \frac{s_{12}^2}{\sqrt{s_{11}^2} \sqrt{s_{22}^2}} & \dots & \frac{s_{18}^2}{\sqrt{s_{11}^2} \sqrt{s_{88}^2}} \\ \frac{s_{21}^2}{\sqrt{s_{22}^2} \sqrt{s_{11}^2}} & \frac{s_{22}^2}{\sqrt{s_{22}^2} \sqrt{s_{22}^2}} & \dots & \frac{s_{28}^2}{\sqrt{s_{22}^2} \sqrt{s_{88}^2}} \\ \vdots & \vdots & \ddots & \vdots \\ \frac{s_{81}^2}{\sqrt{s_{88}^2} \sqrt{s_{11}^2}} & \frac{s_{82}^2}{\sqrt{s_{88}^2} \sqrt{s_{22}^2}} & \dots & \frac{s_{88}^2}{\sqrt{s_{88}^2} \sqrt{s_{88}^2}} \end{bmatrix} \quad (\text{B.8})$$



For reference

Not to be taken from the room.

